AN EVALUATION OF ATMOSPHERIC CORRECTION ALGORITHMS IN THE ESTIMATION OF SOIL ORGANIC CARBON FROM HYPERION IMAGE

Thesis
Submitted in partial fulfillment of the requirements for the
degree of
DOCTOR OF PHILOSOPHY

By
MINU S

DEPARTMENT OF APPLIED MECHANICS AND
HYDRAULICS
NATIONAL INSTITUTE OF TECHNOLOGY KARNATAKA
SURATHKAL, MANGALURU-575 025
JUNE – 2018

AN EVALUATION OF ATMOSPHERIC CORRECTION ALGORITHMS IN THE ESTIMATION OF SOIL ORGANIC CARBON FROM HYPERION IMAGE

Thesis
Submitted in partial fulfillment of the requirements for the
degree of
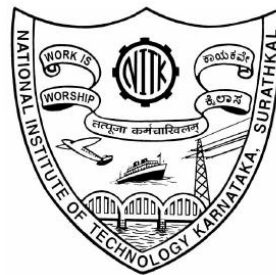**DOCTOR OF PHILOSOPHY**

By
MINU S

Under the guidance of
Dr. AMBA SHETTY
Professor
Dept. of Applied Mechanics & Hydraulics
NITK, Surathkal

DEPARTMENT OF APPLIED MECHANICS AND HYDRAULICS
NATIONAL INSTITUTE OF TECHNOLOGY KARNATAKA
SURATHKAL, MANGALURU-575 025
JUNE – 2018

D E C L A R A T I O N

By the Ph.D. Research Scholar

I hereby *declare* that the Research Thesis entitled **An evaluation of Atmospheric Correction Algorithms in the Estimation of Soil Organic Carbon from Hyperion image** which is being submitted to the **National Institute of Technology Karnataka, Surathkal** in partial fulfilment of the requirements for the award of the Degree of **Doctor of Philosophy** in **Applied Mechanics and Hydraulics Department** is a *bonafide report of the research work* carried out by me. The material contained in this Research Thesis has not been submitted to any University or Institution for the award of any degree.

135010 AM13P01, MINU S

(Register Number, Name & Signature of the Research Scholar)

Department of Applied Mechanics and Hydraulics
National Institute of Technology Karnataka, India

Place: NITK-Surathkal

Date:

C E R T I F I C A T E

This is to *certify* that the Research Thesis entitled **An evaluation of Atmospheric Correction Algorithms in the Estimation of Soil Organic Carbon from Hyperion image** submitted by **MINU S** (Register Number: 135010 AM13P01) as the record of the research work carried out by her, is *accepted as the Research Thesis submission* in partial fulfilment of the requirements for the award of degree of **Doctor of Philosophy**.

Dr. Amba Shetty

Professor

Research Guide

(Name and Signature with Date and Seal)

Chairman - DRPC

(Signature with Date and Seal)

Department of Applied Mechanics and Hydraulics

National Institute of Technology Karnataka, India

ACKNOWLEDGEMENTS

Dedication

To my parents for all their love and support and putting me through the best education as possible,

To all my former teachers through whom the Almighty led me to the world of knowledge and wisdom,

&

To my loving husband Mr. Aravind K. and my in-laws for their constant source of encouragement and inspiration during the period of my research work.

ABSTRACT

Soil organic carbon (SOC) is one of the most important constituents of soil due to its capacity to affect plant growth both as a source of energy and a trigger for nutrient availability through mineralization. Conventional laboratory methods of determination of SOC content are very laborious, time consuming and costly. For practical application, estimation of SOC from spaceborne VNIR/SWIR (Visible Near Infrared and Short wave infrared, 400-2500 nm) image using statistical regression is considered as an alternative technique.

Spatial and spectral information from spaceborne hyperspectral VNIR/SWIR data can be used for quantification and better characterization of soil properties. The potential of this data has not been fully extracted till now because of noisy atmospheric components in spectral signature retrieved from spaceborne hyperspectral image. Though there are different atmospheric correction algorithms, retrieving biophysical characteristics from spaceborne hyperspectral data is a challenge. In this research, influence of atmospheric correction algorithms on the estimation of SOC is investigated.

Research was initiated with ground VNIR/SWIR (400-2500 nm) spectroradiometer reflectance spectra obtained from bare agricultural sites in Narrabri, Australia, to find the effect of various pre-processing methods and estimation models on the estimation of SOC. Partial least square regression (PLSR) model performs better with Savitzky Golay as the best pre-processing method. The output from PLSR model was used to identify wavelengths that are significant in estimating SOC using a relative score defined as the product of the Variable Importance for Projection (VIP) values and the absolute value of PLS regression coefficient values. The most significant wavelengths in this PLSR model were located in the 600–680, 1860–1900, and 2180–2250 nm spectral regions. And, secondary significant wavelengths were located around 1000 and 2070 nm.

Study was conducted to find the influence of atmospheric correction algorithms in the estimation of SOC from Hyperion data in sites located in two different geographical settings viz. Karnataka in India and Narrabri in Australia. Commonly used atmospheric correction algorithms, (1) ATmospheric CORection (ATCOR), (2) Fast Line-of-sight Atmospheric Analysis of Spectral Hypercubes (FLAASH), (3) 6S, and (4) QUick Atmospheric Correction (QUAC), were employed for retrieving spectral reflectance from radiance image. The results showed that ATCOR corrected spectra coupled with PLSR model, produced the best SOC estimation, in terms of coefficient of determination (R^2), Residual Prediction Deviation (RPD) and Ratio of Performance to Inter-Quartile (RPIQ), irrespective of the study area. Comparing the results across study areas, sites in Karnataka gave lower estimation accuracy than sites in Narrabri. This may be explained due to difference in spatial arrangement of field conditions. A spectral similarity comparison of atmospherically corrected Hyperion spectra of soil samples with field-measured VNIR/SWIR spectra was performed. Among the atmospheric correction algorithms, ATCOR corrected spectra is found to capture the pattern in soil reflectance curve near 2200 nm. ATCOR's finer spectral sampling distance in shortwave-infrared wavelength region compared to other models was identified as the main reason for its better performance.

Two hybrid atmospheric correction (HAC) algorithms incorporating a modified empirical line (EL_m) method were proposed. The first HAC model (named HAC_1) combines i) a radiative transfer (RT) model based on the concepts of radiative transfer equations, which uses real-time *in situ* atmospheric and climatic data and ii) an EL_m technique. The second one (named HAC_2) combines i) the well-known ATCOR model and ii) an EL_m technique. Both HAC algorithms and their component single atmospheric correction algorithms (ATCOR, RT and EL_m) were applied to radiance data acquired by Hyperion satellite sensor over study sites in Australia. The performances of both HAC algorithms were analysed in two ways. Firstly, the Hyperion reflectances obtained by five atmospheric correction algorithms were analysed and compared using spectral metrics. Secondly, performance of each atmospheric correction algorithm was analysed for estimation of SOC using Hyperion

reflectances obtained from atmospheric correction algorithms. The estimation model of SOC was built using PLSR model. The results show that i) both the hybrid models produce a good spectrum with lower Spectral Angle Mapper (SAM) and Spectral Information Divergence (SID) values and ii) both hybrid algorithms provided better SOC estimations accuracy, in terms of R^2, RPD and RPIQ statistics. Thus, HAC algorithms, developed using EL_m technique, may be recommended for atmospheric correction of Hyperion radiance data, when archived Hyperion reflectance data have to be used for SOC estimation mapping.

TABLE OF CONTENTS

LIST OF FIGURES

models using *N* ground targets, over Narrabri site#2 image.

LIST OF TABLES

LIST OF ABBREVIATIONS

Abbreviation	Description
ACORN	Atmospheric CORrection Now
ANN	Artificial Neural Network
ATCOR	ATmospheric CORrection
ATREM	ATmospheric REMoval
ASD	Analytical Spectral Devices
β	Regression Coefficients
EL	Empirical Line
EL_m	Modified Empirical Line
EO-l	Earth Observing-l
FLAASH	Fast Line-of-sight Atmospheric Analysis of Spectral Hypercubes
GPS	Global Positioning System
GS	Gaussian Smoothing
GT	Ground Target
HAC	Hybrid Atmospheric Correction
HATCH	High-accuracy ATmosphere Correction for Hyperspectral data
HITRAN	HIgh-resolution TRANsmission molecular absorption
MA	Moving Average
MF	Median Filter
MIR	Mid Infrared
MLR	Multiple Linear Regression
MODTRAN	MODerate resolution atmospheric TRANsmission

NF	Optimum number of PLS components
PC	Principal Component
PCR	Principal Component Regression
PLSR	Partial Least Square Regression
QUAC	QUick Atmospheric Correction
R^2	Coefficient of determination
RMSE	Root Mean Square Error
RPD	Residual Prediction Deviation
RPIQ	Ratio of Performance to Inter-Quartile
RT	Radiative Transfer
6S	Second Simulation of a Satellite Signal in the Solar Spectrum
SAM	Spectral Angle Mapper
SG	Savitzky Golay
SIC	Soil Inorganic Carbon
SID	Spectral Information Divergence
SNR	Signal to Noise Ratio
SOC	Soil Organic Carbon
SOM	Soil Organic Matter
SSD	Spectral Sampling Distance
SWIR	Shortwave-Infrared
TOA	Top-of-atmosphere
VIP	Variable Importance in PLS projections
VNIR	Visible Near-Infrared

<div align="right">

CHAPTER 1

INTRODUCTION

</div>

1.1 BACKGROUND

Soil is a composite heterogeneous material with highly variable physical and chemical properties. It supports life and vegetation on earth and is a valuable gift of nature. For better management of soil, one has to have a thorough knowledge of soil properties in general, and top soil in particular. Topsoil is the upper, outermost layer of soil, usually the top 0 to 20 cm.

Soil organic carbon (SOC) is one of the most important constituents of top soil due to its capacity to affect plant growth both as a source of energy and a trigger for nutrient availability through mineralization (USDA 2009). SOC also plays a vital role in the carbon cycling of terrestrial ecosystems (Li et al. 2012). Information on spatial and temporal variations in SOC content is needed in agronomic, soil studies (Stevens et al. 2006) and climate change studies (Albaladejo et al. 2013, McBratney et al. 2014).

Conventional laboratory methods of determination of SOC content are very laborious, time consuming and expensive. Determination of SOC content from Visible Near-infrared and Shortwave infrared (VNIR/SWIR, 400-2500 nm) laboratory and field spectroscopy is considered to be an alternative technique (e.g. McCarty et al. 2002; Martin et al. 2002; Viscarra-Rossel et al. 2006). SOC has a substantial effect on soil reflectance in VNIR/SWIR region of electromagnetic spectrum. Thus it significantly affects the pattern of a soil reflectance spectrum.

Statistical regression techniques (e.g. Ben-Dor and Banin 1995; Chang and Laird 2002) may be used to estimate SOC from the VNIR/SWIR laboratory and field soil reflectance

An evaluation of atmospheric correction algorithms in the estimation of SOC from Hyperion image.
Ph.D. Thesis, 2018, NITK, Surathkal, India.

1

spectra. Though many researchers have successfully demonstrated the potential of laboratory or field spectroscopy for SOC estimation, such laboratory and field techniques cannot be extended to large area. A soil spectrum derived from hyperspectral remote sensing images can be available solution. But this technique has a number of limitations, and there is scope for improvements which needs to be addressed.

1.2 REMOTE SENSING IN THE STUDY OF SOIL PROPERTIES

Remote sensing is the science and art of acquiring information about an object from measurements made from a distance without coming into physical contact with the object (Lillesand et al. 2009). The advent of satellite remote sensing technology has revolutionized the world in acquiring information in a cost-effective and temporal basis. It makes possible to gather information from locations which otherwise would have been very hard to traverse. Remote sensing technique can observe the earth surface from outer space using satellites (spaceborne) or from the air using aircrafts (airborne).

Remotely sensed images provide repetitive spatial and spectral data that can be used for quantification and better characterization of top soil properties. The spectral behaviour of soil is a cumulative property reliant on its composition. Variation in spectral signature about absorption features may indicate the presence or absence of chemical chromophores (Das et al. 2015). Spectral signature derived from remote sensing data when processed with standard/well-established procedures produce better results in its end applications.

Airborne remote sensing, compared to spaceborne remote sensing, offers the advantage of increased control over the data collection process. The spatial resolution can be adjusted by flying the sensor at different altitudes or changing the focal length of the sensor (Moses et al. 2012). The intervening atmosphere is significantly less at typical aircraft altitudes (~4 km) than the altitudes of typical spaceborne platform (~700 km).

An evaluation of atmospheric correction algorithms in the estimation of SOC from Hyperion image.
Ph.D. Thesis, 2018, NITK, Surathkal, India.

2

However, such data collection is an expensive effort with high cost per unit area of ground coverage. Airborne remote sensing missions are often carried out as one-time operations, whereas spaceborne remote sensing missions offer the possibility of continuous monitoring of the earth. Airborne imaging spectrometer (AIR) developed by JPL NASA, Digital Airborne Imaging Spectrometer (DAIS 7915) developed by the European Union and DLR, Airborne Visible / Infrared Imaging Spectrometer (AVIRIS) and AVIRIS- Next Generation developed by JPL NASA, Compact Airborne Spectrographic Imager (CASI) by ITRES, etc. are a few examples.

Spaceborne VNIR/SWIR sensors provide spectral data over large coverage and at regular intervals. Most of the spaceborne VNIR/SWIR sensors are multispectral sensors (< 10 spectral bands), such as ASTER, LANDSAT or SPOT (Abrams and Hook 2003; Roy et al. 2014). Spaceborne hyperspectral remote sensing is the future of remote sensing, and provides digital imagery of earth surface in narrow continuous spectral bands, along the electromagnetic spectrum rather than few data points averaged over broad wavelengths. Hyperspectral data are thus spectrally continuous remotely sensed data that is used to get spectral signature of an object (Figure 1.1). EO-1 Hyperion Imaging Spectrometer is a spaceborne VNIR/SWIR hyperspectral sensor (> 100 spectral bands) with a spatial resolution of 30 m, a spectral resolution of 10 nm and a swath of 7.5 km (Folkman et al. 2001). The potential of this spaceborne hyperspectral Hyperion sensor has not been fully explored yet because of its signal-to-noise ratio (SNR) around 50:1 (Folkman et al. 2001), due to atmospheric and instrumental perturbations. SNR is dependent on the strength of the signal reflected by the target and it varies spectrally. SNR of a sensor is often specified as a single number that is the maximum value calculated based on a standard target (Moses et al. 2012). While instrumental perturbations may not be corrected on the spectra, atmospheric perturbations may be reduced using atmospheric correction algorithms.

An evaluation of atmospheric correction algorithms in the estimation of SOC from Hyperion image.
Ph.D. Thesis, 2018, NITK, Surathkal, India.

3
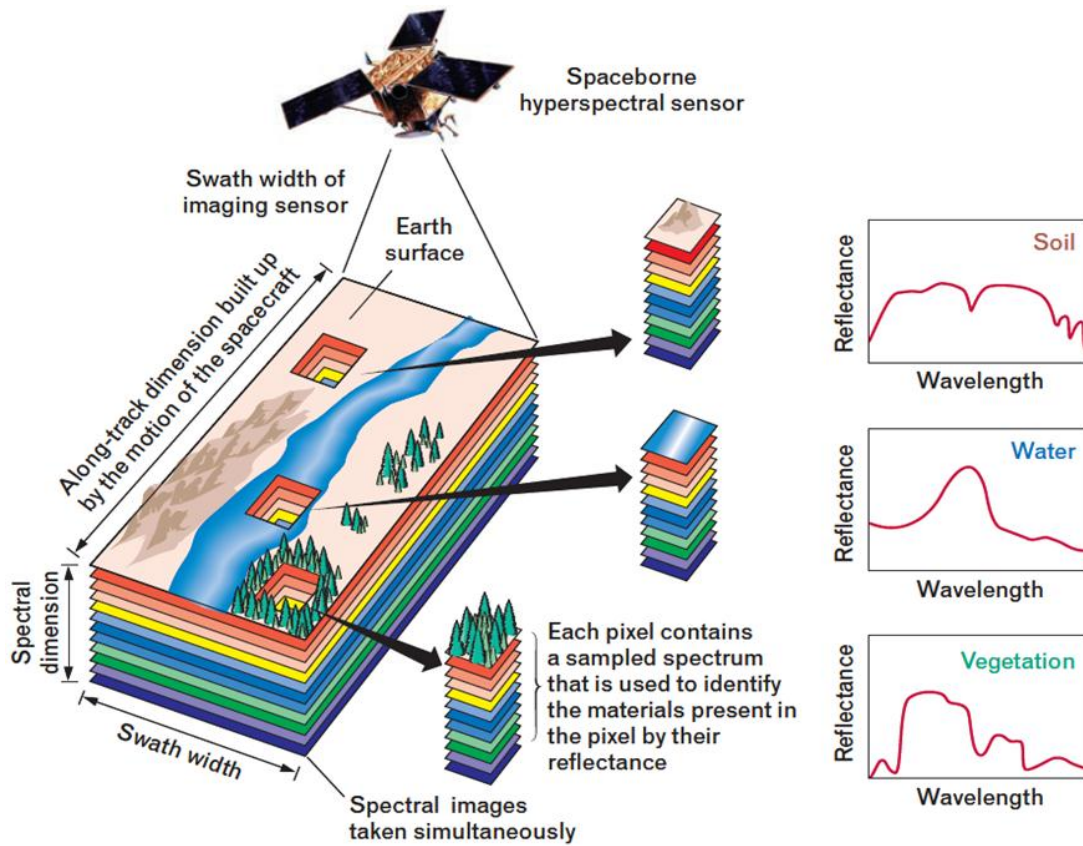
Figure 1.1 Concept of hyperspectral imaging (source: Shaw and Burke 2003)

Over the past decade hyperspectral image analysis has developed into a potent and rapidly growing technology in the field of remote sensing. With the increased amount of spectral data, researchers were able to derive precise information about Earth's surface from an image pixel using characteristic absorption features in its spectral signature. Table 1.1 gives some of the spaceborne hyperspectral instruments in the world.

An evaluation of atmospheric correction algorithms in the estimation of SOC from Hyperion image.
Ph.D. Thesis, 2018, NITK, Surathkal, India.

4

Table 1.1 Some of the Spaceborne hyperspectral instruments worldwide

Satellite/ Sensor	Country	Launch -End of life	No. of bands	Spectral range	Band width	Spatial resolution	Purpose
EO1– Hyperion	NASA, USA	2000-2017	220	400 to 2500 nm	10 nm	30 m	Mineral exploration, resource mapping
PROBA – CHRIS	ESA, UK	2001-≥2018	82	415 to 1050 nm	12 nm	18 or 36 m	Agriculture, Land Natural Disasters
IMS1 – HySI-T	ISRO, India	2008-2018*	64	450 to 950nm	8 nm	500 m	Land observation and detailed vegetation classification
HJ 1A – HSI	CAST, China	2008-≥2018	115	450 to 950 nm	5 nm	100 m	Earth observation
HICO on ISS	NASA/ ONR, USA	2009-2014	102	380 to 960 nm	5.7 nm	90 m	Bathymetry, water optical properties
Resurs-P – GSA	Roscosmos, Russia	2013-≥2021	216	400 to 1100 nm	5 -10 nm	25m	Vegetation process study

* present status is unclear

Additionally, at least five hyperspectral VNIR/SWIR satellite sensors are planned to be launched in the years to come. The Italian PRISMA (PRecursore IperSpettrale della Missione Applicativa) (Lopinto and Ananasso 2013) and German EnMAP (Environmental Mapping and Analysis Program) (Stuffler et al. 2007) satellite sensors are expected to be launched in 2018. And the American HyspIRI (Hyperspectral Infrared Imager), Italy-Israel SHALOM (Spaceborne Hyperspectral Applicative Land and Ocean

Mission) (Bussoletti 2012) and French HYPXIM (HYPerspectral X Imagery) (Carrere et al. 2013) are under study. These sensors would open up a significant way of digital SOC mapping.

1.3 LIMITATIONS IN THE USE OF HYPERSPECTRAL REMOTE SENSING DATA FOR SOIL STUDIES

The constraints in the use of hyperspectral remote sensing data for soil studies are atmospheric attenuation of spectral measure, low signal-to-noise ratio (Lagacherie et al. 2008), spatial resolution (Gomez et al. 2015a) and non-homogeneity of field area (Ben-Dor et al. 2002). There is a performance decrease of SOC estimation obtained by remote sensing compared to performance obtained by lab/field spectroscopy. There is also a performance decrease of SOC estimation obtained by spaceborne compared to performance obtained by airborne spectroscopy owing to poor signal-to-noise ratio of satellite data (e.g., 50:1 for Hyperion, e.g., Gomez et al. 2008) than airborne data (e.g., 500:1 for HyMap, e.g., Selige et al. 2006), and the spatial resolution that is lower in satellite data (e.g., 30 m for Hyperion) than airborne data (e.g., 5 m for HyMap). The low estimation value is mainly due to the atmospheric media along the sun-surface-sensor path which cause significant attenuation of the signal recived at the sensor.

Success level of estimation, to a large extent, also depends on soil property variation, field size and non-homogeneity of field area. Due to which a pixel may straddle more than one field and so may include several types of surface roughness and soil humidity due to different types of ploughing between fields. When it comes to fields of smaller size typically found in India, challenges are manifold. Another disadvantage is the shortage of hyperspectral data and the huge volume and complexity of these data when they are available. Fast computers with large data storage capacities and skilled human

An evaluation of atmospheric correction algorithms in the estimation of SOC from Hyperion image.
Ph.D. Thesis, 2018, NITK, Surathkal, India.

6

resources are needed for analysing hyperspectral data. Effort is going on in India by the Indian Space Agency in training manpower in processing of hyperspectral data.

1.4 ATMOSPHERIC INTERFERENCE ON SPACEBORNE HYPERSPECTRAL IMAGES

The atmospheric interference on the spaceborne hyperspectral data received depends on absorption and scattering by atmospheric gases and aerosols. Magnitude of this interference depends on the nature, concentrations and particle sizes of various atmospheric constituents like aerosols, water vapour, oxygen, ozone, carbon dioxide etc. Atmospheric correction is required to remove atmospheric components of a spectral signature obtained from a spaceborne hyperspectral image. The quality of the remotely sensed hyperspectral data depends on the quality of the atmospheric correction algorithms applied, which in turn affects its end application (Borengasser et al. 2008). In the current study, the efficacy of spaceborne hyperspectral data in the retrieval of SOC with the best possible accuracy is explored.

1.5 PROBLEM IDENTIFICATION

Soil organic carbon is an important index in reflecting soil fertility. To date, only a few studies have attempted the exploitation of existing satellite's hyperspectral capabilities for SOC retrieval. It may be due to the attenuated quality of remotely sensed reflectance data mainly caused by atmospheric interference. Thus, the role of atmospheric correction algorithms needs to be investigated. If it is possible to extract pure spectra from satellite data, when it is integrated with other statistical approaches, it would open the windows of new possibilities.

An evaluation of atmospheric correction algorithms in the estimation of SOC from Hyperion image.
Ph.D. Thesis, 2018, NITK, Surathkal, India.

7

1.6 OBJECTIVES

The specific objectives of the present study are:

1. To evaluate the accuracy of estimation of SOC from ground-based VNIR/SWIR reflectance spectra using advanced statistical techniques viz. principal component regression (PCR), partial least square regression (PLSR) and artificial neural network (ANN) coupled with different spectra preprocessing methods; and to identify the appropriate statistical technique for further analysis.

2. To compare four popularly used atmospheric correction algorithms (QUAC, ATCOR, FLAASH, 6S) in deriving soil spectra from Hyperion data and estimation of SOC in agricultural fields of India and Australia.

3. To explore the use hybrid atmospheric correction algorithm that combines the concepts of radiative transfer equations and empirical line techniques and incorporates real-time *in situ* atmospheric and climatic data.

4. To compare hybrid atmospheric correction algorithm with their component algorithms in deriving soil spectra from Hyperion data and estimation of SOC.

1.7 ORGANIZATION OF THE THESIS

The rest of this thesis is organized as follows:

Chapter 2 contains a review of literature and is divided into four themes. Firstly, previous studies on estimation of soil organic carbon from spectroscopy are surveyed. Secondly, various preprocessing techniques and atmospheric correction algorithms for remotely sensed data developed during the past years are reviewed. Thirdly, the previous researches on the use of airborne and spaceborne hyperspectral remote sensing data in estimation of various soil properties are reviewed. Lastly, previous studies on comparison of atmospheric correction algorithms in various applications are reviewed.

An evaluation of atmospheric correction algorithms in the estimation of SOC from Hyperion image.
Ph.D. Thesis, 2018, NITK, Surathkal, India.

8

Areas under investigation and data used are described in **Chapter 3**. The chapter also briefs an overall methodology adopted for the study.

A study on estimation of SOC content through ground-based VNIR/SWIR reflectance spectroscopy is presented in **Chapter 4**. The results obtained from this study are discussed and used for further analysis.

A study comparing influence of four popularly used atmospheric correction algorithms in the estimation of SOC from Hyperion data is presented in **Chapter 5**. The results obtained are discussed.

Development of hybrid atmospheric correction algorithms, incorporating a modified empirical line technique is described in **Chapter 6**. A study evaluating their performance in estimating SOC content from spaceborne hyperspectral data is also presented. The spectral similarity indices and estimation accuracies of corrected reflectance spectrum is evaluated and compared with their component algorithms. The performances of hybrid algorithms were analysed in two ways. Firstly, the Hyperion reflectances obtained by hybrid algorithms and their component algorithms were analysed and compared using spectral metrics. Secondly, performance of each atmospheric correction algorithm was analysed for estimation of SOC using Hyperion reflectances obtained from atmospheric correction algorithms.

Finally, **Chapter 7** contains the summary and conclusions and provides scope for the future studies.

In order to arrive at the objective of research, literatures were focused on selected themes and review of the same presented in the following chapter.

An evaluation of atmospheric correction algorithms in the estimation of SOC from Hyperion image.
Ph.D. Thesis, 2018, NITK, Surathkal, India.

9

<div align="right">

CHAPTER 2

</div>

<div align="center">

LITERATURE REVIEW

</div>

2.1 INTRODUCTION

This chapter outlines a comprehensive review of relevant literature to bring out the background of the study undertaken and to achieve the objectives of the research. The literature review is organized under four themes namely:

I. Estimation of soil organic carbon from reflectance spectroscopy.

II. Preprocessing techniques and atmospheric correction algorithms developed during the past years for hyperspectral airborne/spaceborne data.

III. Use of airborne/spaceborne imaging spectroscopy to study soil properties.

IV. Past studies that focus on comparing atmospheric correction algorithms in various applications.

The survey of literature carried out under these themes is presented in the sections to follow.

2.2 THEME I: ESTIMATION OF SOIL ORGANIC CARBON FROM REFLECTANCE SPECTROSCOPY

Soil reflectance is a cumulative property, derived from inherent spectral behaviour of the heterogeneous combination of mineral, organic matter and soil moisture (Van der Meer, 2001). Carbon is a measurable component of soil organic matter. Since soil organic matter (SOM) is difficult to measure directly, laboratories tend to measure and report soil

An evaluation of atmospheric correction algorithms in the estimation of SOC from Hyperion image.
Ph.D. Thesis, 2018, NITK, Surathkal, India.

10

organic carbon. A conversion factor is available to report soil organic matter when required. SOC has strong influence on soil reflectance, absorbing light through the VNIR/SWIR region. It affects the shape and nature of a soil reflectance spectrum.

Henderson et al. (1992) found that for soils formed from same parent materials, reflectance in the visible region (425-695 nm) gave the best correlation with SOC content. However, those bands also respond significantly to iron and manganese oxide content. They also found that for soils formed from different parent materials, 1955–1965, 2215, 2265, 2285–2295, and 2315–2495 nm gave the best correlation with SOC content.

Ben-Dor et al. (1997) suggested that, reflectance slope between 450 and 638 nm of soil spectrum may be useful for identifying the degradation condition and the parent material status of organic matter and the reflectance slope between 680 and 800 nm may be used as a general parameter for monitoring organic matter and the region 900 to 1220 nm is good for mapping SOM.

Bartholomeus et al. (2008) studied the spectral reflectance with a large range of SOC content. They observed that besides an overall decrease in reflectance with an increase in SOC, the shape of the spectral signature also varies. They found that in the spectral range from 400 to 800 nm there is a change from convex to concave when the SOC content decreases, and a flatter spectral profile at higher SOC contents. In the spectral range from 1600 to 1800 nm overall level of reflectance varies, but hardly any variance in the pattern of the reflectance curve is noticed. In the spectral response from 2000 to 2300 nm, the reflectance pattern varies; the dip in the spectral profile flattens when the SOC content increases. Peon et al. (2017) identified significant wavelengths for SOC prediction as 2000 to 2450 nm and visible regions of electromagnetic spectrum.

An evaluation of atmospheric correction algorithms in the estimation of SOC from Hyperion image.
Ph.D. Thesis, 2018, NITK, Surathkal, India.

11

Using statistical regression methods several studies established relationships between soil reflectance and SOC. Multiple Linear Regression (MLR), Principal Components Regression (PCR), Partial Least Squares Regression (PLSR) or Artificial Neural Networks (ANN) etc. have been used as estimation models by several researchers.

Dalal and Henry (1986) studied NIR (Near Infrared) diffuse reflectance spectrophotometry, within the wavelength range 1100 to 2500 nm in the prediction of SOC content of air-dried soils. Calibration equations for SOC prediction were formed by a combination of three wavelengths, i.e. 1744, 1870 and 2052 nm, in a multiple regression analysis. McCarty et al. (2002) compared the potential of NIR and MIR (Mid Infrared) spectral regions to quantify total, organic, and inorganic C in soil samples by PLSR analysis. They found that both spectral regions contained significant information on organic and inorganic C in soils studied and MIR analysis outperformed NIR. Cozzolino and Moron (2006) studied the potential of NIR reflectance spectroscopy to predict SOC in different particle-size fractions using PLSR model. They concluded that NIR spectra gave a global signature of chemical composition and could be useful in understanding interactions of SOC in different soil fractions and different agricultural systems. Morgan et al. (2009) studied the potential of *in situ* VNIR spectra to predict soil organic and inorganic C by PLSR analysis. It was found that *in situ* spectroscopy measure organic and inorganic C with some loss of accuracy compared to dried ground samples. To improve *in situ* inorganic C predictions, they performed soil reaction with 1 N HCl. Bellon-Maurel and McBratney (2011) reviewed the studies that have been undertaken on near-infrared and mid-infrared spectroscopy applied for determining SOC content.

The advent of satellite remote sensing technology has revolutionized the world in acquiring information in a cost-effective and temporal basis. For practical application, airborne/spaceborne VNIR/SWIR data can be used to extract reflectance spectra. But, the

An evaluation of atmospheric correction algorithms in the estimation of SOC from Hyperion image.
Ph.D. Thesis, 2018, NITK, Surathkal, India.

12

potential of spaceborne hyperspectral sensors (e.g Hyperion) has not been fully explored yet, due to atmospheric and instrumental perturbations in the acquired spectral signature. While instrumental perturbations may not be corrected on the spectra, atmospheric perturbations may be reduced. The present study is focussed on evaluating different preprocessing techniques in the estimation of SOC from spaceborne hyperspectral data. Relevant literatures on the same is reviewed in the following sections.

2.3 THEME II: PREPROCESSING TECHNIQUES FOR REMOTELY SENSED DATA

Preprocessing techniques utilized may be broadly classified into two categories:

(i)   Atmospheric correction algorithms,

(ii)   Spectral smoothening methods.

2.3.1 Atmospheric correction algorithms

Atmospheric correction algorithms were developed since mid-1980s which were applied on data obtained from airborne and spaceborne multispectral and hyperspectral sensors. Over the years atmospheric correction algorithms have evolved from empirical approach to rigorous radiative transfer modeling (Gao et al. 2009). Basically, an atmospheric correction algorithm converts at-sensor radiance spectrum to corresponding ground reflectance spectrum by removing all the external atmospheric components. Atmospheric correction algorithms can be classified into three types: empirical models, radiative transfer models and hybrid models and are explained in the following sections.

2.3.1.1 Empirical models

Initial algorithms were scene-based empirical models that depend on image statistics or availability of field reflectance measurements to predict the surface reflectance. The Internal Average Reflectance (IAR) approach (Kruse 1985) calculates the relative

An evaluation of atmospheric correction algorithms in the estimation of SOC from Hyperion image.
Ph.D. Thesis, 2018, NITK, Surathkal, India.

13

reflectance spectrum for a pixel from the ratio of spectrum of the pixel to the average spectrum of a scene. This method suits for dry areas without vegetation. The Flat Field (FF) approach (Roberts et al. 1986) produces relative reflectance by dividing reflectance at each pixel by mean spectrum of a user-defined region of interest in the image. The region of interest should be spectrally flat material within the wavelength range of the sensor. The flat-field chosen should have a high albedo to avoid decreasing signal-to-noise ratio. Conel et al. 1987 introduced empirical line (EL) method that used field measurements of reflectance spectra of two contrasting targets for correction. It forces the image spectra to match reflectance spectra collected from the field. It requires at least two targets (light and dark) whose field reflectance and at-sensor radiance are known and are linearly regressed to obtain gain and offset. The gain and offset are then applied to the whole image and surface reflectance for the entire image is derived. This method can produce accurate results, but it requires *in situ* reflectance.

QUick atmospheric correction (QUAC) (Bernstein et al. 2005), is a semi-empirical algorithm for atmospheric correction and aerosol retrieval. It requires only approximate specification of sensor band locations (i.e., central wavelengths). QUAC is based on the assumption that the average reflectance of a collection of diverse material spectra, such as the end member spectra in a scene, is essentially scene independent. The gain parameter is obtained from endmember average and offset parameter is from baseline subtraction. Lowest reflectance value for each channel defines the baseline spectrum.

2.3.1.2 Radiative Transfer Models

The dependence of empirical approaches on image statistics or availability of field reflectance measurements in retrieving surface reflectance led to theoretical modelling techniques, which simulate absorption and scattering effects of atmospheric components using radiative transfer (RT) equations.

An evaluation of atmospheric correction algorithms in the estimation of SOC from Hyperion image.
Ph.D. Thesis, 2018, NITK, Surathkal, India.

14

Research on atmospheric modelling led to the development of the 5S atmospheric radiation model in 1990s. Since then numerous RT models have been developed. MODTRAN code developed by Spectral Science, Inc. and Air Force Research Laboratory is the most popular among them. Other generally used RT codes are LOWTRAN (Kneizys et al. 1988), MODTRAN (Berk et al. 1989), 5S (Tanre et al. 1990) and 6S (Vermote et al. 1997 a).

RT codes can be used for the calculation of standard reference tables for varying atmospheric and geometrical conditions. Discrete values of atmospheric parameters from reference tables are often interpolated to obtain intermediate values when needed. RT codes assume a flat and Lambertian landscape and use different kinds of methods for the simulation of the radiative transfer in the atmosphere, such as Eddington approximation (Shettle and Weinman 1970), the discrete ordinates method (Liou 1973), Monte Carlo method (Collins et al. 1972), the spherical harmonics method (Benassi et al. 1984) etc.

There are a range of software programs available to model the atmosphere including ATREM (ATmospheric REMoval algorithm), ATCOR (ATmospheric CORrection), FLAASH (Fast Line-of-sight Atmospheric Analysis of Spectral Hypercubes), ISDAS (Imaging Spectrometer Data Analysis System), HATCH (High-accuracy ATmosphere Correction for Hyperspectral data) and ACORN (Atmospheric CORrection Now).

ATREM (Gao et al. 1993), uses channel band ratio technique (Gao and Goez 1990) to estimate water column; narrowband spectral model (Malkmus 1967), based on HITRAN 92 (Rothman et al. 1992) database to derive transmittance spectra of atmospheric gases and the 5S code to model scattering effects due to atmospheric molecules and aerosols. In the later upgrades line-by-line atmospheric transmittance model (Gao and Davis 1997) and the HITRAN2000 line database (Rothman et al. 2003, 2005) were used, and 5S code was replaced with 6S code for modeling atmospheric scattering effects.

An evaluation of atmospheric correction algorithms in the estimation of SOC from Hyperion image.
Ph.D. Thesis, 2018, NITK, Surathkal, India.

15

ATCOR (Richter 1996), uses lookup tables based on MODTRAN4/5. Several versions of ATCOR codes (Richter 1998; Richter and Schlaepfer 2002) were developed. ATCOR 2 is used for flat terrain while ATCOR 3 handles rugged terrain by integrating a DEM. ATCOR4 performs the combined atmospheric and topographic correction for airborne scanner data, whereas ATCOR 2 and 3 perform correction of satellite remote sensing systems.

ISDAS (Staenz et al. 1998) is an atmospheric correction software package developed at Canada Center for Remote Sensing. The ISDAS tools are coded in C.

FLAASH (Adler-Golden et al. 1999), is MODTRAN4 based atmospheric correction software package. Atmospheric multiple scattering is computed using scaled DISORT (DIScrete Ordinate Radiative Transfer) algorithm and the correlated-k algorithm (Lacis and Oinas 1991) is used to model absorption for regions presenting considerable absorption effects.

HATCH (Qu et al. 2001; Qu et al. 2003) uses correlated-k algorithm for gaseous absorption calculation. It is based on HITRAN 96 database, and provides an explicit way to account for the interaction between multiple scattering and absorption. It uses smoothness test to retrieve water vapour amount and absorbing gases, such as carbon dioxide and methane. HATCH also allows different aerosol types to be mixed externally.

ACORN developed by Analytical Imaging and Geophysics, LLC (ACORN 2002), works on MOTRAN-4 code. It uses spectral fitting to estimate water vapour and suppress effects of liquid water on the surface.

The SIERRA code (Spectral reflectance Image Extraction from Radiance with Relief and Atmospheric correction) (Lenot et al. 2009) extracts ground reflectance and water vapour

An evaluation of atmospheric correction algorithms in the estimation of SOC from Hyperion image.
Ph.D. Thesis, 2018, NITK, Surathkal, India.

16

content over mountainous areas from hyperspectral imagery. A correction of the bi-directional effects is considered for large incidence or emergence angles.

Even though radiative transfer models were theoretically well portrayed, the surface reflectance values produced still show residual atmospheric absorptions and scattering effects. These residual errors may affect their end application.

2.3.1.3 Hybrid Models

Hybrid models include combinations of radiative modeling and empirical approaches for the derivation of surface reflectance from hyperspectral imaging data. Clark et al. (1995) first suggested the use of combination of ATREM radiative transfer correction method followed by ground calibration using EL method that produced better results than radiative or empirical models alone. It provides sound correction, while removing artifacts from errors in the radiative models and solar spectrum. Ben-Dor et al. (2004) showed that combined HATCH and EL produce good results when tested using synthetic imaging spectroscopy data. Tuominen and Lipping (2011) showed that combined ATCOR4 and EL method produces better results compared to model-based ATCOR alone. The disadvantage is that EL method requires *in-situ* field measurements. Even though hybrid models give promising results, seldom studies concentrate on development of hybrid methods in processing of spaceborne hyperspectral data.

A review of atmospheric correction algorithms for hyperspectral imageries is published in Minu and Shetty 2015.

2.3.2 Spectral smoothening methods

Noise is unwanted signal generated by the instrument used to make measurement. By spectral smoothing, one tries to reduce the random noise in the instrumental signal.

An evaluation of atmospheric correction algorithms in the estimation of SOC from Hyperion image.
Ph.D. Thesis, 2018, NITK, Surathkal, India.

17

Smoothing reduces the effect of noise by smoothing out local variations in the data. The data values are modified such that values which are higher than the immediately adjacent values are reduced, and values which are lower than adjacent values are increased. However, smoothing can also remove real variations in the data (i.e., variations not caused by noise) and can add uncertainties to the data as actual values get replaced by local averages.

Moving average and Savitzky Golay method are the most commonly used smoothing techniques. Derivatives eliminate the effect of baseline drift and gentle background interference. The first derivative removes only the baseline; the second derivative removes both baseline and linear trend. The first and second derivatives of the spectrum can be computed by the finite difference method.

The Savitzky Golay (SG) smooth is based on the least-squares fitting of polynomials to segments of the data. It retains the shape of the original signal. It is capable of differentiation as well as smoothing. It has two degrees of freedom: the polynomial order and the window length.

Rinnan et al. 2009 reviewed the most common pre-processing techniques for near-infrared spectra in chemometry. Hively et al. 2011 compared 15 spectral math preprocessing treatments showed that a simple first derivative worked well for all cases. Miglani et al. 2011, Buddenbaum and Steffens 2012 and Peng et al. 2014 also systematically compared the effect of pre-treatment methods on chemometric spectroscopy. However, there are no guidelines on choosing of spectral smoothening techniques for the problem at hand.

An evaluation of atmospheric correction algorithms in the estimation of SOC from Hyperion image.
Ph.D. Thesis, 2018, NITK, Surathkal, India.

18

2.4 THEME III: USE OF AIRBORNE/SPACEBORNE IMAGING SPECTROSCOPY TO STUDY SOIL PROPERTIES

With the pre-processed spectral data from airborne/spaceborne imaging spectroscopy, estimation models (e.g MLR, PCR, PLSR ANN etc.) can be established. Spectral reflectance in the visible, NIR and SWIR regions has been widely used in many studies for the assessment of soil fertility. Some of the soil properties studied were soil organic carbon (SOC), soil inorganic carbon (SIC), total nitrogen (TN), pH, moisture content (MC), electrical conductivity (EC), Phosphorous (P), Potassium (K), Calcium (Ca), Magnesium (Mg), Sodium (Na), Manganese (Mn), Zinc (Zn) and Iron (Fe) with various levels of prediction accuracy.

MLR correlates response variable (i.e., soil property) with two or more independent variables (i.e., spectral wavelength) using linear equations. In PCR principal component analysis of spectra is followed by regression against soil properties. While, in PLSR a rotated PCA is applied to both spectra and soil properties and obtains the best relationship between them. Recently, new statistical tools such as artificial neural networks (ANN), boosted regression trees (BRT) etc. are adopted for the same.

A number of studies use airborne hyperspectral imagery for prediction of soil properties. Even though spaceborne hyperspectral imageries have become available since 2000, only few attempts have been made to use them for mapping soil properties. This may be due to their low signal to noise ratio. A review of the works carried out by airborne and spaceborne hyperspectral imageries to predict soil properties is published in Minu et al. 2016.

An evaluation of atmospheric correction algorithms in the estimation of SOC from Hyperion image.
Ph.D. Thesis, 2018, NITK, Surathkal, India.

19

Several surface soil properties were modeled from airborne hyperspectral imagery. Table 2.1 summarizes some of the earlier works in the field. Soil properties predicted, airborne hyperspectral sensor used, its spectral range and spatial resolution, nature of study area and its location, preprocessing method adopted during the prediction method, prediction model used, accuracy of prediction in terms of R^2 values of different studies are tabulated. These studies point out the great potential of airborne hyperspectral data to map surface soil properties. However, it is noted that a research on the influence of preprocessing techniques were not carried out. Standard modules available as part of commercial software were used for atmospheric corrections in these studies. It is also noted that earlier studies are concentrated only in developed countries. In Indian context, studies using airborne data are limited. It may be due to (i) cost involved in the study, (ii) less importance given to advancement in agriculture in a developing country like India, and (iii) smaller and scattered agricultural fields.

An evaluation of atmospheric correction algorithms in the estimation of SOC from Hyperion image.
Ph.D. Thesis, 2018, NITK, Surathkal, India.

20

Table 2.1 Summary of Soil properties Prediction, using airborne hyperspectral imagery

Soil Property	Platform/ spectral range/ spatial resolution	Field nature	Country	Preprocessing method	Prediction technique	R^2	Author
Fe	AVIRIS (400-2500 nm) (20 m)	Pasture and seasonal crops	Brazil	MODTRAN-based (Green, et al. 1993)	Regression equations	0.83	Galvao et al. 2001
TiO$_2$						0.74	
Al$_2$O$_3$						0.68	
OM	DAIS-7915 (400-2500 nm) (5 m)	Agriculture fields	Israel	Minimum Noise Fraction (MNF) (Green et al. 1988) for noise reduction; EL technique	Visible and NIR analysis	0.827	Ben-Dor et al. 2002
MC						0.647	
EC						0.665	
EC	RDACS/H3 (471 - 828 nm) (1 m)	Bare soil of corn-soybean rotation field	Missouri	Calibrated with chemically treated reference traps with known reflectance	SMLR	0.66	Hong et al. 2002
pH						0.68	
Mg						0.67	
K						0.59	
OM						0.55	
OM	CASI (408.73 - 947.07 nm) (2m)	Corn field with clay-loam soil	Canada	CAM5S model (O'Neill et al. 1997)	SMLR	0.49	Uno et al. 2005
					ANN	0.592	

An evaluation of atmospheric correction algorithms in the estimation of SOC from Hyperion image.
Ph.D. Thesis, 2018, NITK, Surathkal, India.

21

Table 2.1 *(Continued)*

Soil Property	Platform/ spectral range/ spatial resolution	Field nature	Country	Preprocessing method	Prediction technique	R^2	Author
Iron oxide	CASI-A (400-1000 nm) (3m)	Sand dunes	Israel	EL technique	Spectral indices based model	0.59	Ben-Dor et al. 2006
gravel coverage %	DAIS-7915 (400-2500 nm) (5 m)	Alluvial fan	Negev desert, Israel	MNF technique for noise reduction and EL technique	Ferric absorption feature depth(AFD) model	0.83	Crouvi et al. 2006
					Al-OH AFD model	0.67	
					Carbonate AFD model	0.57	
SOC	HyMap (450-2500 nm) (3.5 m)	Agriculture fields	Germany	ATCOR	MLR	0.9	Selige et al. 2006
TN						0.92	
Sand						0.95	
Clay						0.71	
SOC					PLSR	0.86	
TN						0.87	
Sand						0.87	
Clay						0.65	

An evaluation of atmospheric correction algorithms in the estimation of SOC from Hyperion image.
Ph.D. Thesis, 2018, NITK, Surathkal, India.

22

Table 2.1 *(Continued)*

Soil Property	Platform/ spectral range/ spatial resolution	Field nature	Country	Preprocessing method	Prediction technique	R^2	Author
EC	HyMap (420 - 2480 nm) (6 m)	Wetland	Western Australia	Corrected for atmospheric effects and MSC techniques	PLSR	0.86	Farifteh et al. 2007
					ANN	0.86	
EC	AVNIR (429 to 1010 nm) (1.2 m)	Cotton field	California	Atmospheric calibrated with black and grey reference panels	MLR	0.6696	De-Tar et al. 2008
Ca						0.6188	
Mg						0.582	
Na						0.6224	
Cl						0.7376	
Clay	HyMap (400 to 2500 nm) (5m)	Area is mainly devoted to vineyards	France	ATCOR4, Savitzky–Golay filter	PLSR	0.64	Gomez et al. 2008b
$CaCO_3$						0.77	
Clay					Continuum removal	0.58	
$CaCO_3$						0.47	
MC	HyMap (440 to 2470nm) (4 m)	Sandy substrata and low vegetation cover area	Germany	MODTRAN4 based ACUM algorithm	Normalized Soil Moisture Index model	0.819	Haubrock et al. 2008

An evaluation of atmospheric correction algorithms in the estimation of SOC from Hyperion image. Ph.D. Thesis, 2018, NITK, Surathkal, India.

23

Table 2.1 *(Continued)*

Soil Property	Platform/ spectral range/ spatial resolution	Field nature	Country	Preprocessing method	Prediction technique	R^2	Author
Clay	HyMap (400 to 2500 nm) (5m)	Vineyards	France	ATCOR4	Continuum removal analysis	0.58	Lagacherie et al. 2008
CaCO₃						0.47	
SOC	AHS-160 (430–2540 nm) (2.6 m)	Agriculture Fields	Belgium	ATCOR4	PLSR	RPD= 1.47	Stevens et al. 2008
Clay	HyMap (400 to 2500 nm) (5m)	Vineyards	France	ATCOR4	PLSR	0.64	Lagacherie et al. 2010
CaCO₃						0.77	
SOC	AHS-160 (430–2540 nm) (2.6 m)	Cropland	Luxembourg	MODTRAN4 based algorithm	PLSR	0.71	Stevens et al. 2010
					PSR	0.75	
					Support vector machine	0.69	
C	HyperSpecTIR (400–2450 nm) (2.5m)	Tilled agricultural fields	MD, USA	Image processing by ENVI 4.7; & different signal smoothening methods	PLSR	0.65	Hively et al. 2011
Al						0.76	
Fe						0.75	
Silt						0.79	

An evaluation of atmospheric correction algorithms in the estimation of SOC from Hyperion image.
Ph.D. Thesis, 2018, NITK, Surathkal, India.

24

Table 2.1 *(Continued)*

Soil Property	Platform/ spectral range/ spatial resolution	Field nature	Country	Preprocessing method	Prediction technique	R^2	Author
Clay	MIVIS (430–1270 nm) (4.8m)	Maize field, but the crop had not emerged	Central Italy	MODTRAN4 based model	PLSR	0.78	Casa et al. 2013
Silt						0.56	
Sand						0.81	
SOC	CASI 1500 (380 - 1050 nm) (0.2 m)	Compost added soil	Italy	EL Calibration	Correlation analysis	0.85	Matarrese et al. 2014
Iron oxide	HyMap (400-2450 nm) (4.5 m)	Agricultural area	Spain	Fifth order Savitzky–Golay smoothing	PLSR	0.66	Steinberg et al. 2016
Clay						0.64	
SOC	AHS-160 (450 – 2500 nm) (2.6 m)	Agricultural area	Luxembourg			0.74	

An evaluation of atmospheric correction algorithms in the estimation of SOC from Hyperion image.
Ph.D. Thesis, 2018, NITK, Surathkal, India.

25

Concept of hyperspectral remote sensing emerged in recent years. Very few investigations were carried out using spaceborne hyperspectral data for prediction of soil properties. NASA's EO1 Hyperion data is employed in most of the studies. Table 2.2 presents a summary of previous studies on prediction of soil properties across the globe using spaceborne hyperspectral data. Soil properties predicted, spaceborne hyperspectral sensor used, its spectral range and spatial resolution, nature of the study area and its location, preprocessing method adopted during the prediction method, prediction model used, accuracy of prediction in terms of R^2 values of different studies are tabulated.

It is noted that studies on utilization of spaceborne data in the determination of soil properties are less explored globally, especially in the Indian context. It is expected that the technological advancements in this field will attract more studies and will increase the usage of these data. Das et al. 2015 reviewed the preparedness and opportunities for using remotely sensed hyperspectral data for soil assessment in India.

An evaluation of atmospheric correction algorithms in the estimation of SOC from Hyperion image.
Ph.D. Thesis, 2018, NITK, Surathkal, India.

26

Table 2.2 Summary of soil properties prediction, using spaceborne hyperspectral imagery

Soil Property	Platform/ spectral range/ spatial resolution	Field nature	Country	Preprocessing method	Prediction technique	R^2	Author
SOC	EO1 Hyperion (400–2500 nm) (30m)	Cotton crops and pasture.	Australia	ATREM	PLSR	0.5	Gomez et al. 2008
OM	EO1 Hyperion (400–2500 nm) (30m)	Agriculture field.	Central Indiana, USA	FLAASH	PLSR	0.74	Zheng 2008
TN						0.72	
TP						0.67	
TN	EO1 Hyperion (400–2500 nm) (30m)	Arid regions.	Shanxi, China	EL atmospheric correction	Linear regression model	0.84	Wu et al. 2009
MC	EO1 Hyperion (400–2500 nm) (30m)	Bare field	Central Indiana, USA	ACORN	PLSR	0.79	Zhang et al. 2009
OM						0.89	
TN						0.70	
TP						0.69	
TC						0.86	
Clay						0.49	
OM	EO1 Hyperion (400–2500 nm) (30m)	Agriculture -pasture mixed area.	Hengshan County, China	Internal average relative reflectance	Land degradation spectral response units model	0.722	Wang et al. 2010

An evaluation of atmospheric correction algorithms in the estimation of SOC from Hyperion image. Ph.D. Thesis, 2018, NITK, Surathkal, India.

27

Table 2.2 *(Continued)*

Soil Property	Platform/ spectral range/ spatial resolution	Field nature	Country	Preprocessing method	Prediction technique	R^2	Author
Clay	CHRIS-PROBA (415–1050 nm) (17 m)	Maize field, but the crop had not emerged	Central Italy	FLAASH	PLSR	0.6	Casa et al. 2013
Silt						0.3	
Sand						0.62	
OM	EO1 Hyperion (400–2500 nm) (30m)	Wheat and potato fields	China	FLAASH	PLSR	0.63	Lu et al. 2013
pH						0.68	
P						0.62	
N	EO1 Hyperion (400–2500 nm) (30m)	Scattered paddy fields	Karnataka India	FLAASH, Moving average	PLSR	0.63	Gopal et al. 2014
				Savitzky–Golay		0.63	
POM	EO1 Hyperion (400–2500 nm) (30m)	Coastal soils densely covered with vegetation	Florida, USA	FLAASH, MNF filter	PLSR	0.67	Anne et al. 2014
MAOM						0.74	
labile C						0.93	
labile N						0.96	

An evaluation of atmospheric correction algorithms in the estimation of SOC from Hyperion image.
Ph.D. Thesis, 2018, NITK, Surathkal, India.

28

2.5 THEME IV: COMPARISON OF ATMOSPHERIC CORRECTION ALGORITHMS IN VARIOUS APPLICATIONS

Previous studies assessed different atmospheric correction algorithms in various contexts like mineral mapping (e.g. San and Suzen 2010), forest biomass estimation (e.g. López et al. 2016), vegetation mapping (Marcello et al. 2016), canopy growth monitoring (Kim et al. 2016) etc. Performance of algorithms will differ depending on the final biophysical character under study.

San and Suzen (2010) compared the impact of three atmospheric correction models (ATCOR, ACORN, and FLAASH) for mineral mapping using Hyperion data and found that ACORN performed the best. It was because ACORN could detect more number of absorption features in mineral spectra. ACORN was recommended as a better atmospheric correction algorithm for lithological and mineralogical mapping of natural earth materials from Hyperion data.

Though atmospheric correction algorithms are inevitable for spaceborne hyperspectral data, few research papers compared atmospheric correction algorithms on multispectral data. López-Serrano et al. (2016) and Marcello et al. (2016) found that 6S works well in case of vegetation mapping using multispectral satellite images. López-Serrano et al. (2016) evaluated four atmospheric correction algorithms: ATCOR2, COST (Cosine of the Sun Zenith Angle), FLAASH and 6S, in estimating aboveground forest biomass using multivariate adaptive regression splines (MARS) analysis in temperate forests in the northeast of the state of Durango, Mexico. They used Landsat 5 TM imagery and best results were obtained after application of 6S algorithm. Marcello et al. (2016) assessed the performance of five atmospheric correction algorithms: DOS (Dark Object Subtraction), QUAC, FLAASH, ATCOR and 6S, using high resolution Worldview-2 imagery in the vegetation estimation. Superior performance of 6S algorithm was

An evaluation of atmospheric correction algorithms in the estimation of SOC from Hyperion image.
Ph.D. Thesis, 2018, NITK, Surathkal, India.

29

identified, achieving reflectance estimations very close to *in situ* measurements. Kim et al. (2016) evaluated performance of three atmospheric correction methods: QUAC, FLAASH and ATCOR to distinguish the canopy growth of paddy rice using RapidEye image data. The results of the atmospheric correction using ATCOR on the satellite images were found to be favourable among the tested ones.

However, previous studies did not clearly say among the different algorithms available which one to use. In fact, it is understood that the choice of atmospheric correction algorithm depends on the biophysical characteristics under study and also the spectral resolution of the satellite data. When the interest is to retrieve SOC data, limited guidelines are available.

2.6 CONCLUSIONS

Following inferences were gathered from the literature review:

- All the atmospheric correction algorithms discussed were built on their own assumptions and thus have limitations. An idealized universal atmospheric correction system has not been developed yet. The method used for atmospheric correction should be a function problem type, remote sensing data type, amount of available *in situ* atmospheric information and the accuracy of biophysical information extracted from the remote sensing data.

- Empirical models are not always reliable, especially for hyperspectral data since they depend on image statistics only. These methods are used for quick correction of images for preliminary analysis. The EL method which involves field calibration produces more accurate results. Radiative transfer models produce precise results under optimal conditions. Hybrid methods despite the promising research results are not often used in the processing of hyperspectral data. Hybrid

An evaluation of atmospheric correction algorithms in the estimation of SOC from Hyperion image.
Ph.D. Thesis, 2018, NITK, Surathkal, India.

30

methods can be tried with physical models and other scene dependent properties of the area. New approaches like atmospheric correction of hyperspectral imageries using neural networks (Achard and Lesage 2010), open possibilities for the improvement of the topic.

- Only a few studies systematically compared the effect of preprocessing methods on chemometric spectroscopy. The best spectral preprocessing/smoothening method will be the one that finally produces a robust model with the best predictive ability. Unfortunately, there seem to be no hard rules to decide which spectral preprocessing method to use and often the only approach is trial and error. The development of a methodology that would allow a systematic approach would be beneficial.

- Studies conducted using airborne hyperspectral images in the prediction of soil properties had a moderate accuracy. However, research on the influence of preprocessing techniques are not carried out. Also, earlier studies are concentrated only in developed countries. In Indian context, studies using airborne data are limited. It may be due to (i) cost involved in the study, (ii) less importance given to advancement in agriculture, and (iii) smaller field size.

- Despite the vast coverage of spaceborne hyperspectral images, a few studies concentrate on top soil properties investigation. It is expected that the technological advancements in this field will attract more studies and will increase the usage of these data. An encouraging trend in this direction is the NASA-ISRO joint venture of AVIRIS-NG.

- The limitation of spaceborne hyperspectral data is mainly due to its low signal to noise ratio and loss of information from atmospheric components. The importance of apt preprocessing/atmospheric correction technique is understood at this

An evaluation of atmospheric correction algorithms in the estimation of SOC from Hyperion image.
Ph.D. Thesis, 2018, NITK, Surathkal, India.

31

juncture. If it is possible to extract uncontaminated information from satellite data, it would open the windows of new possibilities.

- It is perceived that there is a performance decrease of SOC prediction obtained by remote sensing compared to performance obtained by lab/field spectroscopy (Stevens et al. 2008, Lu et al. 2013). There is also a performance decrease of SOC prediction obtained by satellite sensors (R^2 between 0.5 and 0.63, from e.g., Gomez et al. 2008; Lu et al. 2013) compared to airborne spectroscopy (R^2 between 0.74 and 0.85, for e.g. Uno et al. 2005; Stevens et al. 2010). The low prediction value is due to the attenuated quality of remotely sensed reflectance data. Thus, the role of atmospheric correction algorithms needs to be investigated.

- Previous studies assessed different atmospheric correction algorithms in various contexts like mineral mapping (e.g. San and Suzen 2010), forest biomass estimation (e.g. López et al. 2016), vegetation mapping (Marcello et al. 2016), canopy growth monitoring (Kim et al. 2016) etc. Performance of algorithms will differ depending on the final biophysical character under study. When the interest is to retrieve SOC data, limited guidelines are available.

Conclusions drawn from the literature survey guides the objectives of this research. Formulated objectives address few issues of importance specifically to estimate SOC from spaceborne data and are presented in Chapter 1.

Description of areas under investigation and data used for the present study are outlined in next chapter.

An evaluation of atmospheric correction algorithms in the estimation of SOC from Hyperion image.
Ph.D. Thesis, 2018, NITK, Surathkal, India.

32

<div align="right">

CHAPTER 3

</div>

<div align="center">

STUDY AREA AND MATERIALS

</div>

3.1 INTRODUCTION

This chapter includes the description of:

- Geographical location and characteristics of the study areas,

- Data products and software used in the study,

- Overall methodology adopted for the study.

3.2 STUDY AREAS

This work utilised data from cultivated sites of India and Australia. Table 3.1 summarizes the details of study area.

The Southern Karnataka sites covering a part of Dakshina Kannada and Udupi Districts in India, between latitude 13°00'N and 13°08'N and longitude 74°45'E and 74°52'E (Figure 3.1) and encompasses an area of 53 km². It is characterised by paddy fields scattered and small in size. Study area predominantly consists of loamy, sandy and gravelly clay soils. The paddy fields considered are homogeneous in terms of ploughing and phytosanitary treatments. The average sizes of the fields are approximately 30 m x 30 m. The area follows tropical climate and consists of plane region with an average elevation of 20 m above mean sea level.

An evaluation of atmospheric correction algorithms in the estimation of SOC from Hyperion image.
Ph.D. Thesis, 2018, NITK, Surathkal, India.

33

Table 3.1: Details of study area

Study area	Location	Latitude & Longitude	Field type	Soil type	No of samples	Data source
India	Southern Karnataka	74°45'E to 74°52'E & 13°00'N to 13°08'N	Paddy fields	Clay soils	111	Gopal, 2014
Australia	Narrabri, NSW	Narrabri Site#1: 149°35'E to 149°40'E & −30°07'S to −30°13'S	Cotton fields	Vertisols	46	Gomez et al., 2008
		Narrabri Site#2: 149°40'E to 149°46'E & −30°15'S to −30°19'S	Pastures		52	

The Narrabri sites is located in north western New South Wales (NSW), Australia. The study area consists of two sub sites: cotton fields of Namoi (referred as Narrabri Site#1 hereadter) (149°37'E, −30°10'S), that extends in 70 km² area and Pastures in town of Narrabri (referred as Narrabri Site#2 hereafter) (149°43'E, −30°17'S), that extends in 69 km² area. The Australian fields are continuous and large in size (approximately 500m x 900 m) (Figure 3.2). This region is dominated by Vertisols. The area follows subtropical climate and consist of plane region with an average elevation of 210 m above mean sea level.

An evaluation of atmospheric correction algorithms in the estimation of SOC from Hyperion image.
Ph.D. Thesis, 2018, NITK, Surathkal, India.

34
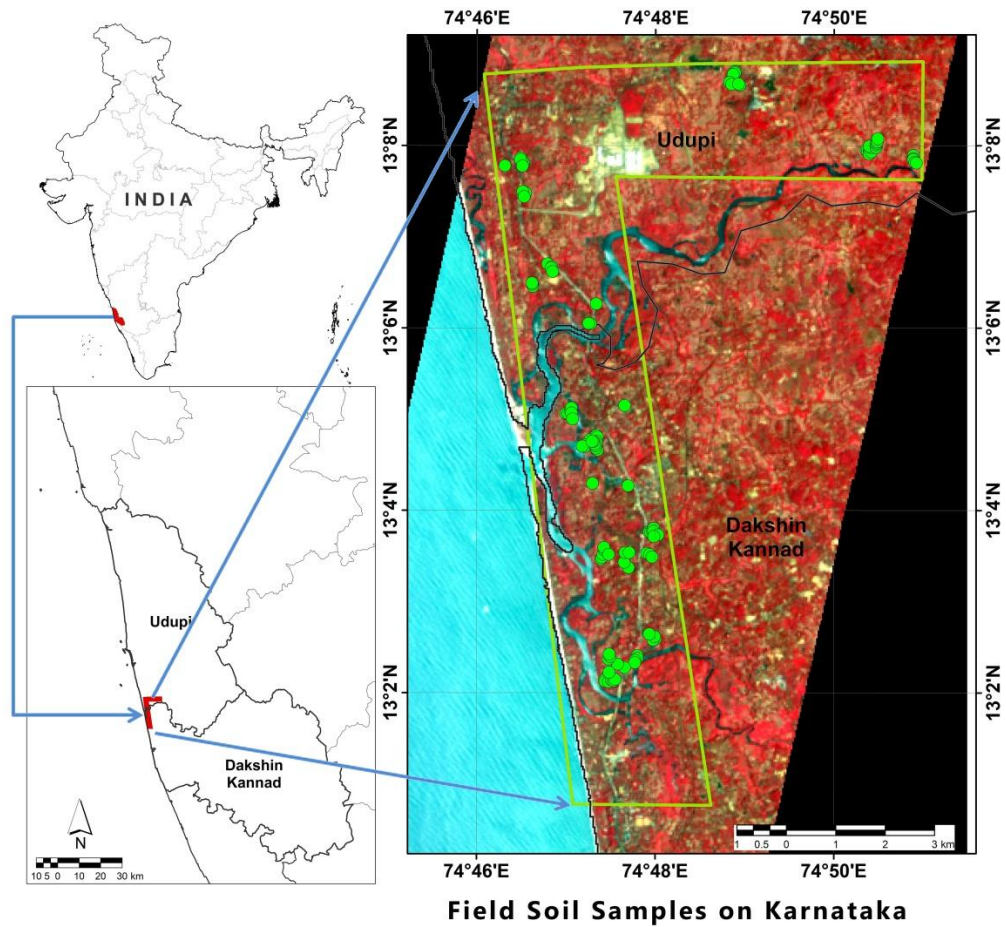
Figure 3.1: Location of the sample sites on false colour composite (spectral bands used: 864 nm, 650 nm, 549 nm) of Hyperion images over Karnataka sites. Green circles represent GPS locations of collected soil samples.

An evaluation of atmospheric correction algorithms in the estimation of SOC from Hyperion image. Ph.D. Thesis, 2018, NITK, Surathkal, India.

35
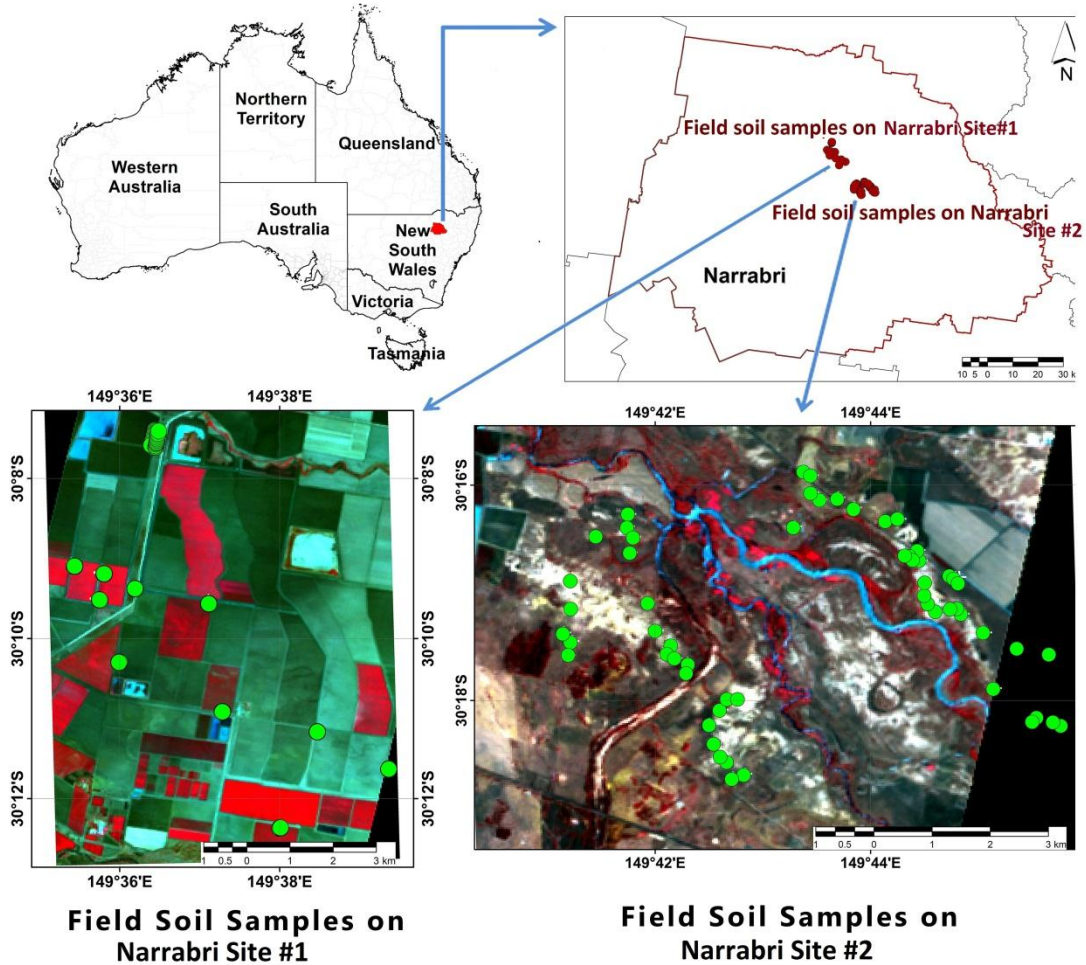
Figure 3.2: Location of the sample sites on false colour composite (spectral bands used: 864 nm, 650 nm, 549 nm) of Hyperion images over Narrabri sites. Green circles represent GPS locations of collected soil samples.

3.3 EO-1 HYPERION REMOTE SENSING DATA

Earth Observing 1 (EO-1) spacecraft was launched from Vandenberg Air Force Base on November 21, 2000 as part of NASA's New Millennium Program. After 17 years in orbit, its operations ended in March 2017. The EO-1 has a sun-synchronous orbit with an

An evaluation of atmospheric correction algorithms in the estimation of SOC from Hyperion image.
Ph.D. Thesis, 2018, NITK, Surathkal, India.

36

altitude of 705 km. The orbit inclination is 98.2 degree and the orbital period is 98.9 minutes. The velocity of the EO-1 nadir point is 6.74 km/sec with 16 days repeat cycle (Folkman et al. 2001).

Hyperion is a hyperspectral instrument on EO-1. It is a push-broom, imaging spectrometer. It provides radiometrically calibrated spectral data from 400 to 2500 nm, with 242 spectral bands with approximately 10 nm spectral resolution and 30 m spatial resolution. Each image contains data for a 7.65 km wide (cross-track) by 185 km long (along-track) region. Hyperion has a single telescope and two spectrometers, one visible near-infrared spectrometer and one short-wave infrared spectrometer. A detailed description of Hyperion characteristics, operations and applications can be found in Folkman et al. (2001).

In this study one Hyperion image was acquired on 4th March 2012 at 05:15 UT over Karnataka study area (Figure 3.1). And two Hyperion images were acquired over Narrabri study area: the first one was acquired on 13th December 2006 at 23:51 UT over pasture soils of Narrabri Site#2 and the second one was acquired on 17th January 2007 at 23:47 UT over cropping soils and travelling stock routes of Narrabri Site#1 (Figure 3.2). Terrain-corrected and georeferenced Hyperion images in L1T format were downloaded from EarthExplorer website of the United States Geological Survey, which is a scientific agency of the United States government (http://earthexplorer.usgs.gov/). All Hyperion images were cloud-free over study sites.

The metadata of Hyperion imageries over Karnataka, Narrabri Site#1 and Narrabri Site#2 study sites are given in Tables 3.2, 3.3 and 3.4 respectively.

An evaluation of atmospheric correction algorithms in the estimation of SOC from Hyperion image. Ph.D. Thesis, 2018, NITK, Surathkal, India.

37

Table 3.1 Metadata of Hyperion image over Karnataka image

Data Set Attribute	Attribute Value
Entity ID	EO1H1460512012064110KZ_PF2_01
Acquisition Date	04 March 2012
Cloud Cover	0 to 9% Cloud Cover
Target Path	146
Target Row	51
Station	PF2
Processing Level	L1T Product
Scene Start Time	2012:064:05:15:18.642
Scene Stop Time	2012:064:05:15:33.642
Sun Azimuth	121.828749
Sun Elevation	55.066599
Satellite Inclination	98.14
Look Angle	23.758
Center Latitude	12°35'46.85"N
Center Longitude	74°43'39.75"E

An evaluation of atmospheric correction algorithms in the estimation of SOC from Hyperion image.
Ph.D. Thesis, 2018, NITK, Surathkal, India.

38

Table 3.2 Metadata of Hyperion image over Narrabri Site#1 image

Data Set Attribute	Attribute Value
Entity ID	EO1H0910802007017110KT_AGS_01
Acquisition Date	17 January 2007
Cloud Cover	0 to 9% Cloud Cover
Target Path	91
Target Row	80
Station	AGS
Processing Level	L1T Product
Scene Start Time	2007:017:23:49:23.360
Scene Stop Time	2007:017:23:49:55.360
Sun Azimuth	81.85906
Sun Elevation	56.640028
Satellite Inclination	98.19
Look Angle	9.7812
Center Latitude	31°08'36.80"S
Center Longitude	149°25'29.92"E

An evaluation of atmospheric correction algorithms in the estimation of SOC from Hyperion image.
Ph.D. Thesis, 2018, NITK, Surathkal, India.

39

Table 3.3 Metadata of Hyperion image over Narrabri Site#2 image

Data Set Attribute	Attribute Value
Entity ID	EO1H0910802006347110KV_WPS_01
Acquisition Date	13 December 2006
Cloud Cover	0 to 9% Cloud Cover
Target Path	91
Target Row	80
Station	WPS
Processing Level	L1T Product
Scene Start Time	2006:347:23:53:10.298
Scene Stop Time	2006:347:23:53:41.298
Sun Azimuth	82.791116
Sun Elevation	61.875154
Satellite Inclination	98.18
Look Angle	17.179
Center Latitude	31°12'07.74"S
Center Longitude	149°32'37.71"E

An evaluation of atmospheric correction algorithms in the estimation of SOC from Hyperion image.
Ph.D. Thesis, 2018, NITK, Surathkal, India.

40

3.4 SOIL SAMPLES

3.4.1 Soil samples collection over Karnataka sites

A total of 111 soil samples were selected from Karnataka sites. Soil samples were collected by researchers from 'National Institute of Technology, Karnataka' during the first week of March 2012 (Gopal, 2014; Gopal et al., 2015). These soil samples were located over the Hyperion scene. Soil samples were collected in the same week as that of Hyperion data acquisition. Samples were collected over harvested paddy fields devoid of vegetation in and around the radius 90-100 m to ensure pure soil spectra. Since paddy fields were very random and dispersed as a small patch of land, adopting grid sampling technique was difficult. Random sampling method was adopted based on the availability of fields. Soil samples were collected from 0-20 cm depth. As the soil samples were collected over cultivated fields, this depth corresponds to the ploughed soil horizon and the Hyperion measurement may be considered as representative of this sampled depth. A mixture of soils taken at 5 spots of radius 10 m at a location represented one sample. Soil sampling sites were located using a GPS with 2 m accuracy. SOC content of the Indian soil samples was measured by Dichromate oxidation (Walkley-Black) technique (IS 2720-Part22 1972). Over Karnataka sites, the soil samples collection and Hyperion data acquisition were realised in the same time; so, SOC content may be considered as stable between both data collections (samples and image).

3.4.2 Soil samples collection over Narrabri sites

A total of 98 soil samples were selected from Australia, Narrabri sites. Soil samples were collected by researchers from 'The University of Sydney, Australia' (Gomez et al. 2008) over the study sites. It includes 46 samples over cropping soils and travelling stock routes of Narrabri Site#1 collected in October 2006 (realized in the same semester as of Hyperion data) and 52 samples collected over pastures of Narrabri Site#2 in December

An evaluation of atmospheric correction algorithms in the estimation of SOC from Hyperion image.
Ph.D. Thesis, 2018, NITK, Surathkal, India.

41

2006 (realized in the same month as of Hyperion data). Soil samples were collected over bare soil fields. SOC content may be considered as stable between sampling and image acquisition, as in the field the organic matter was neither added nor consumed because of the absence of vegetation during this period in the sampling locations. Changes of the climate, particularly the temperature and rainfall, affect SOC by accelerating SOC decomposition. However a short duration of 3 months from October 2006 to January 2007 in Narrabri Site#1 was safely assumed that SOC was fairly stable between the measurements. Soil samples were collected from 0 to10 cm depth. As the soil samples were collected over cultivated fields, this depth corresponds to the ploughed soil horizon and the Hyperion measurement may be considered as representative of this sampled depth (same as over Karnataka context). And soil samples are the average of sub-samples collected at the centre and four corners of perimeter of a 20 m× 20 m area.

SOC content of soil samples was measured by laboratory mid-infrared (MIR) spectroscopy. For the MIR analysis, samples were ground to 200 μm for analyses as neat powders. MIR spectral reflectance of each soil sample were measured using a Tensor 37_Fourier Transform Infrared spectrometer from Bruker Optics, in the range 2500 to 25000 nm with 8 cm^{-1} resolution and 64 scans per second. Predictions of SOC content of each soil sample were made using PLSR from MIR calibrations (more details in Gomez et al. 2008). The calibration used 13 factors and the test set validation root mean squared error of the model was 0.15 dag/kg and R^2 of 0.91. Over Narrabri sites, the soil samples collection and Hyperion data acquisition were realised in the same semester so SOC content may be considered as stable between sampling and image acquisition.

An evaluation of atmospheric correction algorithms in the estimation of SOC from Hyperion image.
Ph.D. Thesis, 2018, NITK, Surathkal, India.

42

3.4.3 SOC values

The distribution of SOC in both study areas is represented in box plot (Figure 3.3). Unit of SOC content is expressed as weight of organic carbon as percentage of the total weight of the soil sample. In Karnataka sites SOC content varies between 0.07 % and 5.22 % with its mean, median and standard deviation which are 2.31, 1.98 and 1.21 respectively. In Narrabri sites it ranges from 0.002 % to 5.1 %. But it is noted that only one sample in the dataset has 5.1 % of SOC which is considered as an outlier and removed. So SOC ranges from 0.002 % to 3.6 % with its mean, median and standard deviation are 1.56, 1.47 and 0.97 respectively. It is noted that the SOC distribution over the Karnataka fields are spread out and normally distributed whereas that of Narrabri fields are skewed towards lower SOC content.
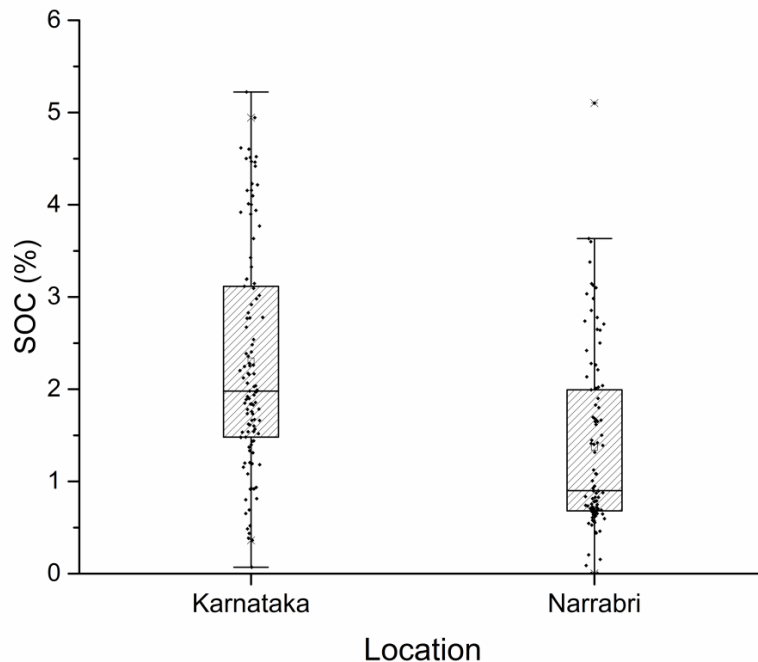

Figure 3.3: SOC distribution (in %) in both field sample sets

An evaluation of atmospheric correction algorithms in the estimation of SOC from Hyperion image. Ph.D. Thesis, 2018, NITK, Surathkal, India.

43

3.5 ANCILLARY DATA

Climate data such as mean temperature, mean pressure and daily rainfall for the date of acquisition of Hyperion images were obtained from 'global surface summary of day' product produced by the National Climatic Data Center (NCDC) (www.ncdc.noaa.gov) are shown in Table 3.5. Climatic data from the nearest climatological station of the study area were downloaded from the website. The nearest station of Karnataka site is Mangalore (located at 12.9169°N, 74.8828°E and elevation of 102 m) and that of Narrabri site is Narrabri airport (located at 30.3154°S, 149.8302°E and elevation of 229 m). Atmosphere was clear and precipitation was zero in all cases on the date of acquisition of images.

Concentration of atmospheric components was obtained on the date of acquisition of satellite image from NASA's Earth Observations (NEO) website (http://neo.sci.gsfc.nasa.gov/) are given in Table 3.6. Owing to the small size of the study area in relation to spatial resolution of MODIS (Moderate Resolution Imaging Spectroradiometer) and OMI (Ozone Mapping Instrument) data (which is 0.25 degree), spatial variations were not considered.

Table 3.5: Climate data for the acquisition dates

Place	Year-month-date	Mean temperature (°C)	Mean pressure (mbar)	Daily rainfall (mm)
Karnataka	4 March 2012	25.8	996.6	0
Narrabri Site#1	17 January 2007	27.1	989.9	0
Narrabri Site#2	13 December 2006	27.1	988.8	0

An evaluation of atmospheric correction algorithms in the estimation of SOC from Hyperion image.
Ph.D. Thesis, 2018, NITK, Surathkal, India.

44

Table 3.6: Atmospheric data for the acquisition dates

Sl no.	Parameter	Sensor/ Satellite	Unit	Karnataka: 4 March 2012	Narrabri Site#1 17 January 2007	Narrabri Site#2 13 December 2006
1	Aerosol optical thickness_550	MODIS/ Terra	-	0.23	0.25	0.26
2	Carbon monoxide	MOPITT / Terra	ppb (v)	145	72	83
3	Ozone optical thickness	OMI/ Aura	DU	255	258	263
4	Water vapour	MODIS/ Terra	cm	2.5	3.1	2.8

3.6 SPECTRORADIOMETRIC DATA

A gist of spectroradiometric data collected on Indian sites as adopted by Gopal 2014 and on Australian sites as adopted by Gomez et al. 2008 is presented here.

Field reflectance measurement of Karnataka soil samples was obtained with an ASD handheld Spectroradiometer Field Spec® in the range 375-1075 nm with spectral resolution of 1 nm. The instrument was mounted on a tripod with 30 cm vertical distance from soil sample and an external halogen light source was used. It was optimized to the halogen light source and calibrated with white reference panel. Soils were placed on black chart paper to avoid reflection. Reflectance spectra of air dried and sieved soil samples were obtained.

An evaluation of atmospheric correction algorithms in the estimation of SOC from Hyperion image.
Ph.D. Thesis, 2018, NITK, Surathkal, India.

45

The reflectance of the Narrabri soil samples was measured on the field during sample collection with the AgriSpec portable spectroradiometer in the range 350–2500 nm with spectral resolution of 1 nm. The AgriSpec spectrometer has a light source and measurements are made using the contact probe. A white spectralon panel (5 cm × 5 cm) provided the absolute reflectance factor for field measurements. The surface scanned was a core of 10 cm and 10 scans were made per sample.

3.7 SOFTWARE USED

The following software were used for processing the hyperspectral data and modelling the soil properties:

3.7.1 ArcGIS 10.1®

ArcGIS® is professional GIS software developed by Environmental Systems Research Institute (ESRI). ArcGIS can be used for creating maps, conducting spatial analysis and sharing intelligent visualizations for better decision making. It provides a set of comprehensive data visualization and analysis tools which greatly simplifies the processing of geo-spatial data. The study employs ArcGIS version 10.1 for visualizing the soil sampling locations from GPS data and to prepare location maps.

3.7.2 ENVI 4.7®

ENVI® is an acronym for "ENvironment for Visualizing Images" and is a geospatial imagery analysis and processing application marketed by Exelis Visual Information Solutions. ENVI® bundles together a number of scientific algorithms for image processing and analyses all types of imagery such as multispectral, hyperspectral, LiDAR, and SAR. Version 4.7 has been used in this study to perform preprocessing of FLAASH and QUAC atmospheric corrections on Hyperion imagery.

An evaluation of atmospheric correction algorithms in the estimation of SOC from Hyperion image.
Ph.D. Thesis, 2018, NITK, Surathkal, India.

46

3.7.3 ReSe Software

ReSe Applications Schläpfer provides atmospheric correction software ATCOR for remote sensing images. Trial version of ATCOR2® processed in Interactive Data Language (IDL) is used here (https://www.rese-apps.com/software/atcor/index.html). Interpretation of data and powerful application solving are its key functions.

3.7.4 MATLAB R2015a ®

MATLAB® (MATrix LABoratory) is a proprietary fourth-generation programming language developed by MathWorks. It provides an interactive environment for algorithm development, data visualization, data analysis, and numerical computations. MATLAB® enables matrix manipulations, graphics for visualizing data, implementation of algorithms and interfaces to C/C++, Java, .NET, Python, SQL, and Microsoft Excel, etc. It also has add-on toolboxes for a wide range of engineering and scientific applications. The study employs MATLAB R2015a® for coding and analysis. PCR, PLSR and ANN models were coded in MATLAB®. Also, hybrid atmospheric correction algorithms were also coded in MATLAB®. The codes are presented in Appendix I.

3.7.5 VisualSixS

6S was processed in alpha version of VisualSixS 1.1.2. Since the software is under development, its trial copy was used for this study. Emanuele Mandanici, from DICAM, University of Bologna has provided this software upon request.

3.8 OVERALL METHODOLOGY

The present study can be divided into three sub-studies which are inter-related and answers the four objectives of the study. Figure 3.4 presents overall methodology used in this study. As part of first objective, the accuracy of estimation of SOC from ground

An evaluation of atmospheric correction algorithms in the estimation of SOC from Hyperion image.
Ph.D. Thesis, 2018, NITK, Surathkal, India.

47

based VNIR/SWIR reflectance spectra using advanced statistical techniques viz. principal component regression (PCR), partial least square regression (PLSR) and artificial neural network (ANN) coupled with different spectra preprocessing methods were analysed. It was to identify the best estimation model and spectra smoothing method to be used for further analysis. The study is explained in detail in chapter 4. As part of the second objective, the influence of four popularly used atmospheric correction algorithms in the estimation of SOC from hyperspectral spaceborne Hyperion VNIR/SWIR data was analysed in fields located in two different geographical settings viz. Karnataka in India and Narrabri in Australia. This study is explained in detail in chapter 5. Results from this study were used for the development of hybrid atmospheric correction algorithms especially for retrieving soil reflectance. Later, two hybrid atmospheric correction algorithms are developed and evaluated for finding their potential in deriving soil spectra from Hyperion data and estimation of SOC. One of them uses radiative transfer equations with *in situ* atmospheric data followed by calibration using field reflectance values taken from optimum number of locations. Whereas, the second one combines an existing algorithm and calibration using field reflectance values. The study is explained in Chapter 6 and it answers third and fourth objectives of this research.

An evaluation of atmospheric correction algorithms in the estimation of SOC from Hyperion image.
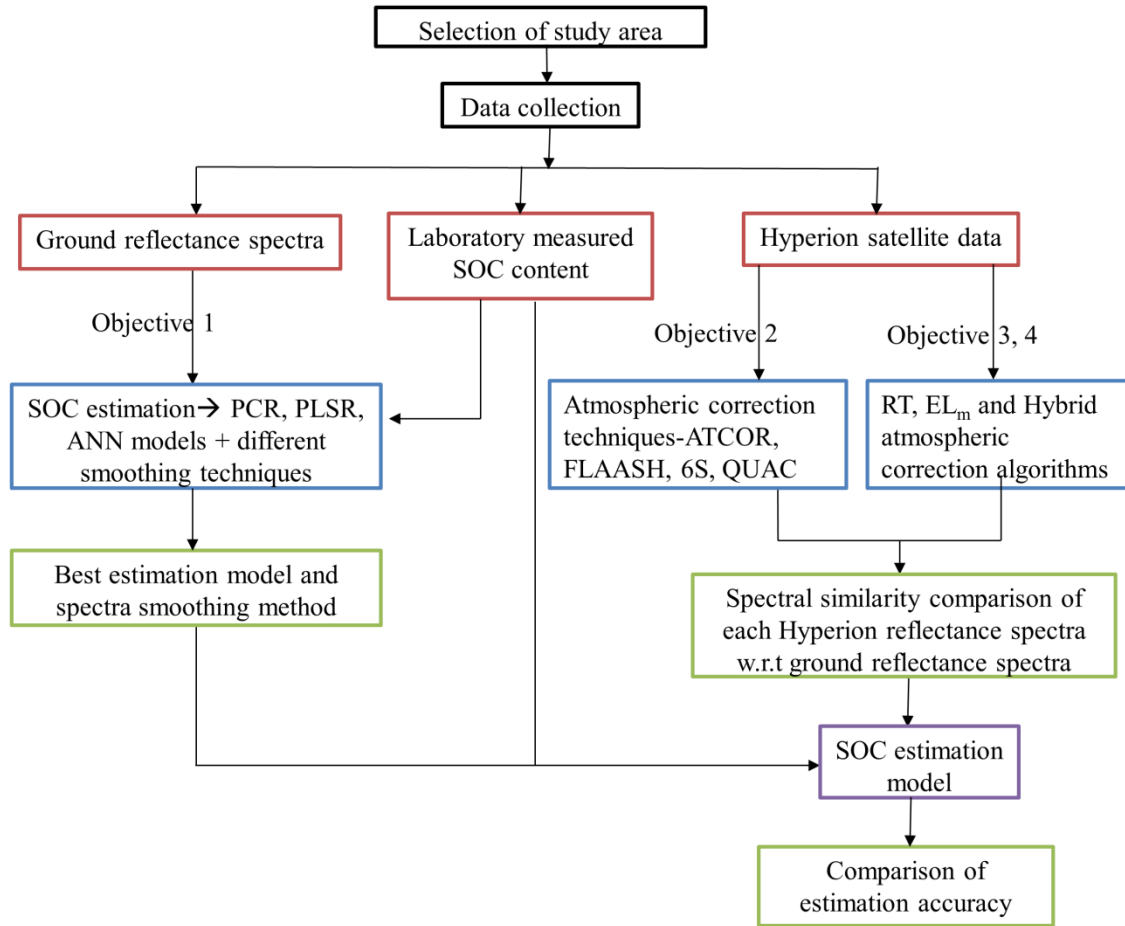*Ph.D. Thesis, 2018, NITK, Surathkal, India.*

48

Figure 3.4 Overall methodology

The next chapter explains detailed methodology, results and discussions of the first sub-study which answers objective 1 of this research.

An evaluation of atmospheric correction algorithms in the estimation of SOC from Hyperion image.
Ph.D. Thesis, 2018, NITK, Surathkal, India.

49

<div align="right">**CHAPTER 4**</div>

ESTIMATION OF SOC CONTENT THROUGH GROUND-BASED VNIR/SWIR SPECTROSCOPY

4.1 INTRODUCTION

Reflectance data from VNIR/SWIR regions were explored in estimating SOC (e.g. Gao et al. 2014, Peng et al. 2014, Jiang et al. 2016) and the studies were further extended to mid-infrared regions (Minasny et al. 2008). Henderson et al. 1992, Ben-Dor et al. 1997, Bartholomeus et al. 2008, Peon et al. 2017 etc. studied the relationship of soil spectrum and SOC content.

In the current study, as SOC is not measured under controlled environment, direct dependence of reflectance and SOC content cannot be established. Additionally SOC-specific spectral features in the reflectance signal are not strong enough or there are overlapping features due to some other quantity in the soil (e.g soil moisture). Thus first principle approaches is not applied here. The response of soil properties specifically SOC from spectral features is established using well-developed statistical techniques.

Viscarra-Rossel et al. (2006) reviewed various statistical methods of obtaining soil properties from different regions of electromagnetic spectrum. Stevens et al (2010) and Stevens et al (2012) compared several multivariate calibration models to estimate SOC using soil spectrum obtained from airborne hyperspectral sensor. Estimation accuracy of SOC from reflectance spectroscopy depends on many of the factors which include the smoothening effect of reflectance data, the soil type and statistical model used for estimation.

An evaluation of atmospheric correction algorithms in the estimation of SOC from Hyperion image.
Ph.D. Thesis, 2018, NITK, Surathkal, India.

50

Preprocessing methods are required to remove noise and other irrelevant information from the spectral data and thereby to improve the calibration of model. There is a need to define global applicability of role of preprocessing technique in SOC estimation from reflectance spectroscopy. As of now, there are no guidelines in choosing of spectral smoothening techniques for the problem at hand.

The present study investigates the accuracy of estimation of SOC from ground based VNIR/SWIR reflectance spectra using advanced techniques viz. principal component regression (PCR), partial least square regression (PLSR) and artificial neural network (ANN) coupled with different spectra preprocessing methods.

The study is published in Minu and Shetty, 2018. The methodology adopted in the study is explained in the section below.

4.2 METHODOLOGY

Methodology adopted in the study is shown in Figure 4.1. Ground measured reflectance signatures and laboratory measured SOC contents of Narrabri sites were used in this study since full range spectroradiometer reflectance were available. These ground reflectance spectra were preprocessed using different smoothing methods such as: moving average, median filtering, gaussian smoothing and Savitzky Golay smoothing. PCR, PLSR and ANN models were applied to estimate SOC content from preprocessed signal. The three statistical techniques were also applied to unsmoothed raw data. The implementation of models were carried out in MATLAB environment and the codes used are presented in Appendix I.

An evaluation of atmospheric correction algorithms in the estimation of SOC from Hyperion image.
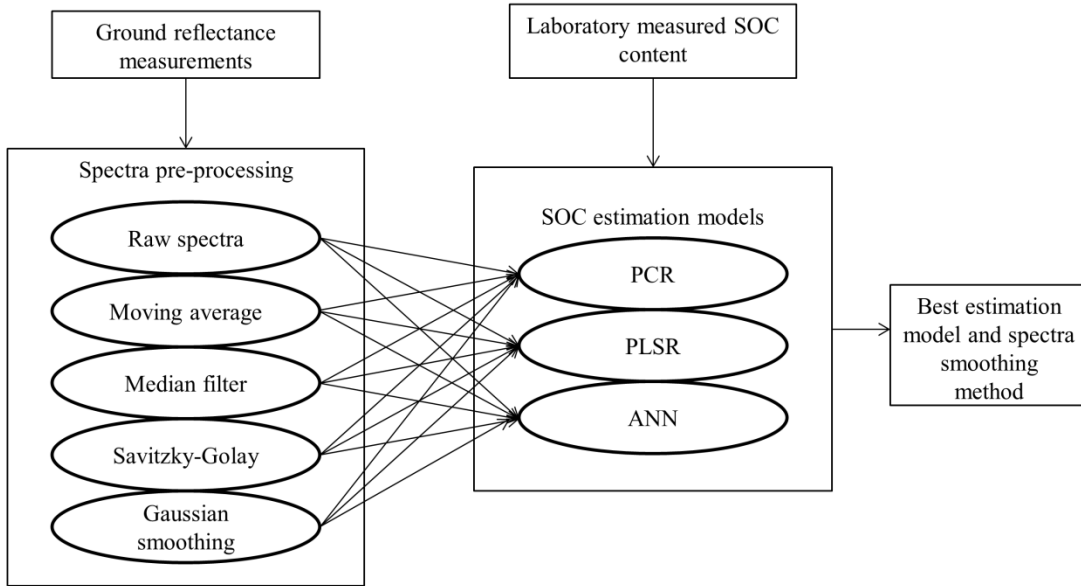*Ph.D. Thesis, 2018, NITK, Surathkal, India.*

51

Figure 4.1 Methodology adopted

The performance of estimation models in the calibration and validation sets was evaluated using performance matrices given in Equations 4.1–4.4.

(1) coefficient of determination (R^2) over calibration database (R^2_{cal}) and validation database (R^2_{val}),

(2) root mean square error (RMSE) calibration database (RMSE$_{cal}$) and validation database (RMSE$_{val}$),

(3) residual prediction deviation (RPD) over calibration database (RPD$_{cal}$) and validation database (RPD$_{val}$), (Chang et al. 2001) and

(4) ratio of performance to inter-quartile range (RPIQ) over calibration database (RPIQ$_{cal}$) and validation database (RPIQ$_{val}$) (Bellon-Maurel et al. 2010).

An evaluation of atmospheric correction algorithms in the estimation of SOC from Hyperion image.
Ph.D. Thesis, 2018, NITK, Surathkal, India.

52

$$R^2 = 1 - \frac{\sum\limits_{i=1}^{n} (\hat{y}_i - y_i)^2}{\sum\limits_{i=1}^{n} (\hat{y}_i - \bar{y})^2} \qquad (4.1)$$

$$RMSE = \sqrt{\sum\limits_{i=1}^{n} \frac{(\hat{y}_i - y_i)^2}{n}} \qquad (4.2)$$

$$RPD = \frac{sd}{RMSE} \qquad (4.3)$$

$$RPIQ = \frac{Q3 - Q1}{RMSE} \qquad (4.4)$$

where,

$\hat{y}_i$ is predicted value of the ith observation,

y_i is measured value of the ith observation,

$\bar{y}$ is the mean measured value,

n is the number of samples in each set,

sd is the standard deviation,

Q3 and Q1 are 3rd and 1st quartiles of the sample set, respectively.

The RPD scales model error by population dispersion and facilitates comparison of results from datasets with different degrees of variability. In contrast, the RPIQ accounts for the spread of a population in datasets with a skewed distribution by using the interquartile range instead of the standard deviation.

Performance categories used in this study are defined according to Veum et al. 2015 where PLSR model was used in estimating soil organic carbon along with other soil parameters.

- 'Category A' models are most reliable with $R^2 \geq 0.75$, RPD ≥ 2.0, and RPIQ ≥ 3.0,
- 'Category B' models with $R^2 \geq 0.63$, RPD ≥ 1.6, and RPIQ ≥ 1.9 and

An evaluation of atmospheric correction algorithms in the estimation of SOC from Hyperion image.
Ph.D. Thesis, 2018, NITK, Surathkal, India.

53

- 'Category C' models with $R^2 \geq 0.50$, RPD ≥ 1.4, and RPIQ ≥ 1.5.

- All other models were considered as not recommendable.

A brief description of preprocessing methods used and estimation models tested are given in following sections.

4.2.1 Spectra preprocessing methods

Spectroradiometer signatures were preprocessed using four different smoothening filters viz. moving average (MA) filter, median filter (MF), Savitzky Golay (SG) smoothing and Gaussian smoothing (GS). These pre-processing methods resolve overlapping spikes, remove linear baselines and eliminate spectral noises.

Moving average filter smoothens data by replacing each data point with an average of neighbouring data points defined within the span. Median filter is run through the signal, replacing each entry with the median of neighbouring entries. Savitzky Golay filter (Savitzky and Golay 1964), also called as digital smoothing polynomial filter or least-squares smoothing filter, is a generalized moving average filter. The filter coefficients are derived by performing unweighted linear least-squares fit using a polynomial of a given degree. It fits a local polynomial regression on the signal and requires equidistant bandwidth. A higher degree polynomial makes it possible to achieve a high level of smoothing without attenuation of data features. Mathematically, it operates merely as a weighted sum of neighbouring values. A third order Savitzky Golay filter was the choice in this study. Gaussian filter modifies the input signal by convolution with a Gaussian function (Rojas-Lertxundi et al. 2015). All filters were applied in a span size of 51 nm.

Figure 4.2 shows the plot of a spectra smoothed through each of these filters and comparing them to raw spectrum. An inspection of the raw spectrum shows that, the spectrum is affected by instrumental noises espectially in the visible and SWIR region of

An evaluation of atmospheric correction algorithms in the estimation of SOC from Hyperion image.
Ph.D. Thesis, 2018, NITK, Surathkal, India.

54

the spectrum. It takes us to the conclusion that smoothing is required as an initial preprocessing step of the spectrum.
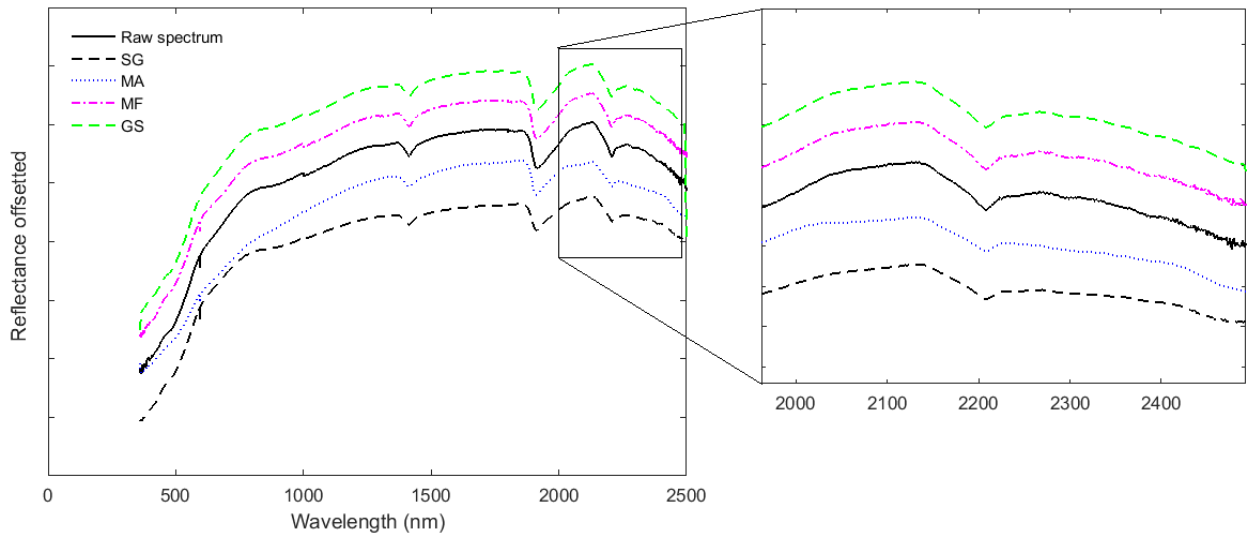

Figure 4.2 Smoothed and raw spectrum

4.2.2 Division of dataset for calibration/training and validation/testing

Of the total dataset (i.e. SOC content and corresponding soil reflectance) 3/4 is grouped as calibration set and remaining as validation set. To begin with, SOC values were sorted in ascending order. Initially, sample with lowest SOC content was placed in the validation set. The next three samples were placed in calibration set. The procedure is continued by alternately placing the following sample in validation set and the next three samples in calibration set. This ensures that datasets including entire range of SOC are evenly distributed across calibration range (Mark and Workman 2003).

In this study, PLSR, PCR and ANN uses the same calibration/training and validation/testing sets.

An evaluation of atmospheric correction algorithms in the estimation of SOC from Hyperion image.
Ph.D. Thesis, 2018, NITK, Surathkal, India.

55

4.2.3 Estimation Models

To estimate SOC from reflectance spectra various linear and non-linear estimation models have been used. Principal component regression (PCR) and partial least squares regression (PLSR) are linear models coupled with dimension reduction methodologies. While PCR is applied without consideration of correlation between spectra and SOC content during the process, PLSR takes into account the correlation. PLSR selects orthogonal factors that maximize covariance between spectra and SOC content. It handles multicollinearity and is strong in considering data noise and missing values. Unlike PCR, PLSR balances the two objectives of explaining response and predictor variation and performs the decomposition and regression in a single step (Viscarra-Rossel et al. 2006). ANN model possesses characteristics such as non-linearity, parallelism, noise tolerance, and learning and generalization capability (Chiang et al. 2004).

The models used in the study are explained in following sections.

4.2.3.1 Principal component regression

PCR consists of two stages (Maesschalck et al. 1999). In the first stage the number of input bands are reduced to few principal components (PC). These PCs describe the spectral variance across all samples. In the second stage these PCs are regressed against SOC content and calibration models are constructed. The model is validated using separate data (validation set). Selection of calibration and validation sets are defined as explained in section 4.2.2.

In the present sample sets, three principal components were used in the regression calculations which explained about 90% of variance (Figure 4.3). Regression modelling using principal components was carried out in MATLAB® software. The function 'pca' is used to get principal components which are then regressed and y (i.e., SOC) is estimated.
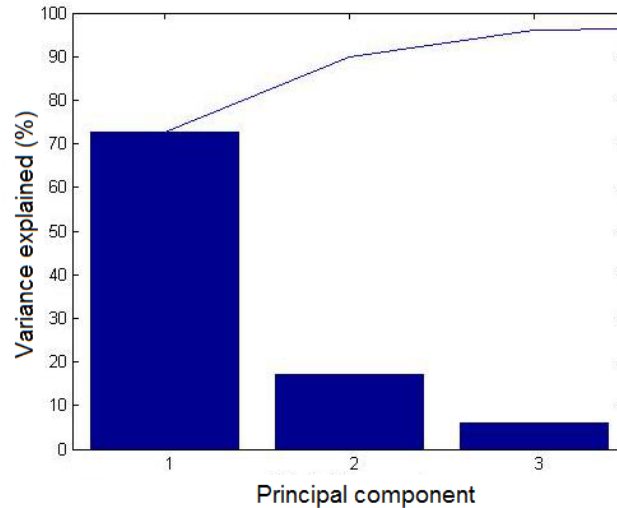
An evaluation of atmospheric correction algorithms in the estimation of SOC from Hyperion image.
Ph.D. Thesis, 2018, NITK, Surathkal, India.

56

Figure 4.3 Percentage of variance explained by each principal component

4.2.3.2 Partial least square regression

PLSR is a multivariate analysis technique used in cases where there are a large number of independent variables or predictors and these independent variables are highly collinear. It was developed by Wold et al. (1983). PLSR is used by several researchers in soil property studies at different scales such as laboratory, *in situ* spectral analysis and airborne and spaceborne hyperspectral image analysis (Viscarra-Rossel et al. 2006, Stevens et al. 2008, Lu et al. 2013, Anne et al. 2014). The PLSR method reduces the entire reflectance spectra to a small number of relevant factors and regresses them to the dependent variable. It decomposes both the predictor (Spectral reflectance) and response (soil properties) variables and identifies a few underlying latent vectors that maximize the co-variability between them (Wold et al. 2001). The general idea of PLSR is to extract these latent factors, accounting for as much of the manifest factor variation as possible while modelling the responses well.

Selection of calibration and validation sets are defined as in section 4.2.2. An optimum number of PLS components, which minimizes the mean square prediction error in cross-

An evaluation of atmospheric correction algorithms in the estimation of SOC from Hyperion image.
Ph.D. Thesis, 2018, NITK, Surathkal, India.

57

validation was identified for each dataset. This ensures dimensionality reduction in subsequent regression analysis. MATLAB function 'plsregress' is used for the regression. It calculates regression coefficients (β coefficients) from the calibration set and use them for estimating y values.

4.2.3.3 Artificial neural network

ANN is a non-linear estimation model carried out using graphical user interface 'nntool' in MATLAB® software for SOC estimation from reflectance spectrum. Data were divided into training and test sets. Selection of samples in the training sets and test sets were defined as in section 4.2.2. The neural network used is feed-forward back-propagation network and consists of input, hidden and output layers as shown in Figure 4.4. Input layer consists of reflectance values and the number of wavelengths in this layer was reduced by averaging three successive wavelengths in order to reduce the size of the matrix formed. Output layer consists of SOC values. The number of neurons in the hidden layer was found out by a trial-and-error approach which resulted in lower training error (Chiang et al. 2004). Tan-sigmoid (non-linear) and purelin (linear) functions were selected for the hidden and output layers, respectively. Levenberg-Marquardt was used as the training algorithm.
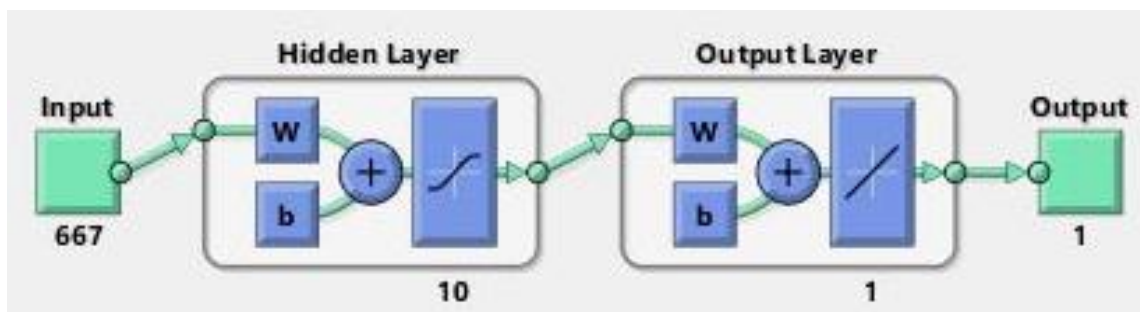

Figure 4.4 Artificial neural network structure used in this study

An evaluation of atmospheric correction algorithms in the estimation of SOC from Hyperion image.
Ph.D. Thesis, 2018, NITK, Surathkal, India.

58

4.3 RESULTS AND DISCUSSION

4.3.1   Model performance

Model performance was evaluated in terms of R^2, RMSE, RPD and RPIQ for each SOC estimation model. The analysis was performed on raw and smoothed reflectance spectra. The calibration and validation results of SOC estimation are summarized in Table 4.1.

Table 4.1 Performance matrices of PCR, PLSR and ANN models

Model	Pre-processing	NF*	Calibration set				Validation set			
			R^2_{cal}	$RMSE_{cal}$	RPD_{cal}	$RPIQ_{cal}$	R^2_{val}	$RMSE_{val}$	RPD_{val}	$RPIQ_{val}$
PCR	Nil	3	0.54	0.61	1.52	2.49	0.50	0.64	1.43	2.11
	MA		0.71	0.51	1.87	2.99	0.70	0.52	1.93	2.99
	MF		0.66	0.56	1.71	2.75	0.65	0.58	1.76	2.72
	SG		0.71	0.51	1.87	2.99	0.70	0.53	1.93	2.99
	GS		0.65	0.55	1.71	2.74	0.65	0.58	1.76	2.72
PLSR	Nil	5	0.77	0.46	2.11	3.34	0.66	0.52	1.77	2.86
	MA	6	0.83	0.39	2.46	3.87	0.77	0.48	2.13	3.08
	MF	5	0.83	0.39	2.47	3.90	0.76	0.49	2.09	3.03
	SG	5	**0.84**	**0.38**	**2.55**	**4.02**	**0.77**	**0.48**	**2.17**	**3.19**
	GS	7	0.81	0.41	2.32	3.66	0.75	0.50	2.07	3.00
ANN	Nil	10	0.61	0.61	1.58	2.58	0.60	0.65	1.69	2.60
	MA		0.63	0.57	1.67	2.68	0.66	0.58	1.76	2.72
	MF		0.78	0.44	2.17	3.48	0.74	0.50	2.05	3.15
	SG		0.78	0.44	2.18	3.49	0.77	0.47	2.17	3.16
	GS		0.71	0.50	1.90	3.05	0.64	0.59	1.72	2.66
* NF is no. of PC in PCR model, no. of PLS components in PLSR model and no. of neurons in ANN										
In bold are represented the best performances										

A good model has higher values of R^2, RPD and RPIQ and a lower RMSE. Analysis on raw spectra did not give good results irrespective of the estimation model used. Smoothening is essential in order to remove any abnormal peaks or noise from the spectrum. Results of this study also reveal that the choice of signal smoothening technique affects model output and the best one among the four is Savitzky Golay filter for all the estimation models considered. Even though all the three models used in the study have the potential to estimate SOC content from reflectance spectrum (fall into category A or B as Veum et al. 2015, refer section 4.2), PLSR model outperforms the other two. The superiority of PLSR is because it considers correlation between dependent and independent variables, whereas it is not considered in PCR.

Previous studies by Wijewardane et al. (2016) showed that nonlinear techniques like ANN outperformed PLSR in soil carbon modeling. But ANN gives good results only when it has sufficient number of training samples. It may produce better results if the spread and number of training samples are increased. In the present study, estimation models are built with limited data, mostly this kind of scenarios prevail in field measurement of environmental parameters especially at the local scale. The results obtained recommend that, PLSR model performs better with Savitzky Golay method (SG-PLSR model) as the best pre-processing method yielding $R^2_{cal} = 0.84$, $RPD_{cal} = 2.55$ and $RPIQ_{cal} = 4.02$ in the calibration set and $R^2_{val} = 0.77$, $RPD_{val} = 2.17$ and $RPIQ_{val} = 3.19$ in the validation set and the same is highlighted in Table 4.1. The scatterplot obtained for SG-PLSR model is shown in Figure 4.5.
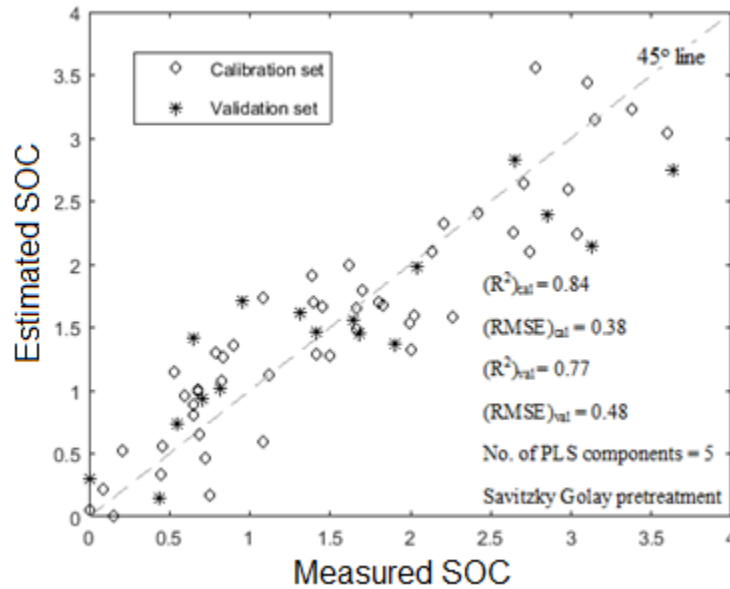
An evaluation of atmospheric correction algorithms in the estimation of SOC from Hyperion image.
Ph.D. Thesis, 2018, NITK, Surathkal, India.

60

Fig. 4.5 Estimated vs. Measured plot of SOC content (%) from SG-PLSR model

4.3.2 Significant wavelengths for SOC estimation

The output from SG-PLSR model was analysed for identifying significant wavelengths for SOC estimation. The spectral responses of functional groups are dispersed over several adjacent wavelengths, leading to strong collinearity in some regions of the spectra, while other regions may be corrupted by noise or contain irrelevant information (Gosselin et al. 2010). It is necessary that the wavelengths that are relevant for modelling a particular property be identified. In this study, this is achieved by computing the 'Variable Importance in PLS projections' (VIP) and the absolute value of PLS regression coefficients (β) from SG-PLSR model. Higher $|\beta| \times$ VIP scores were identified as a subset of wavelengths significant in estimating the SOC content as opposed to entire range of spectrum.

An evaluation of atmospheric correction algorithms in the estimation of SOC from Hyperion image.
Ph.D. Thesis, 2018, NITK, Surathkal, India.

61

VIP is a weighted sum of squares of the PLS weights, with weights calculated from the amount of Y-Variance of each PLS component (Wold et al. 2001, Mehmood et al. 2012). It accumulates the importance of each variable *j* being reflected by loading weights *w* from each component (Mehmood et al., 2012). The VIP score v_j for the variable *j* is defined as in equation 4.5.

$$v_j = \sqrt{\frac{p \sum_{a=1}^{A}\left[SS_a\left(\frac{w_{aj}}{||w_a||}\right)^2\right]}{\sum_{a=1}^{A} SS_a}} \qquad (4.5)$$

where,

p is the number of predictor variables or wavelengths,

SS_a is the sum of squares explained by the ath component

$\frac{w_{aj}}{||w_a||}$ represents the importance of the jth variable

The product of absolute regression coefficient and VIP score ($|\beta| \times$ VIP) from the SG-PLSR model is plotted in Figure 4.6. The significant wavelengths were identified by setting thresholds for $|\beta| \times$ VIP scores. The most significant wavelengths identified in PLSR model are located in the 600-680nm, 1860- 1900nm and 2180–2250nm spectral regions. And secondary significant wavelengths are located around 1000 nm and 2070 nm (Figure 4.6). Ben-Dor et al. (1997), Bartholomeus et al. (2008), Viscarra-Rossel and Behrens (2010), Vohland and Emmerling (2011), and Sarkhot et al. (2011), Bellon-Maurel and McBratney (2011) etc. have also reported association of important wavelengths for estimating SOC, which are in accordance with these results.

An evaluation of atmospheric correction algorithms in the estimation of SOC from Hyperion image.
Ph.D. Thesis, 2018, NITK, Surathkal, India.

62
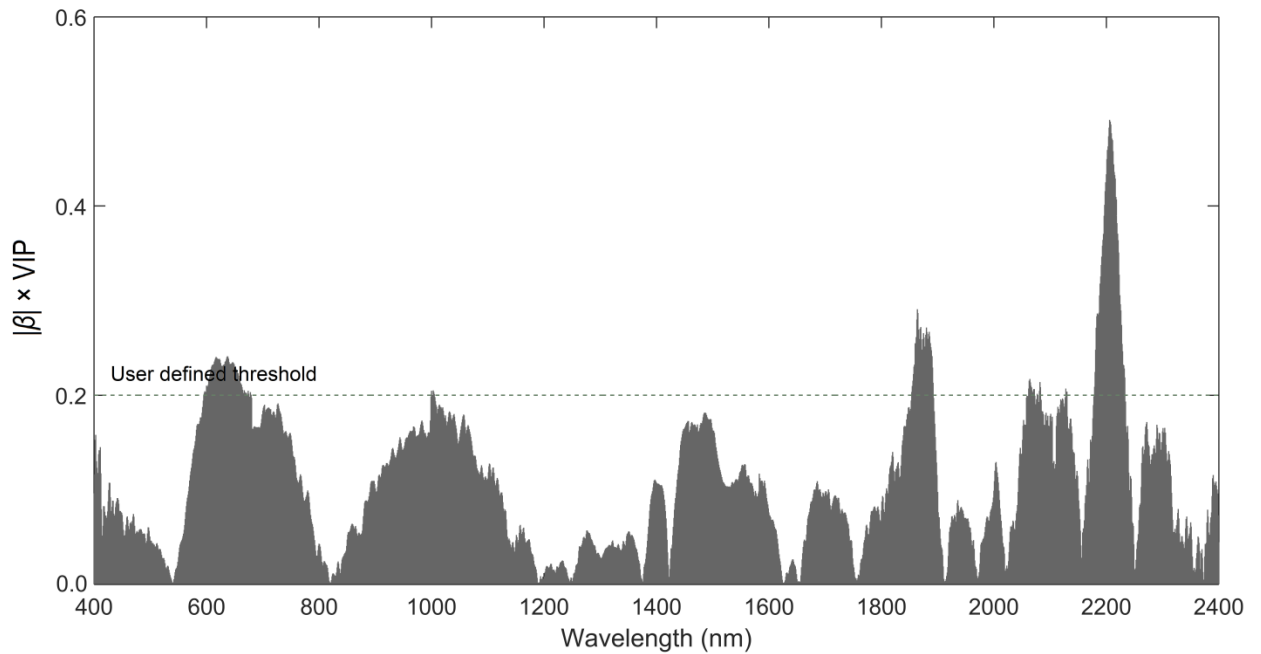
Figure 4.6: $|\beta| \times$ VIP scores for wavelengths from field spectra over Narrabri.

Earlier studies on interaction of SOC and reflectance spectra point out that, different wavelengths can contribute to SOC estimation. There is an overall decrease in reflectance with an increase in SOC. Henderson et al. (1992) found that for soils formed from different parent materials, 1955–1965, 2215, 2265, 2285–2295, and 2315–2495 nm gave the best correlation with SOC content. Ben-Dor et al. (1997) reported that based on the degree of decomposition or the type of organic matter, several changes occur in the soil spectrum. They showed that 400–600 nm slope of soil spectrum is influenced based on decomposition stage of organic material. Ben-Dor et al. (2002) assigned certain spectral features in soil spectrum to organic matter such as around 700 nm due to chlorophyll, around 1000 nm due to oil and cellulose, around 1600 nm due to pectin, starch, and cellulose, and around 2300 nm due to humic acid.

An evaluation of atmospheric correction algorithms in the estimation of SOC from Hyperion image.
Ph.D. Thesis, 2018, NITK, Surathkal, India.

63

Bartholomeus et al. (2008) studied on spectral regions suitable for soil SOC quantity. They reported that SOC determination from soil spectroscopy depends on reflectance variation due to cellulose, starch, and lignin content at different regions in the VNIR/SWIR region of the electromagnetic spectrum. They found the highest correlation between the inverse of reflectance and SOC at wavelengths between 640 and 690 nm. They also found that the area of the absorption feature between 2050 and 2200 nm shows a negative relation with SOC.

4.4 LIMITATION OF THE STUDY

Soil reflectance is a cumulative property, derived from inherent spectral behaviour of heterogeneous combination of mineral and organic matter/SOC, soil moisture, and soil texture. However, in the present study, the soil was not understood completely and SOC was only measured. The limitation of the present study is that, other components influencing spectral behavior were not separated, which is infact the most practical condition. Direct dependence of reflectance and SOC content cannot be established. Additionally, SOC-specific spectral features in the reflectance signal are not strong enough or there are overlapping features due to some other quantity in the soil (e.g soil moisture).

4.5 CONCLUSIONS

This study highlights that a properly pre-processed reflectance spectra show tremendous potential in soil organic carbon estimation. Among the smoothening techniques compared Savitzky Golay method outperforms others. PLSR models performed better than PCR and ANN models in cross-validation. Thus PLSR model using Savitzky Golay smoothened soil reflectance signals is recommended for SOC estimation from reflectance data in the study area when the spread and number of calibration samples are limited.

An evaluation of atmospheric correction algorithms in the estimation of SOC from Hyperion image.
Ph.D. Thesis, 2018, NITK, Surathkal, India.

64

Significant wavelengths for SOC estimation were identified as 600-680 nm, 950-1050 nm, 1860-1900 nm, 2050-2090 nm and 2180-2250 nm regions from the output of SG-PLSR model.

SG-PLSR model is adopted in further analysis for estimation of SOC from spaceborne Hyperion data and finding out the role of atmospheric correction algorithm on estimation accuracy as explained in Chapter 5.

An evaluation of atmospheric correction algorithms in the estimation of SOC from Hyperion image.
Ph.D. Thesis, 2018, NITK, Surathkal, India.

65

CHAPTER 5

INFLUENCE OF ATMOSPHERIC CORRECTION ALGORITHMS IN THE ESTIMATION OF SOC FROM HYPERION DATA

5.1 INTRODUCTION

Chapter 4 demonstrates the potential of field spectroscopy for estimation of SOC. SG-PLSR model was recommended for the same. In this part of the study, the potential of spaceborne hyperspectral VNIR/SWIR data is explored for quantification and better characterization of SOC. Remotely sensed target reflectance is affected by the presence of atmosphere in between. This study tries to evaluate popularly used atmospheric correction algorithms for the estimation of SOC from hyperspectral spaceborne sensor, specifically Hyperion (VNIR/SWIR, 400-2500 nm) data in fields located in two different geographical settings viz. Karnataka in India and Narrabri in Australia. The study is published in Minu et al. 2017. The methodology adopted in the study is discussed in the section follows.

5.2 METHODOLOGY

A broad outline of process flow adopted in this study is illustrated in Figure 5.1. ρ_{s_ATCOR}, ρ_{s_FLAASH}, ρ_{s_6S} and ρ_{s_QUAC} are the reflectances obtained after applying ATCOR, FLAASH, 6S and QUAC algorithms respectively and are described in the following sections.

An evaluation of atmospheric correction algorithms in the estimation of SOC from Hyperion image.
Ph.D. Thesis, 2018, NITK, Surathkal, India.

66
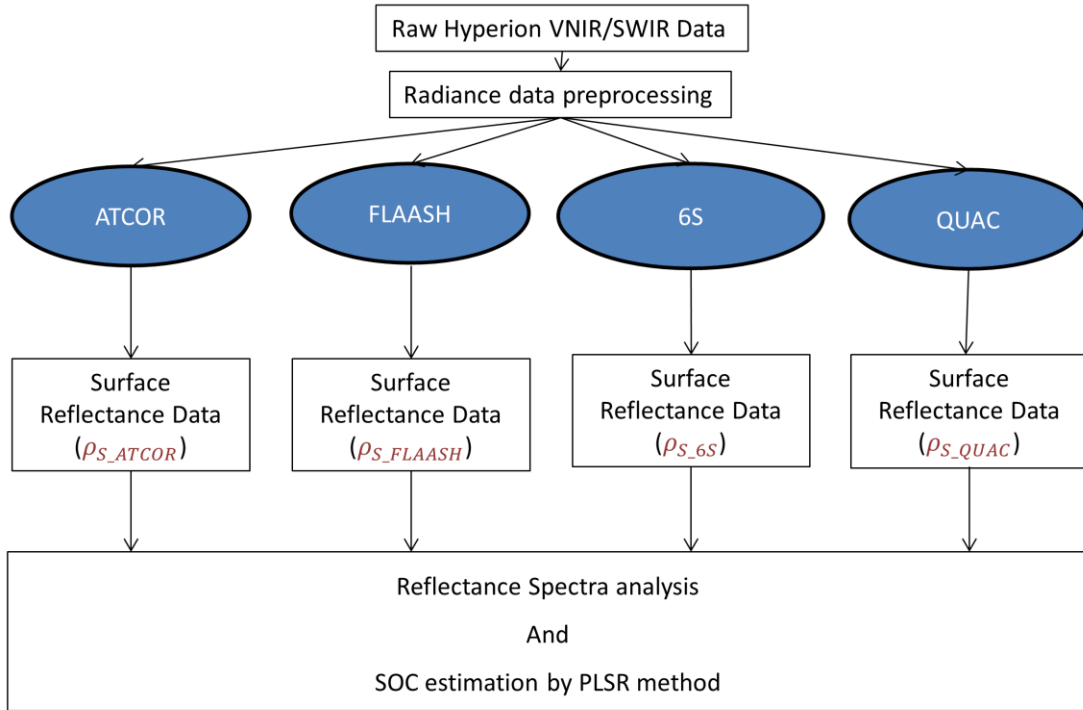
Figure 5.1 An outline of process flow adopted in the study

5.2.1 Radiance Hyperion data preprocessing

In order to reduce the processing time, spatial and spectral sub-setting was performed. Initially regions of interest were subset from the Hyperion images. Following which, out of 242 Hyperion bands, uncalibrated bands 1-7 (355-416 nm), 58-78 (overlapping bands between VNIR and SWIR focal planes), 121-126 (1356-1406 nm), 165-181 (1800-1961 nm), 185-186 (2002-2012 nm), and 221-242 (2365-2577 nm) were removed from the image. The remaining 167 bands were available for further analysis.

5.2.2 Atmospheric correction algorithms

An ideal atmospheric correction algorithm removes intrinsic atmospheric components from a satellite-derived top-of-atmosphere radiance data and converts to surface

An evaluation of atmospheric correction algorithms in the estimation of SOC from Hyperion image.
Ph.D. Thesis, 2018, NITK, Surathkal, India.

67

reflectance. Four commonly used atmospheric correction algorithms tested in this study are: QUAC, 6S, FLAASH and ATCOR. A brief note on the four atmospheric correction algorithms tested in this study is explained below.

5.2.2.1 QUAC

Quick atmospheric correction (QUAC) is a semi-empirical, solar reflective spectral region (400-2500 nm), atmospheric correction method (Bernstein et al. 2005). It is based on the empirical finding that, the average reflectance of diverse material spectra is not dependent on the specific scene, provided that there are atleast ten diverse materials in a scene, spectral standard deviation of reflectance for a collection of diverse materials is nearly wavelength-independent constant and there are sufficiently dark pixels in a scene to allow for a good estimation of the baseline spectrum. QUAC also allows for any view or solar elevation angle.

It does not use any radiative transfer (RT) equations and determines atmospheric compensation parameters directly from the image, without any ancillary information. It does not consider spectral sampling distance. It is faster than physics-based methods and produces a uniform correction; however, it is an approximate method. In the present study, QUAC model was applied using ENVI$^®$ software.

The parameters for QUAC include selecting an input file, specifying a sensor type, and setting output file defaults. The 'sensor type' was specified as 'Hyperion' so that algorithm identifies specification of sensor band locations and their radiometric calibration (Bernstein et al. 2012). The reflectance values in the output image from QUAC were scaled by 10000.

5.2.2.2 6S

6S, which stands for Second Simulation of a Satellite Signal in the Solar Spectrum code, is one of the most widely used RT codes, based on successive orders of scattering

An evaluation of atmospheric correction algorithms in the estimation of SOC from Hyperion image.
Ph.D. Thesis, 2018, NITK, Surathkal, India.

68

approximations (Vermote et al. 1997a). It uses a wavenumber grid of 20 cm^{-1} with spectral sampling distance varying from 0.32 nm to 12.4 nm depending on wavelength in 400-2500 nm region.

6S considers a plane parallel to atmosphere. So it cannot handle spherical atmosphere and as a result, it cannot be used for limb observations. Also, the decoupling used for absorption and scattering effects does not allow using the code in the presence of strong absorption bands (Vermote et al. 1997a). Mandanici (2010) compared 6S with MODTRAN based 'FLAASH' algorithm over arid and vegetated land cover types and found a weaker water vapour absorption band modelling. 6S cannot handle clouds. Its employment in hyperspectral image pre-processing chain has been limited.

In the current study, 6S was processed in alpha version of VisualSixS software. 6S assumes Lambertian surface and considers adjacency effects caused by contributions from pixels surrounding the pixel of interest. Sensor and viewing geometry such as sensor type, scene centre location, sensor altitude, target elevation, month and day of the flight, satellite zenith and azimuth angles, solar zenith and azimuth angles were provided for each image. Tropical atmospheric model was assumed for Indian sites, whereas midlatitude summer model was assumed for Australian sites. Continental aerosol model with 30 km visibility was assumed for both sites.

5.2.2.3 FLAASH

Fast line-of-sight atmospheric analysis of spectral hypercubes (FLAASH) is a physics-based atmospheric correction method (Adler-Golden et al. 1999). It uses MODTRAN4 code to calculate the parameters required for RT equations which in turn gives surface reflectance (FLAASH 2006). Atmospheric multiple scattering is computed using scaled DISORT (DIScrete Ordinate Radiative Transfer) algorithm, and the correlated *k* algorithm is used to model the absorption for regions presenting considerable absorption effects. FLAASH with 5 cm^{-1} resolution (FLAASH 2006) translates to varying spectral

An evaluation of atmospheric correction algorithms in the estimation of SOC from Hyperion image.
Ph.D. Thesis, 2018, NITK, Surathkal, India.

69

sampling distance from 0.08 nm to 3.12 nm depending on wavelength in 400-2500 nm region. FLAASH assumes Lambertian surface and considers adjacency effect.

In the current study, input images were corrected with FLAASH algorithm using the 'FLAASH atmospheric correction' module in ENVI®. The input image for FLAASH is radiometrically calibrated radiance image in band-interleaved-by-line (BIL) or band-interleaved-by-pixel (BIP) format. Hyperion radiance data in units of $W/(m^2.\mu m.sr)$ can be obtained by multiplying VNIR bands (i.e bands 1-70, 400 to 1000nm) with a scaling factor of 40 and SWIR bands (i.e bands 71-242, 900 to 2500 nm) with a scaling factor of 80 (Beck 2003). However, FLAASH algorithm requires input data to have units of $\mu W/(cm^2.nm.sr)$. Thus, to obtain proper units appropriate scaling factors (40 and 80 for the VNIR and SWIR, respectively) as well as a factor of 10 to convert the units are to be applied. Thus, a scaling factor of 400 is applied to the bands of VNIR region and 800 for bands of SWIR region in FLAASH algorithm.

Information such as scene centre location, sensor type, sensor altitude, ground elevation, flight date, flight time, satellite zenith and azimuth angles were provided for each image. Tropical atmosphere and rural aerosol models were used for Indian sites, whereas mid-latitude summer atmosphere and rural aerosol model were used for the Australian sites. Initial visibility, aerosol scale height and CO_2 mixing ratio were kept as default as 30 km, 1.5 km and 390 ppm respectively in all cases. The surface reflectance values, after FLAASH correction, is scaled up by 10000.

5.2.2.4 ATCOR

ATmospheric CORrection (ATCOR) uses MODTRAN5 code for atmospheric correction (Richter and Schlaepfer 2012) with latest HIgh-resolution TRANsmission molecular absorption (HITRAN) database. It is a large atmospheric database at a high spectral resolution (Richter and Schlaepfer 2012). MODTRAN5 is an upgraded version which includes finer spectral resolution and treatment of auxiliary atmospheric gases (Berk et al.

An evaluation of atmospheric correction algorithms in the estimation of SOC from Hyperion image.
Ph.D. Thesis, 2018, NITK, Surathkal, India.

70

2004, Berk et al. 2008). ATCOR uses a variable wavenumber grid to obtain a constant spectral sampling distance of 0.4 nm in the 400-2500 nm region (Richter and Schlaepfer 2012).

In this study, trial version of ATCOR2 was processed in IDL. It supports calibrated image file in band-sequential (BSQ) format. ATCOR assumes Lambertian surface and requires information such as sensor type, flight date, solar zenith angle, sensor view geometry, average ground elevation and adjacency range for each image. Initial visibility was assumed as 30 km. For the sensor Hyperion, the spectral definitions are stored in a calibration file called 'hyperion_167.cal' as provided by ATCOR. Atmospheric database i.e., look-up-tables of radiative transfer calculations, covering a wide range of weather conditions and sun angles are available. The user is provided the choice of selecting the standard MODTRAN model for atmosphere and aerosol types to represent the scene, and a unique MODTRAN solution is computed for each image. In ATCOR model CO_2 level is set at default 380 ppm. *In situ* ozone column in Dobson Units (DU) was also entered. The atmospheric file used is "h99000_wv10_rural.atm" which represents a file with the symbolic altitude of 99,000 m, water vapour column 1.0 cm, and rural aerosol.

QUAC being a semi empirical method does not require atmospheric parameters. 6S, FLAASH and ATCOR are physics-based methods. A summary of atmospheric parameters used by the algorithms is reported in Table 5.1. The difference in treating the input parameters by these atmospheric correction algorithms has a direct bearing on the reflectance simulation.

An evaluation of atmospheric correction algorithms in the estimation of SOC from Hyperion image.
Ph.D. Thesis, 2018, NITK, Surathkal, India.

71

Table 5.1 Atmospheric input parameters applied on 6S, FLAASH and ATCOR algorithms

Parameters	*6S*		*FLAASH*		*ATCOR2*	
	Karnataka	*Narrabri*	*Karnataka*	*Narrabri*	*Karnataka*	*Narrabri*
Atmospheric Model	Tropical	Midlatitude Summer	Tropical	Midlatitude Summer	h99000_wv10_rura	h99000_wv10_rura
Adjacency correction	1 km	No	Yes	No	1 km	0 km
Aerosol model	Continental	Continental	Rural	Rural	Zone 1	Zone 1
Visibility	30 km	30 km	30 km	30 km	30 km	30 km
Region for water vapour retrieval	-	-	820 nm	820 nm	940 to1130 nm	940 to1130 nm
Spectral Polishing	-	-	No	No	-	-
CO_2	-	-	390 ppm (user defined)	390 ppm (user defined)	380 ppm (uneditable)	380 ppm (uneditable)
Ozone concentration	-	-	-	-	*In situ* value in DU	*In situ* value in DU

5.2.3 Reflectance Hyperion data treatment

Visual inspection of individual reflectance bands alluded to different degrees of vertical stripping. Discarding these bands from the analysis was found to be beneficial (Jaber et al. 2011). Additionally, calibrated bands near major atmospheric absorption regions (e.g. around 950, 1400, 1900 and 2500 nm water absorption bands) that appear as over/under-corrected reflectance values were also discarded from reflectance spectrum. Few bands with negative or zero reflectance values near 450 nm spectral region after applying FLAASH, 6S and ATCOR algorithms that are not realistic reflectance values were also discarded. This effect is maximum in FLAASH output and not seen in QUAC output. Wavelengths used for further analysis after each atmospheric correction are given in Table 5.2.

Table 5.2: Hyperion wavelength domains used in the analysis

Atmospheric correction algorithm applied	Wavelengths used (nm)
ATCOR	477-925, 962-1114, 1164-1346, 1416-1790, 2022-2345
FLAASH	508-925, 972-1114, 1154-1336, 1487-1790, 2032-2345
6S	457-925, 972-1094, 1164-1336, 1487-1780, 2032-2324
QUAC	437-925, 972-1114, 1154-1336, 1487-1790, 2032-2345

An evaluation of atmospheric correction algorithms in the estimation of SOC from Hyperion image.
Ph.D. Thesis, 2018, NITK, Surathkal, India.

73

5.2.4 Spectral similarity comparison

To compare and validate atmospherically corrected Hyperion images obtained by four atmospheric correction methods, with field spectral measurements Spectral Angle Mapper (SAM) index was used. Spectral resolution of Hyperion images are 10 nm wheras that of field spectroradiometer is 1 nm. Through resampling it was brought to a common resolution of 10 nm. SAM calculates the spectral similarity between a test reflectance spectrum and a reference reflectance spectrum. It calculates the angle between the two spectra and treats them as vectors in space with dimensionality equal to the number of bands (Kruse et al. 1993). The spectral angle is calculated in radians and its value ranges from 0 to 1. The greater the spectral angle, the lower the spectral similarity. Spectral angle, α, between test spectrum t and a reference spectrum r is calculated using equation (5.1). Figure 5.2 shows the schematic representation to measure the angle between two spectra using SAM when two bands of reflectance are considered.

$$\alpha = \cos^{-1}\left[\frac{\sum_{i=1}^{m} t_i r_i}{(\sum_{i=1}^{m} t_i^2)^{1/2}(\sum_{i=1}^{m} r_i^2)^{1/2}}\right] \tag{5.1}$$

where m is the total number of bands used and i referring to each band number.
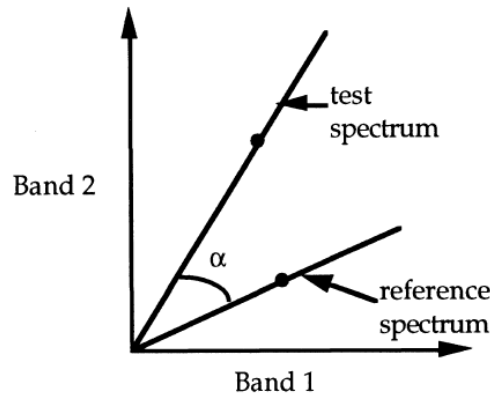
Figure 5.2 Schematic representation of SAM angle (Kruse et al. 1993)

An evaluation of atmospheric correction algorithms in the estimation of SOC from Hyperion image.
Ph.D. Thesis, 2018, NITK, Surathkal, India.

74

This analysis was performed on raw and smoothened reflectance spectra. Both Hyperion reflectance spectra and field reflectance spectra were smoothened by passing through Savitzky Golay smoothing with a third order polynomial and a window size of 50 nm.

To get a deeper understanding of the performance of atmospheric correction algorithm in different regions of electromagnetic spectrum and to compare spectroradiometer working in different wavelength regions, SAM was applied separately in three domains. First domain ranges from 400 to 1050 nm, second from 1500 to 1790 nm and third from 2000 to 2350 nm.

5.2.5 PLSR analysis

To estimate SOC from corrected soil spectra, each dataset (Karnataka and Narrabri) was divided into two groups, one group for calibration of PLSR model (3/4 of the dataset), and a second group for validation/prediction (1/4 of the database). Grouping of data into calibration and validation sets are explained in section 4.2.2 of Chapter 4. An analysis was performed to detect the outliers in the calibration dataset. Outliers are commonly defined as observations that are inconsistent with the majority of the data, such as observations that deviate significantly from normal values. To identify the concentration outliers, the samples with difference between actual and estimated SOC contents lying outside an interval spanning over the mean plus/minus two times standard deviation were considered (Hodge and Austin 2004) as outliers.

For executing PLS regression, an optimum number of PLS components (latent variables) was identified for each model to avoid the problem of overfitting. Cross-validation is a statistically sound method for choosing the number of components in PLSR (Wold et al. 2001). An optimum number of PLS components (NF) minimizes the mean square prediction error in cross validation and ensures dimensionality reduction in subsequent regression analysis.

An evaluation of atmospheric correction algorithms in the estimation of SOC from Hyperion image.
Ph.D. Thesis, 2018, NITK, Surathkal, India.

75

The performance of PLSR models were evaluated using R^2, RMSE, RPD, and RPIQ in both calibration and validation sets. Equations for evaluating these performance statistics are given in equations 4.1 to 4.4.

A higher value for the product of absolute regression coefficient and variable importance for projection ($|\beta| \times$ VIP) of each PLSR model were analyzed to identify a subset of wavelengths that are significant in estimating the SOC content from spectral reflectance data as opposed to entire range of spectrum (see section 4.4 of Chapter 4).

5.3 RESULTS

5.3.1 Spectral similarity comparison

Mean and standard deviation of SAM values were calculated for raw reflectance spectra and Savitzky Golay smoothened spectra separately (Table 5.3). It is seen that SAM indices of smoothened spectra are better (with lower values) than corresponding SAM indices of raw data. This observation is in accordance with the earlier studies (e.g. Selige et al. 2006, Anne et al. 2014), which points out that smoothening is essential in order to remove any abnormal peaks or noise. Thus, only smoothened spectra were used for further analysis.

The average SAM values vary from 0.020 to 0.312 radians as seen from Table 5.3. High and low SAM index is defined based on clustering noticed in the dataset. Three clusters were identified between 0.02 and 0.081, 0.112 and 0.131, and 0.259 and 0.312 corresponding to low, medium and high SAM values. The first spectral domain (400 - 1050 nm) seems to be strongly affected by the atmospheric correction model, with high to medium SAM values. Whereas second (1500 - 1790 nm) and third (2000 - 2350 nm) spectral domains seem to be slightly affected by the atmospheric correction model, with low SAM values (Table 5.3).

An evaluation of atmospheric correction algorithms in the estimation of SOC from Hyperion image.
Ph.D. Thesis, 2018, NITK, Surathkal, India.

76

Table 5.3: Summary statistics of SAM index: Mean SAM value (μ) and Standard deviation of SAM value (σ) (K= Karnataka set, N= Narrabri set, SG-smooth = Savitzky Golay smoothened).

Spectral domain	Pre-treatment	ATCOR		FLAASH		6S		QUAC	
		μ	σ	μ	σ	μ	σ	μ	σ
Domain 1 400 to 1050 nm (K)	Raw	0.301	0.057	0.309	0.061	0.311	0.050	0.291	0.069
	SG-smooth	0.296	0.064	0.308	0.071	0.312	0.058	**0.259**	0.076
Domain 1 400 to 1050 nm (N)	Raw	0.149	0.079	0.128	0.090	0.133	0.087	0.112	0.073
	SG-smooth	0.130	0.081	0.129	0.091	0.131	0.092	**0.112**	0.072
Domain 2 1500 to 1790 nm (N)	Raw	0.043	0.022	0.071	0.026	0.092	0.048	0.027	0.024
	SG-smooth	0.037	0.020	0.041	0.019	0.047	0.020	**0.020**	0.019
Domain 3 2000 to 2350 nm (N)	Raw	0.069	0.029	0.091	0.027	0.09	0.032	0.086	0.030
	SG-smooth	**0.057**	0.028	0.069	0.022	0.068	0.024	0.081	0.027
In bold is represented the best SAM index (minimal value), per tested domain.									

In terms of spectral similarity, no atmospheric correction model seems to be superior to other one. Indeed, the best SAM index (so the minimal value) is obtained for a different atmospheric correction model depending on the spectral domain (in bold in Table 5.3). ATCOR seems to be a good compromise with best SAM values for third spectral domain.

Even though in first and second domains QUAC model seems to give good compromise with lower values of SAM, in the third spectral domain it gives least compromise with higher SAM values. FLAASH and ATCOR seem to give similar SAM values in first and second spectral domains. 6S model does not provide a good SAM value in any spectral domain. Signals from large homogeneous fields of Narrabri seem to have small SAM values than Karnataka samples.
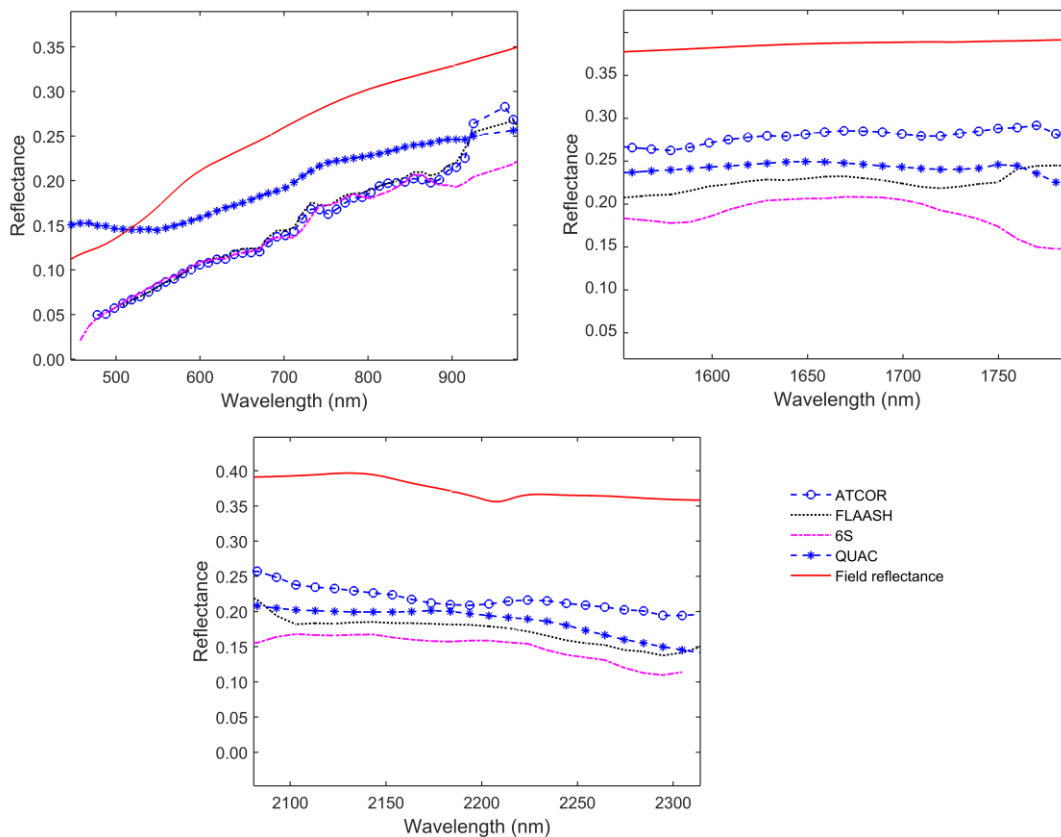
Figure 5.3 Average reflectance spectra of Narrabri pixels (over bare soils) and average field spectra, in the following spectral regions: (*a*) 400 to 1050 nm-Domain 1, (*b*) 1500 to 1790 nm-Domain 2 and (*c*) 2000 to 2350 nm-Domain 3.

Figure 5.3 shows average spectral reflectance pattern of Narrabri sites in three spectral

An evaluation of atmospheric correction algorithms in the estimation of SOC from Hyperion image.
Ph.D. Thesis, 2018, NITK, Surathkal, India.

78

domains. Each corrected Hyperion average reflectance spectrum is compared with field average reflectance spectrum. It is noted that the semi-empirical QUAC model produces a smooth spectrum, contrasting other physical models (ATCOR, FLAASH and 6S), whatever may be the spectral domain (Figure 5.3). Average albedo seems to be underestimated in all the models with 6S having maximum variation. It is identified that only ATCOR corrected spectra is able to capture the pattern of field reflectance curve near 2200 nm (Figure 5.3(*c*)).

5.3.2 Estimation of SOC from Hyperion reflectance data

Over each sites (Karnataka and Narrabri), PLSR models were built for SOC estimation from Hyperion reflectance spectra. So in total, four PLSR models per site were built.

As the first step, optimum number of PLS components (NF) required in each case was identified and the results are tabulated in Table 5.4 and Table 5.5. To arrive at these results, regression was run with ten components as a trial. The graphs of percentage variance in the model explained by each component and MSEP corresponding to ten PLS components were plotted. From the plotted graph, optimum number of factors were identified which minimizes the mean square prediction error in cross-validation. This ensures dimensionality reduction in subsequent regression analysis.

Each PLSR model, run with an optimum number of PLS components, was used to estimate SOC from atmospherically corrected Hyperion spectra. Figures 5.4 to 5.11 show scatter plots of SOC estimation results in calibration and validation datasets for each of the study sites. Qualitatively the spread of estimation with respect to 1:1 line and also the general trend of the estimation is depicted. It is noted that, at lower SOC the trend line shows that the estimation is overestimated whereas at higher SOC it is underestimated across all models. For comparison purpose, the quantitative values are represented by various performance statistics and are tabulated in Table 5.6.

An evaluation of atmospheric correction algorithms in the estimation of SOC from Hyperion image.
Ph.D. Thesis, 2018, NITK, Surathkal, India.

79

Table 5.4 Results of optimum number of PLS component (NF) selection in Karnataka samples

Spectrum used	Variance in Y explained by 10 components	Estimated MSEP in Y for 10 components	NF
ATCOR corrected			6
FLAASH corrected			7
6S corrected			5

QUAC corrected			5

Table 5.5 Results of optimum number of PLS component (NF) selection in Narrabri samples

Spectrum used	Variance in Y explained by 10 components	Estimated MSEP in Y for 10 components	NF
ATCOR corrected			6

An evaluation of atmospheric correction algorithms in the estimation of SOC from Hyperion image.
Ph.D. Thesis, 2018, NITK, Surathkal, India.

81

FLAASH corrected		4
6S corrected		4
QUAC corrected		4

An evaluation of atmospheric correction algorithms in the estimation of SOC from Hyperion image.
Ph.D. Thesis, 2018, NITK, Surathkal, India.

82

Figure 5.4 Measured vs. estimated SOC content obtained from (a) calibration set and (b) validation set of PLSR model using ATCOR corrected signals over Karnataka sites.
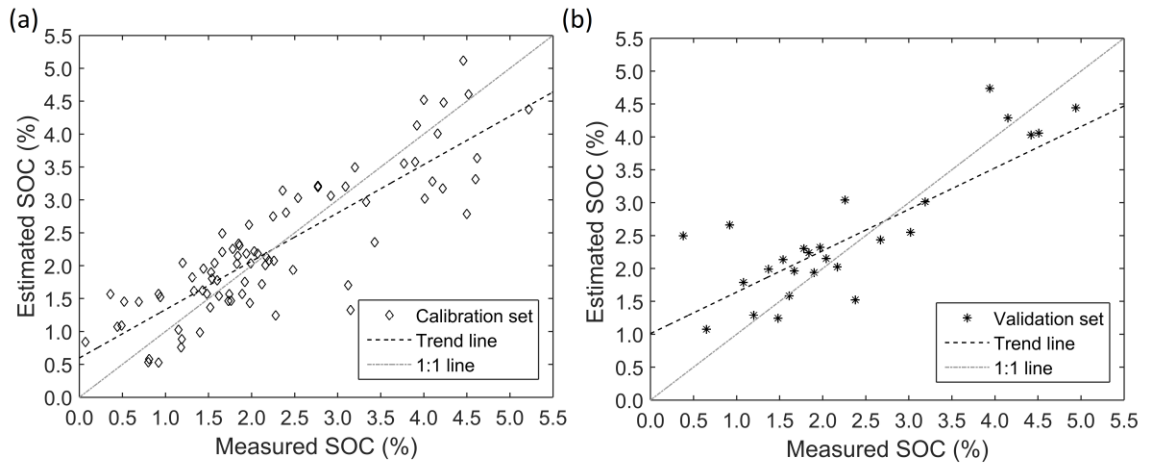
Figure 5.5 Measured vs. estimated SOC content obtained from (a) calibration set and (b) validation set of PLSR model using FLAASH corrected signals over Karnataka sites.

An evaluation of atmospheric correction algorithms in the estimation of SOC from Hyperion image.
Ph.D. Thesis, 2018, NITK, Surathkal, India.

83
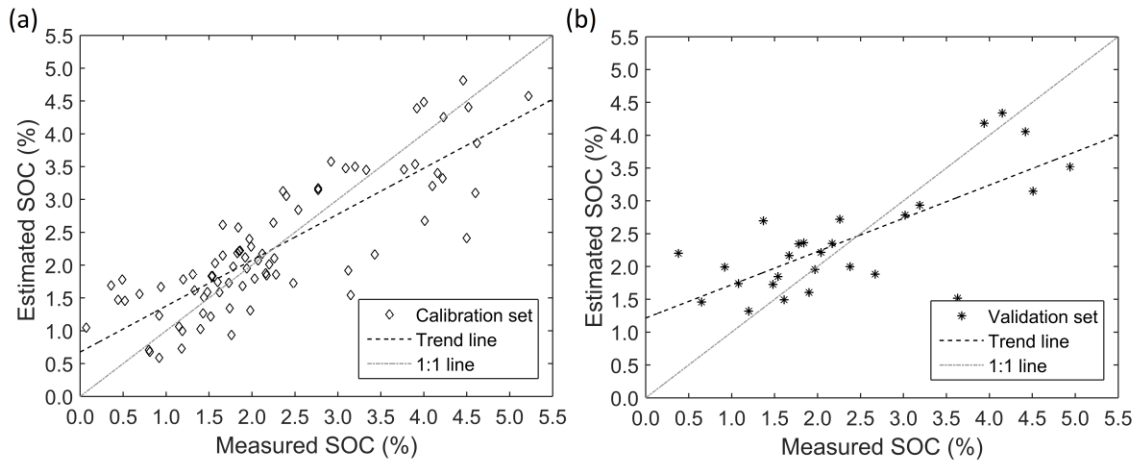
Figure 5.6 Measured vs. estimated SOC content obtained from (a) calibration set and (b) validation set of PLSR model using 6S corrected signals over Karnataka sites.
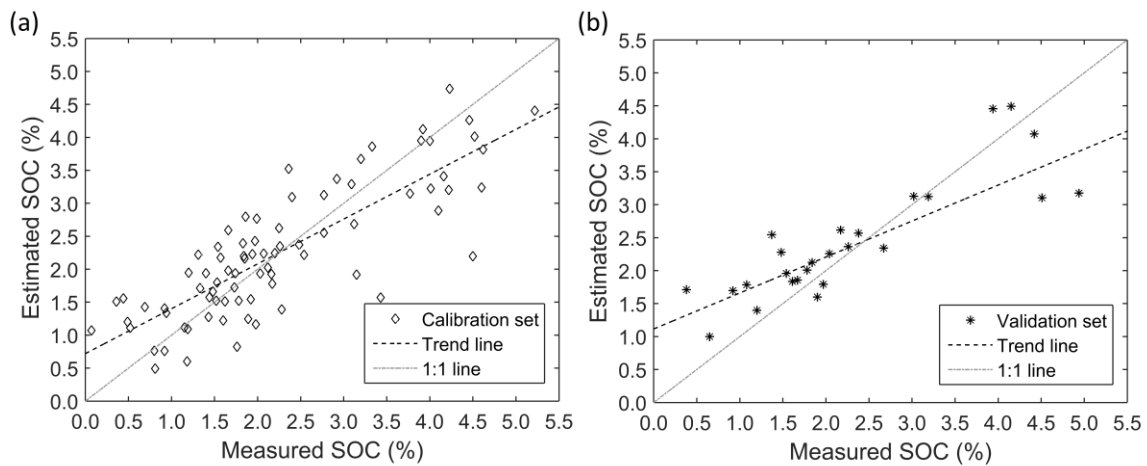
Figure 5.7 Measured vs. estimated SOC content obtained from (a) calibration set and (b) validation set of PLSR model using QUAC corrected signals over Karnataka sites.

An evaluation of atmospheric correction algorithms in the estimation of SOC from Hyperion image.
Ph.D. Thesis, 2018, NITK, Surathkal, India.

84
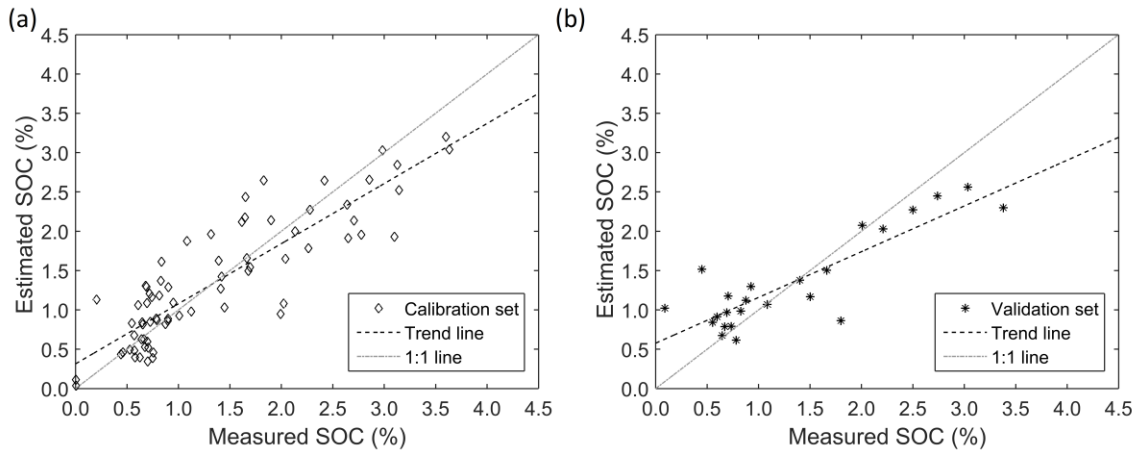
Figure 5.8 Measured vs. estimated SOC content obtained from (a) calibration set and (b) validation set of PLSR model using ATCOR corrected signals over Narrabri sites.
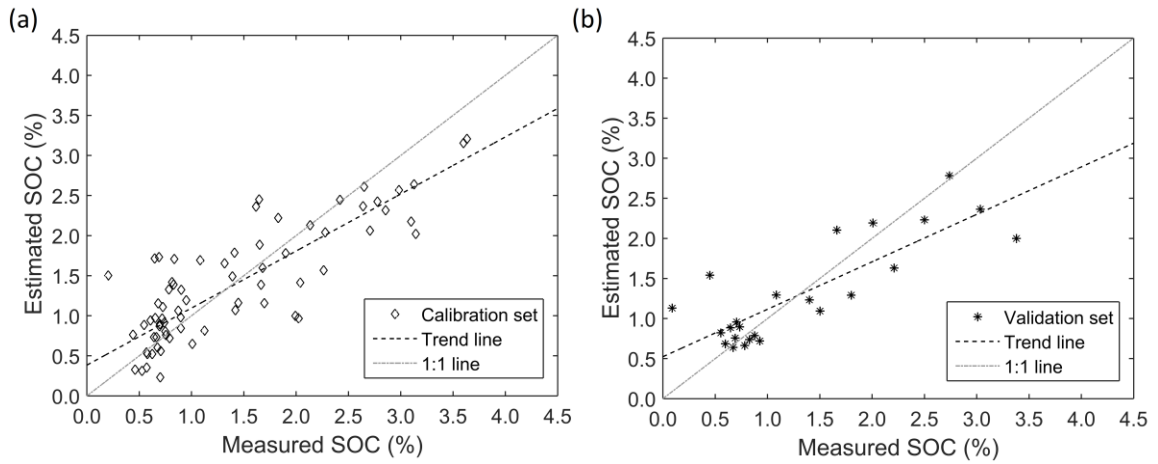
Figure 5.9 Measured vs. estimated SOC content obtained from (a) calibration set and (b) validation set of PLSR model using FLAASH corrected signals over Narrabri sites.

An evaluation of atmospheric correction algorithms in the estimation of SOC from Hyperion image.
Ph.D. Thesis, 2018, NITK, Surathkal, India.

85
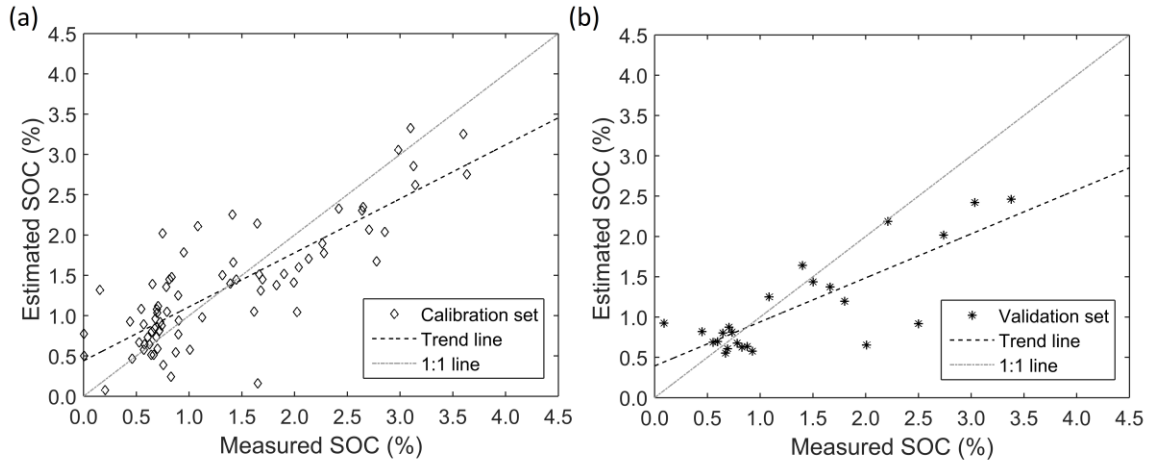
Figure 5.10 Measured vs. estimated SOC content obtained from (a) calibration set and (b) validation set of PLSR model using 6S corrected signals over Narrabri sites.
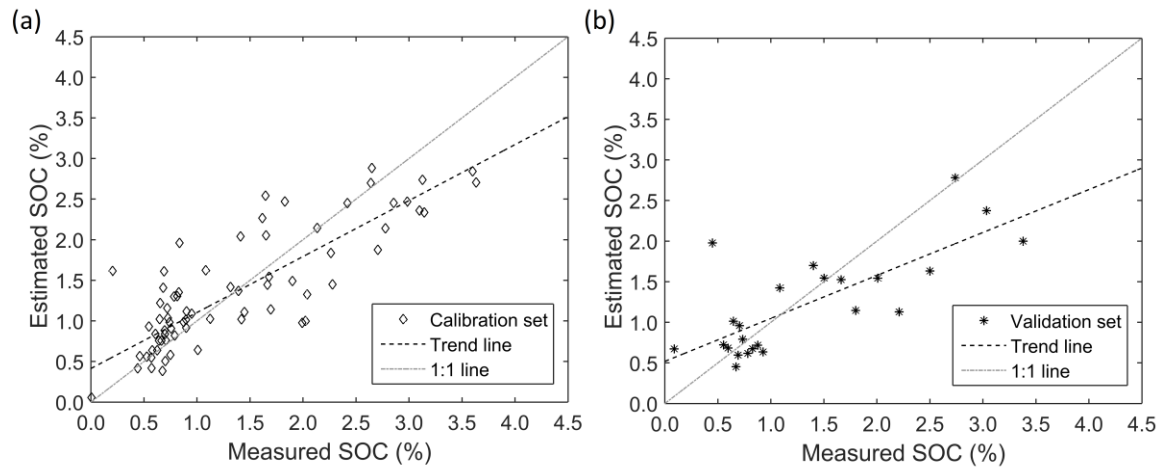
Figure 5.11 Measured vs. estimated SOC content obtained from (a) calibration set and (b) validation set of PLSR model using QUAC corrected signals over Narrabri sites.

An evaluation of atmospheric correction algorithms in the estimation of SOC from Hyperion image.
Ph.D. Thesis, 2018, NITK, Surathkal, India.

86

Table 5.6: Performance matrices of SOC estimation using atmospherically corrected Hyperion spectra over Karnataka sites.

Atmospheric correction algorithm used	Calibration set				Validation set			
	R^2_{cal}	$RMSE_{cal}$	RPD_{cal}	$RPIQ_{cal}$	R^2_{val}	$RMSE_{val}$	RPD_{val}	$RPIQ_{val}$
ATCOR	**0.74**	**0.63**	**1.97**	**2.65**	**0.61**	**0.76**	**1.64**	**2.17**
FLAASH	0.73	0.63	1.95	2.66	0.57	0.81	1.55	2.05
6S	0.69	0.66	1.69	2.47	0.55	0.82	1.52	2.02
QUAC	0.68	0.68	1.77	2.42	0.54	0.82	1.51	2.01
In bold are represented the best performances								

Table 5.7: Performance matrices of SOC estimation using atmospherically corrected Hyperion spectra over Narrabri sites.

Atmospheric correction algorithm used	Calibration set				Validation set			
	R^2_{cal}	$RMSE_{cal}$	RPD_{cal}	$RPIQ_{cal}$	R^2_{val}	$RMSE_{val}$	RPD_{val}	$RPIQ_{val}$
ATCOR	**0.76**	**0.43**	**2.07**	**2.83**	**0.71**	**0.47**	**1.90**	**2.60**
FLAASH	0.71	0.48	1.87	2.56	0.67	0.50	1.78	2.43
6S	0.67	0.52	1.83	2.40	0.58	0.57	1.57	2.14
QUAC	0.68	0.50	1.81	2.47	0.55	0.58	1.53	2.08
In bold are represented the best performances								

The results of SOC estimation from spaceborne Hyperion data are influenced by choice of the atmospheric correction algorithm employed. Though differences among the results from the four atmospheric correction algorithms are rather marginal, when the aim is to rank the model, it matters. The physics-based ATCOR atmospheric correction algorithm

An evaluation of atmospheric correction algorithms in the estimation of SOC from Hyperion image.
Ph.D. Thesis, 2018, NITK, Surathkal, India.

87

allowed to produce the best SOC estimation performances, irrespective of the study area [R^2_{val} = 0.71, RPD$_{val}$ = 1.90 and RPIQ$_{val}$ = 2.60 for Narrabri sites and R^2_{val} = 0.61, RPD$_{val}$ = 1.64 and RPIQ$_{val}$ = 2.17 for Karnataka sites] (Figures 5.4 and 5.8, Tables 5.6 and 5.7). Conversely, the semi-empirical atmospheric correction algorithm QUAC allowed to produce the lowest SOC estimation performances, irrespective of the study area [R^2_{val} = 0.55, RPD$_{val}$ = 1.53 and RPIQ$_{val}$ = 2.08 for Narrabri sites and R^2_{val} = 0.54, RPD$_{val}$ = 1.51 and RPIQ$_{val}$ = 2.01 for Karnataka sites] (Figures 5.7 and 5.11, Tables 5.6 and 5.7). FLAASH and 6S corrected algorithm produced moderate estimation performance (Figures 5.5, 5.6, 5.9 and 5.10, Tables 5.6 and 5.7).The results are also dependant on study areas. Samples of Narrabri sites were estimated more accurately compared to that of Karnataka sites (Tables 5.6 and 5.7).

Significant wavelengths from PLSR estimation models using various atmospherically corrected Hyperion signals over the Narrabri site are presented in Table 5.8 and Figure 5.12. Though the attempt was to compare the significant wavelengths computed from the field model (section 4.4 of Chapter 4) and the Hyperion data, a proper match was not seen (Figure 5.12). It is probably because the atmospherically corrected spectra from any of the algorithms have not completely followed the field pattern. Few wavelengths in 2180-2250 nm of ATCOR and 600-680 nm of QUAC coincide with significant wavelengths identified from field spectra and also, in that region they are parallel to the field reflectance. All in all, one can say that there needs to be further research required to improve on atmospheric correction algorithms.

It is noted that significant wavelengths identified from field spectra in 1860-1900 nm cannot be retrieved in Hyperion image (Figure 5.12). This is because Hyperion images fail to sense reflectance from certain regions of electromagnetic spectrum due to very strong atmospheric absorption, in this case it is in strong water absorption region. These regions cannot be retrieved by any atmospheric correction algorithms.

An evaluation of atmospheric correction algorithms in the estimation of SOC from Hyperion image.
Ph.D. Thesis, 2018, NITK, Surathkal, India.

88
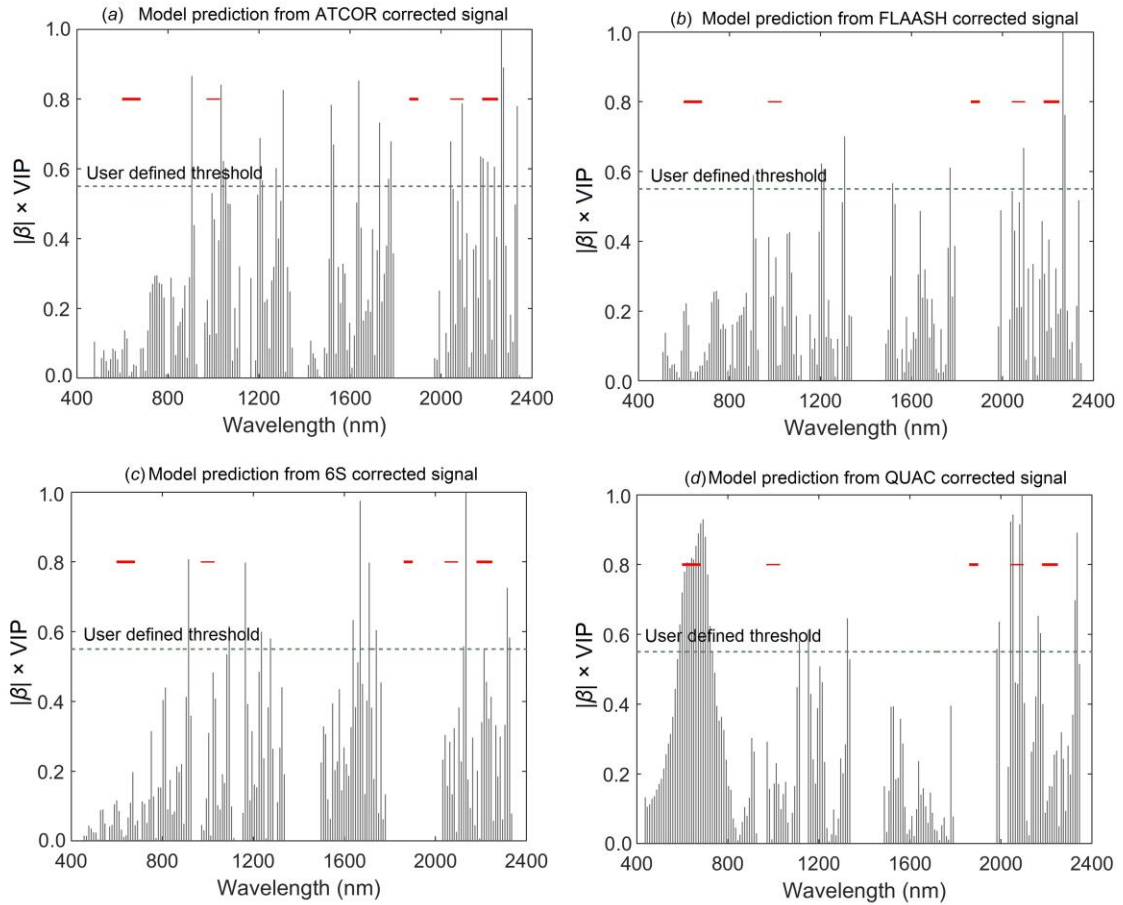
Figure 5.12 Relative scores ($|\beta| \times$ VIP) for wavelengths from PLSR estimation models using (a) ATCOR , (b) FLAASH, (c) 6S and (d) QUAC corrected signals over Narrabri sites. Red lines in the graph represent the significant wavelength sites identified from field PLSR model.

An evaluation of atmospheric correction algorithms in the estimation of SOC from Hyperion image. Ph.D. Thesis, 2018, NITK, Surathkal, India.

89

Table 5.8: Significant wavelengths identified from Hyperion-PLSR models over Narrabri

Atmospheric correction algorithm used	Significant wavelengths identified (nm)
ATCOR	905,1033,1205,1276,1306, 1518,1639,1730,1780,2042, 2093,2184,2204,2234, 2264,2335
FLAASH	640,691,1336,1488,1780, 1790,1982,2083,2093
6S	1084,1104,1114,1195,1205, 1296,1306
QUAC	590-722,1114,1155,1326, 1992,2042,2093,2174,2335

5.4 DISCUSSION

5.4.1 Performances of atmospheric models for SOC estimations using Hyperion data

When Hyperion reflectance spectra were tested in atmospheric correction models, all of them allowed acceptable SOC estimations (fall in category A, B or C as Veum et al. 2015, refer section 4.2) irrespective of the study area. Earlier study by Gomez et al. 2008, used 'Atmospheric Removal Program' (ATREM) algorithm developed by Gao and Goetz (1990) and Gao et al. (1993) that used 5S code for atmospheric correction and estimated SOC with R^2_{val} of 0.493 and RMSE of 0.8 %. The current study uses advanced atmospheric correction algorithms for Hyperion processing which gives better estimation of SOC. Among the tested atmospheric correction models, ATCOR provides more accurate SOC estimations in both study areas (Tables 5.6 and 5.7). FLAASH and 6S produced moderate estimation accuracy, whereas QUAC produced least estimation accuracy. This may be because ATCOR uses the latest HITRAN databases with the MODTRAN 5 whereas FLAASH relies on MODTRAN 4.

An evaluation of atmospheric correction algorithms in the estimation of SOC from Hyperion image.
Ph.D. Thesis, 2018, NITK, Surathkal, India.

90

In 2200 nm, an absorption band occurs in the soil signature. It is due to a combination of metal–OH bonding and O–H stretching (Das et al. 2015). This absorption band is retrieved in an ATCOR corrected signal. As the key SOC spectral feature between 2050 and 2200 nm (Bartholomeus et al. 2008) is retained by ATCOR corrected signal only, may be one of the reasons for its good estimation accuracy. In another key spectral region between 640 and 690 nm (Bartholomeus et al. 2008), QUAC corrected signal is parallel to the field reflectance, whereas the same signal in 400-640 nm region (whose slope influences SOC, Ben-Dor et al. 1997) behaves counter to field reflectance. In the 640-690 nm region, FLAASH and ATCOR behave alike and 6S varies more from field reflectance.

5.4.2 Spectral sampling distance used in atmospheric models as a driver of atmospheric correction quality

The better performance of ATCOR compared to the three other atmospheric models may be due to its spectral sampling distance (SSD). The default spectral resolution in MODTRAN uses a constant wavenumber w (1/cm) grid for the specified wavelength interval.

FLAASH uses MODTRAN with a 5cm^{-1} grid, and wavelength and wavenumber are related by the equation , λ (μm) = 10,000/w

Example, with Δw (grid)=5 cm^{-1}

 at λ =1 μm we have w=10000 and

$\Delta\lambda$= (10000/10000 - 10000/10005)

   = 0.0005 μm = 0.5 nm

At λ=2.2 μm we have w=4545.45 cm^{-1} and

$\Delta\lambda$= (10000/4545.45-10000/4550.45)

An evaluation of atmospheric correction algorithms in the estimation of SOC from Hyperion image. Ph.D. Thesis, 2018, NITK, Surathkal, India.

91

= 0.0024 μm = 2.4 nm

Therefore the wavenumber spacing is decreased to obtain a better wavelength resolution.

6S and FLAASH models use a constant wavenumber grid and obtain a variable SSD in the 400-2500 nm region (section 5.2.2.2 and 5.2.2.3), whereas ATCOR has a narrow and constant SSD of 0.4 nm for the entire spectrum (section 5.2.2.4). 6S model uses an average SSD of 0.72 nm, 1.9 nm and 9.6 nm around central wavelengths of 600 nm, 1000 nm and 2100 nm respectively. FLASSH model uses an average SSD of 0.18 nm 0.5 nm and 2.4 nm around central wavelengths of 600 nm, 1000 nm and 2100 nm respectively. What is to be noted is, owing to narrow SSD in 2000-2500nm wavelength region, ATCOR corrected soil spectra is able to capture an analogous pattern in that region compared to FLAASH or 6S. On the contrary in 400-2000 nm wavelength region, ATCOR corrected spectra is not the best since the SSDs of other algorithms are comparable or even better at some parts in this wavelength region.

According to Bellon-Maurel and McBratney 2011, the spectral range between 1650 and 2500 nm is crucial for SOC estimation. As ATCOR outperforms others in this spectral region and its narrow SSD, may be the reason for its better estimation capacity.

5.4.3 Impact of field conditions of the study area on SOC estimations

Whatever be the atmospheric correction algorithms, the obtained SOC estimation performances are better over Narrabri study area than over Karnataka study area (Tables 5.6 and 5.7). In India, agricultural fields are scattered and small in size (around 30 m x 30 m, as the Hyperion pixel size) while in Australia the fields are large and continuous (around 500 x 900 m, so highly superior to the Hyperion pixel size). This is probably due to the inability to extract pure soil signals from small Karnataka fields due to mixture effects (a Hyperion pixel may straddle more than one field and so may include several types of surface roughness and soil humidity due to the different types of ploughing

An evaluation of atmospheric correction algorithms in the estimation of SOC from Hyperion image.
Ph.D. Thesis, 2018, NITK, Surathkal, India.

92

between fields). This observation is in accordance with the one of Gomez et al. (2015a), where they observed that soil properties estimation performances depend to the spatial resolution of the sensor and the field sizes.

5.5 CONCLUSIONS

- The results showed that ATCOR spectra, among ATCOR, FLAASH, 6S and QUAC corrected spectra, produced the best SOC estimation performances, using PLSR estimation model, irrespective of the study area.

- Comparing the results across study areas, Karnataka sites gave lower estimation accuracy than Narrabri sites. This may be explained due to the difference in spatial arrangement of field conditions. In smaller fields of Karnataka, mixture effects and adjacency effects tamper the quality of spectral signature derived, which in turn affects the SOC estimation.

- A spectral similarity comparison of atmospherically corrected Hyperion spectra of the soil samples with field-measured VNIR/SWIR spectra shows that regarding spectral similarity, no atmospheric correction model seems to be superior to another one. However, the pattern in soil reflectance curve near 2200 nm is captured by ATCOR corrected spectra only. ATCOR's high spectral resolution in the atmospheric database may be the main reason for the better performance.

- Significant wavelengths for SOC estimation identified from each model were found to be different from those identified from ground-based study. This may be because the atmospheric correction algorithms applied have not reached perfection. Also narrow spectral resolution of the ground-based spectroscopy used in the study may estimate it better.

In the next chapter, development and evaluation of hybrid atmospheric correction algorithms in the estimation of SOC from Hyperion data is explained.

An evaluation of atmospheric correction algorithms in the estimation of SOC from Hyperion image.
Ph.D. Thesis, 2018, NITK, Surathkal, India.

93

<div align="right">

CHAPTER 6

</div>

DEVELOPMENT OF HYBRID ATMOSPHERIC CORRECTION ALGORITHMS AND EVALUATION IN THE ESTIMATION OF SOC FROM HYPERION DATA

6.1 INTRODUCTION

In chapter 5, a comparison of four popular atmospheric correction algorithms was carried out for retrieval of soil spectra for SOC estimation from Hyperion data. It was seen that ATCOR performs well among the tested physics-based (i.e. ATCOR, FLAASH and 6S) and empirical based (QUAC) algorithms. In this chapter, hybrid atmospheric correction algorithms, which are combinations of physics-based approaches and empirical approaches are developed. Hybrid algorithms and their component single atmospheric correction algorithms are tested for retrieval of soil spectra from Hyperion images. The methodology adopted is explained in the following section.

6.2 METHODOLOGY

In this study, two hybrid atmospheric correction (HAC) algorithms incorporating a modified empirical line (EL_m) method were proposed.

(1) The first HAC model (named HAC_1) combines i) a radiative transfer model based on the concepts of radiative transfer equations which is referred as 'RT model' hereafter, and ii) an EL_m technique. The 'RT model' applies real-time *in situ* atmospheric and climatic information in the equations of radiative transfer.

(2) The second one (named HAC_2) combines i) the well-known ATmospheric CORrection (ATCOR) model and ii) an EL_m technique.

An evaluation of atmospheric correction algorithms in the estimation of SOC from Hyperion image. Ph.D. Thesis, 2018, NITK, Surathkal, India.

94

Both HAC algorithms and their component single atmospheric correction algorithms (ATCOR, RT and EL_m) were applied to radiance data acquired by Hyperion satellite sensor over study sites in Australia (owing to the availability of full range ground truth reflectance values collected in near real-time to be used in EL_m method). The performances of both HAC algorithms were analysed in two ways. First, the Hyperion reflectances obtained by five atmospheric correction algorithms were analysed and compared using spectral metrics. Second, the performance of each atmospheric correction algorithm was analysed for prediction of SOC using Hyperion reflectances obtained from atmospheric correction algorithms over bare soil pixels. ATCOR model is used in HAC_2 since Chapter 5 found it as the best atmospheric correction algorithm among ATCOR, FLAASH, 6S and QUAC.

A general outline of process flow adopted in this study is illustrated in Figure 6.1. ρ_{s_ATCOR}, ρ_{s_RT}, ρ_{s_ELm}, $\rho_{s\_HAC\_1}$ and $\rho_{s\_HAC\_2}$ are the reflectances obtained after applying ATCOR, RT, EL_m, HAC_1 and HAC_2 algorithms respectively and are described in the following sections.

An evaluation of atmospheric correction algorithms in the estimation of SOC from Hyperion image.
Ph.D. Thesis, 2018, NITK, Surathkal, India.

95
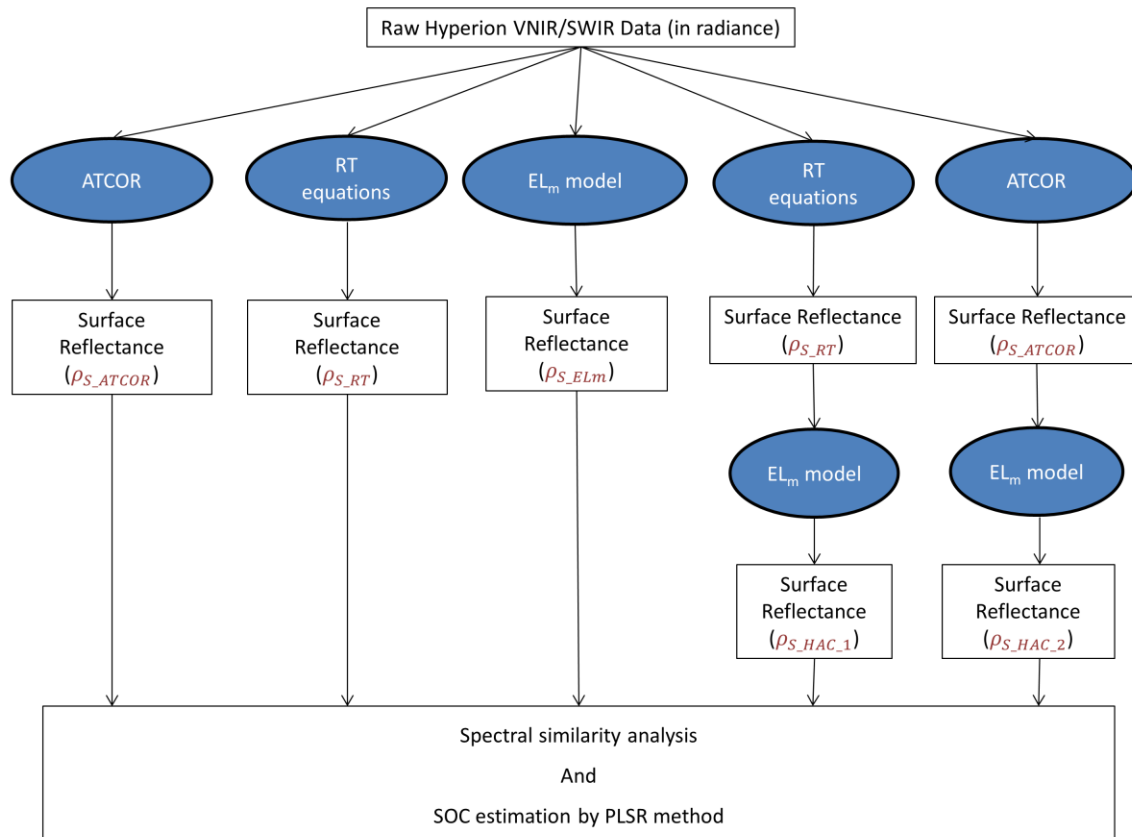
Figure 6.1 An outline of process flow adopted in the study

6.2.1 Atmospheric correction algorithms

6.2.1.1 ATCOR model

From Chapter 5 it was seen that ATCOR corrected signal performs well among the tested ATCOR, FLAASH, 6S and QUAC corrected signals in the estimation of SOC from Hyperion data. Thus, outputs from ATCOR algorithms are compared with hybrid algorithms. ATCOR model is explained in section 5.2.2.4 of Chapter 5.

An evaluation of atmospheric correction algorithms in the estimation of SOC from Hyperion image.
Ph.D. Thesis, 2018, NITK, Surathkal, India.

96

6.2.1.2 Radiative transfer (RT) model

'RT model' was developed based on concepts of RT equations, coupled with real-time *in situ* atmospheric and climatic data. Ancillary data which includes climatic data such as mean temperature, mean pressure and daily rainfall and atmospheric data such as aerosol optical thickness, ozone optical thickness and water vapour over the area for the date of acquisition of Hyperion image as given in Table 3.5 and Table 3.6 of Chapter 3 were used in this model.

Before applying RT algorithm, an initial treatment of Hyperion image is carried out by removing uncalibrated and strong water vapour-affected bands. Reflectance in these regions cannot be quantified by any atmospheric correction algorithms due to poor spectral response. After eliminating these bands, the spectral bands used are 427-925, 933-1336, 1457-1790, 1972-1992, and 2022-2355 nm.

The digital values of the Hyperion Level 1T product are 16-bit radiances and are stored as a 16-bit signed integer. To derive top-of-atmosphere (TOA) radiance image from digital values of Level 1T image, VNIR bands (bands 1-70, 400 to 1000 nm) having a scaling factor of 40 and the SWIR bands (bands 71-242, 900 to 2500 nm) having a scaling factor of 80 (as given in metadata of Hyperion image and documented in Beck 2003) were used. Radiance is the amount of radiation coming from a unit area in a specific direction. The units are W m^{-2} sr^{-1} μm^{-1}. Accordingly, TOA radiance values (L_λ) are derived from equations 6.1 and 6.2.

$$L_{\lambda,1-70} = \text{DN} / 40 \tag{6.1}$$

$$L_{\lambda,71-242} = \text{DN} / 80 \tag{6.2}$$

where DN is the digital values of the Level 1T Hyperion image and λ is the wavelength in μm.

An evaluation of atmospheric correction algorithms in the estimation of SOC from Hyperion image.
Ph.D. Thesis, 2018, NITK, Surathkal, India.

97

Top-of-atmosphere reflectance is the reflectance obtained from satellite sensor above earth's atmosphere. TOA reflectance is computed by normalizing TOA radiances to the band-averaged solar irradiance by classic formulae (equation 6.3, Tanre et al. 1983), which is a function of earth-sun geometry.

$$\rho_{\text{TOA}} = \frac{\pi \, L_\lambda \, d^2}{\text{ESUN}_\lambda \, \cos\theta_0} \tag{6.3}$$

where,

ρ_{TOA} is unitless TOA reflectance

L_λ is spectral radiance at the sensor's aperture

d is earth-sun distance in astronomical unit from nautical handbook which is a function of Julian day for day of satellite pass.

ESUN_λ is Hyperion mean solar exoatmospheric irradiances downloaded from https://eo1.usgs.gov/documents/hyp_irradiance.txt

θ_0 is Solar zenith angle in degrees

The next and the most important stage is to derive surface reflectance from TOA reflectance. TOA reflectance includes information of earth's surface reflectance attenuated by atmospheric processes like scattering by gas mixture (Rayleigh scattering), absorption by gas mixture, absorption by ozone, scattering and absorption by aerosols and absorption by water vapour. To simulate surface reflectance image, the present RT model requires information such as:

   i.   sun-sensor geometry at the time of imaging,
   ii. surface pressure,
   iii. precipitable water vapour in vertical path,

An evaluation of atmospheric correction algorithms in the estimation of SOC from Hyperion image. Ph.D. Thesis, 2018, NITK, Surathkal, India.

98

iv. aerosol type and atmosphere model,

v. aerosol optical thickness at 550 nm and

vi. ozone concentration

Purpose of this atmospheric correction model is to retrieve the target soil reflectance from the satellite image and use it for extracting SOC, so a varying spectral sampling distance is used, giving more importance to significant regions for SOC estimation. Section 4.4 of chapter 4 identifies 600-680 nm, 950-1050 nm, 2060-2080 nm and 2180–2250 nm as critical in estimating SOC. Thus an SSD of 0.4 nm is applied in these regions. For the rest of the wavelength regions, SSD of 1 nm is applied to reduce the computational efforts.

RT model used in the present study applies the concepts of Bird and Riordan (1986) designed for rural terrestrial applications that calculate direct and diffuse spectral irradiance at the earth's surface for cloudless sky conditions. When the surface is assumed as Lambertian and atmosphere is assumed to be horizontally stratified, the TOA spectral reflectance can also be estimated using equation 6.4 (Tanre et al. 1983; Vermote et al. 1997b). Here, the multiple scattering between molecules and aerosols is neglected which makes it unreliable at large zenith angle and at high latitudes (Grey and North, 2009). All calculations are functions of wavelength λ.

$$\rho_{\text{TOA}} = \rho_{\text{r}} + \rho_{\text{a}} + T_{\theta_0} T_{\theta_v} \frac{\rho_{\text{s\_RT}}}{(1 - s\,\rho_{\text{s\_RT}})} \tag{6.4}$$

where,

ρ_{r} and ρ_{a} are the reflectances resulting from Rayleigh and aerosol scattering and detailed expression for the same are given under appropriate heading later in this section

$\rho_{\text{s\_RT}}$ ground reflectance obtained after solving RT equations

s is the spherical albedo of the atmosphere

An evaluation of atmospheric correction algorithms in the estimation of SOC from Hyperion image. Ph.D. Thesis, 2018, NITK, Surathkal, India.

99

T_{θ_0} is the total transmission of the atmosphere from the sun to the surface

T_{θ_v} is the total transmission of the atmosphere from the surface to the sensor.

Figure 6.2 shows a conceptual sketch of the expressions.
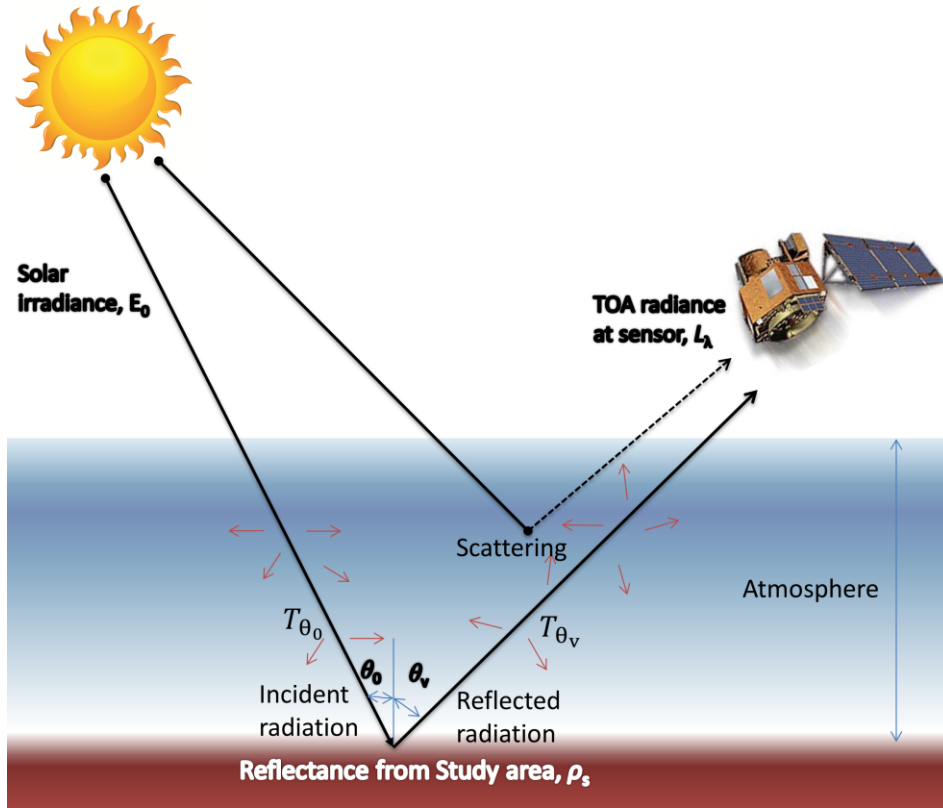
Figure 6.2 Conceptual sketch

The model uses the following expressions (equations 6.5 to 6.11) that use concepts given by Bird and Riordan (1986).

$$T_{\theta_0} = e^{-(\tau_r + \tau_a + \tau_w + \tau_o + \tau_u)/\cos\theta_o} \tag{6.5}$$

$$T_{\theta_v} = e^{-(\tau_r + \tau_a + \tau_w + \tau_o + \tau_u)/\cos\theta_v} \tag{6.6}$$

An evaluation of atmospheric correction algorithms in the estimation of SOC from Hyperion image.
Ph.D. Thesis, 2018, NITK, Surathkal, India.

100

$$\tau_r = \frac{P}{P_0}[\lambda^4(115.6406 - \frac{1.335}{\lambda^2})]^{-1} \qquad (6.7)$$

$$\tau_a = \beta_\lambda \ \lambda^{-\alpha} \qquad (6.8)$$

$$\tau_w = \frac{0.2385a_{w\lambda}W}{(1+20.07a_{w\lambda}W)^{0.45}} \qquad (6.9)$$

$$\tau_o = a_{o\lambda}O_3 \qquad (6.10)$$

$$\tau_u = \frac{P}{P_0}\frac{1.41a_{u\lambda}}{(1+118.3a_{u\lambda})^{0.45}} \qquad (6.11)$$

where,

τ_r is rayleigh optical thickness (Equation 6.7 is numerical approximation for rayleigh optical thickness used in Bird and Riordan (1986) which was adopted from Kneizys et al. 1980.)

τ_a is aerosol optical thickness

τ_w is water vapour optical thickness

τ_o is ozone optical thickness

τ_u is uniform air optical thickness

θ_0 is Solar zenith angle

θ_v is viewing zenith angle

$P_0 = 1013$ mb is the standard pressure at sea level

α and β_λ are obtained for rural aerosol model (Shettle and Fenn 1975). Two α values were used for this aerosol model: $\alpha_1 = 1.0274$ for wavelengths < 550 nm and $\alpha_2 = 1.2060$ for

An evaluation of atmospheric correction algorithms in the estimation of SOC from Hyperion image.
Ph.D. Thesis, 2018, NITK, Surathkal, India.

101

wavelengths > 550 nm. The value of β_λ was chosen appropriately for each wavelength interval to produce aerosol optical depth in a vertical path at 550 nm wavelength. Equation 6.8 is known as Angstrom formula.

$a_{w\lambda}$ is water vapour absorption coefficient (Bird and Riordan 1986)

$a_{o\lambda}$ is ozone absorption coefficient (Bird and Riordan 1986)

$a_{u\lambda}$ is absorption coefficient of uniformly mixed gaseous amount (Bird and Riordan 1986)

P is *in situ* surface pressure in mb

W is *in situ* precipitable water vapour (cm) in a vertical path

O_3 is *in situ* ozone amount (atm-cm)

Rayleigh reflection:

The Rayleigh reflectance, ρ_r, is estimated (Gordon et al. 1988) according to equation 6.12:

$$\rho_r = \tau_r \times p_r(\theta_0, \theta_v, \Delta\phi) \times (4\cos\theta_0 \cos\theta_v)^{-1} \tag{6.12}$$

where

$\Delta\phi$ is the relative azimuth angle between sun and sensor.

The function $p_r(\theta_0, \theta_v, \Delta\phi)$ is given by equation 6.13.

$$p_r(\theta_0, \theta_v, \Delta\phi) = P_r(\Theta_-) + [r(\theta_v) + r(\theta_0)] P_r(\Theta_+) \tag{6.13}$$

where

An evaluation of atmospheric correction algorithms in the estimation of SOC from Hyperion image. Ph.D. Thesis, 2018, NITK, Surathkal, India.

102

$\Theta_{\pm}$ is the scattering angle that is calculated from sun sensor geometry (equation 6.14). The term involving Θ_- in equation 6.13 provides the contribution due to photons which are backscattered from the atmosphere without interacting with the ground surface. The terms involving Θ_+ account for those photons which are scattered in the atmosphere toward the ground surface and then specularly reflected from the surface into the field of view of the sensor as well as photons which are first specularly reflected from the ground surface and then scattered by the atmosphere into the field of view of the sensor.

$$\cos \Theta_{\pm} = \pm \cos \theta_0 \cos \theta_v - \sin \theta_0 \sin \theta_v \cos \left| \phi_o - \phi_v \right| \tag{6.14}$$

where ϕ_o and ϕ_v are the sun and sensor azimuth angles.

$P_r(\Theta)$ is the Rayleigh scattering phase function for scattering angle Θ given by equation 6.15 and $r(\theta)$ is the Fresnel reflectance for air-incident rays at an incidence angle θ given by equations 6.16 and 6.17.

$$P_r(\Theta) = 0.75(1 + \cos^2 \Theta) \tag{6.15}$$

$$r(\theta) = 0.5 \left\{ \frac{\sin^2(\theta - \theta_t)}{\sin^2(\theta + \theta_t)} + \frac{\tan^2(\theta - \theta_t)}{\tan^2(\theta + \theta_t)} \right\} \tag{6.16}$$

$$\theta_t = \sin^{-1}(n_s \sin \theta) \tag{6.17}$$

where θ_t is the angle of transmittance and n_s is the refractive index of soil with respect to air, taken as 1.50.

Aerosol reflection:

Aerosol reflection, ρ_a, is assumed for rural atmosphere as the region under investigation falls in it. ρ_a is given by equation 6.18 (Bilal et al. 2013).

$$\rho_a = \tau_a \times p_a(\theta_0, \theta_v, \Delta\phi) \times w_\lambda \times (4 \cos \theta_0 \cos \theta_v)^{-1} \tag{6.18}$$

An evaluation of atmospheric correction algorithms in the estimation of SOC from Hyperion image.
Ph.D. Thesis, 2018, NITK, Surathkal, India.

103

where,

w_λ is aerosol single scattering albedo (SSA), a function of wavelength, which is given by equation 6.19 (Bird and Riordan 1986):

$$w_\lambda = \mathrm{w}_{0.4}\, e^{-\mathrm{w}\prime\left(\ln\frac{\lambda}{0.4}\right)^2} \tag{6.19}$$

For rural aerosol model, $\mathrm{w}_{0.4} = 0.945$ and $\mathrm{w}\prime = 0.095$.

$p_a(\theta_0, \theta_v, \Delta\phi)$ is aerosol scattering phase function. A modified Henyey–Greenstein phase function (Cornette and Shanks 1992) which is close to the Mie phase function is used and is given by equation 6.20.

$$p_a(\theta_0, \theta_v, \Delta\phi) = \frac{3}{2}\frac{(1-g^2)}{(2+g^2)}\frac{(1+\cos^2(\pi-\Theta))}{[1+g^2-2\,g\,\cos(\pi-\Theta)]^{3/2}} \tag{6.20}$$

where Θ is scattering phase angle calculated from sun sensor geometry (equation 6.14).

g is asymmetry parameter that indicates the relative dominance of forward / back scattering and it remains constant for most of the aerosol models. For rural model it is taken as 0.652.

After calculating all parameters, equation 6.4 is solved for surface reflectance ρ_{s_RT}. The MATLAB codes used are given in Appendix I at the end of the report.

6.2.1.3 Modified Empirical Line (EL$_m$) model

EL$_m$ model uses empirical relationships between TOA reflectance and field reflectance measured in the field using spectroradiometer at different ground targets. Gain and offset were obtained from the slope and intercept parameters estimated using simple linear regression between TOA reflectance and known field reflectance from ground targets (GTs) for each spectral band. The model employed this gain and offset to generate new image with surface reflectance (ρ_{s_ELm}) using equation 6.21 for each band.

An evaluation of atmospheric correction algorithms in the estimation of SOC from Hyperion image.
Ph.D. Thesis, 2018, NITK, Surathkal, India.

104

$$\rho_{\text{s\_ELm}_\lambda} = G_\lambda \times \rho_{\text{TOA}_\lambda} + O_\lambda \tag{6.21}$$

where,

G_λ is the gain for the spectra at wavelength λ,

O_λ is the offset for the spectra at wavelength λ, and

$\rho_{\text{TOA}_\lambda}$ is TOA reflectance at wavelength λ.

Determination of G_λ and O_λ parameters was based on the use of field reflectance spectra acquired over GTs composed of bare soil. In order to fix an optimum number of GTs required to calibrate the G_λ and O_λ parameters in the emiprical line equation (6.21), an experimental approach was adopted.

The number of GTs (N) used was varied till the variation in the index becomes negligible and the optimum number of soil GTs is found out to calibrate empirical line equation (i.e equation 6.21 for EL_m method) for calculating gain and offset parameters. An independent equation was calibrated per Hyperion image. Over Narrabri Site#1 image, GTs were chosen among 46 field VNIR/SWIR spectra, and over Narrabri Site #2 image, the GTs were chosen among 52 field VNIR/SWIR spectra. For each N number of GTs, 100 random combinations of GTs were analysed and so 100 equations (i.e. equation 6.21 for EL_m method) were calibrated. Thus, robustness of model was tested by selecting 100 different combinations of samples for each N. This ensures selection of optimum number of GTs without any dependency of selected field spectra on the model efficiency.

In each case, the performance of EL_m model was evaluated by comparing the corrected image reflectance and the corresponding field reflectance of GTs excluding that used in EL_m method. Comparison is facilitated by calculating two spectral similarity indices:

(1) Spectral Angle Mapper (SAM) and

An evaluation of atmospheric correction algorithms in the estimation of SOC from Hyperion image. Ph.D. Thesis, 2018, NITK, Surathkal, India.

105

(2) Spectral Information Divergence (SID).

SAM index is explained in section 5.2.4 of Chapter 5. SAM index discriminates two spectra by calculating the angle between them using equation 5.1

SID index is used to find the spectral similarity between two spectra *t* and *r* by measuring the discrepancy of probabilistic behaviours between their spectra (Chang 1999). It is calculated using equation 6.22:

$$\text{SID} = \sum_{i=1}^{m} t_i \log\left(\frac{t_i}{r_i}\right) + \sum_{i=1}^{m} r_i \log\left(\frac{r_i}{t_i}\right) \tag{6.22}$$

where *m* is the total number of bands used.

The lower the SAM and SID index, the better is the similarity of both spectral vectors. The *N* spectra that have been used to find gain and offset were removed from the soil dataset, and the similarity of remaining spectra with corresponding field spectra (in terms of SAM and SID index) was evaluated. Gain and offset were calculated separately for both images of Narrabri (over Site #1 and Site #2) and equation 6.21 was solved for each image. The MATLAB codes used are given in Appendix I at the end of the report.

6.2.1.4 HAC_1 model

The first hybrid atmospheric model tested was a combination of EL_m corrections carried out on the output of RT model (explained in section 6.2.1.2), which removes artefacts from errors in the radiative models, and was named as HAC_1. The surface reflectance obtained using radiative transfer equations (ρ_{s_RT}) was then matched with known field reflectance from GTs for each spectral band, which were obtained from remote-sensing overflight, to get gain and offset for each wavelength.

An evaluation of atmospheric correction algorithms in the estimation of SOC from Hyperion image.
Ph.D. Thesis, 2018, NITK, Surathkal, India.

106

To fix an optimum number of GTs, the approach described in section 6.2.1.3 was used. With the optimum number of GTs, gain and offset were calibrated for each spectral band. The HAC_1 model employed this gain and offset to generate new image with surface reflectance ($\rho_{s\_HAC\_1}$) using equation 6.23.

$$\rho_{s\_HAC\_1_\lambda} = G_\lambda \times \rho_{s\_RT_\lambda} + O_\lambda \qquad (6.23)$$

Corrected reflectance image ($\rho_{s\_HAC\_1}$) was obtained separately for both Hyperion images.

6.2.1.5 HAC_2 model

The second hybrid atmospheric correction model tested was a combination of EL_m corrections carried out on ATCOR-retrieved reflectance data and was named HAC_2. This hybrid model removes artefacts from ATCOR model. Gain and offset were obtained from slope and intercept parameters estimated using simple linear regression between ATCOR reflectance (ρ_{s_ATCOR}) and known field reflectance from GTs for each spectral band. To fix an optimum number of GTs, the approach described in section 6.2.1.3 was used. With the optimum number of GTs, gain and offset were calibrated for each spectral band. The HAC_2 model employed this gain and offset to generate new image with surface reflectance ($\rho_{s\_HAC\_2}$) using equation 6.24.

$$\rho_{s\_HAC\_2_\lambda} = G_\lambda \times \rho_{s\_ATCOR_\lambda} + O_\lambda \qquad (6.24)$$

Corrected reflectance image ($\rho_{s\_HAC\_2}$) was obtained separately for both Hyperion images.

6.2.2 Reflectance spectra analysis

Comparison and validation of the atmospherically corrected Hyperion images obtained by the atmospheric correction methods, with field spectral measurements (resampled to Hyperion resolution) from region under investigation, were carried out using the SAM

An evaluation of atmospheric correction algorithms in the estimation of SOC from Hyperion image.
Ph.D. Thesis, 2018, NITK, Surathkal, India.

107

indices. To get a deeper understanding of performance of atmospheric correction algorithm in different regions of electromagnetic spectrum, SAM was applied separately in three wavelength domains (as done in section 5.2.4 of Chapter 5). First spectral domain ranges from 400 to 1050 nm, second from 1500 to 1790 nm and third from 2000 to 2350 nm.

6.2.3 Soil Organic Carbon Estimation

The soil spectra from corrected Hyperion reflectance images were analysed for estimating SOC using PLSR method. The soil dataset (SOC content and corresponding Hyperion reflectance) were divided into two groups: one group for calibration of PLSR model (3/4 of the dataset) and a second group used for validation/prediction (1/4 of the database) (see section 4.2.2 of Chapter 4). However, to estimate SOC after EL_m method, the spectra that have been used to find the gain and offset were removed from the soil dataset. Grouping of data into calibration and validation sets is explained in section 4.2.2 of Chapter 4 and section 5.2.5 of Chapter 5. An optimum number of PLS components (NF) minimizes the mean square prediction error in cross-validation and ensures dimensionality reduction in subsequent regression analysis.

The performance of PLSR models was evaluated using R^2, RPD, and RPIQ in both calibration and validation sets. Equations for evaluating these performance matrices are given in equations 4.1 to 4.4.

Finally, significant wavelengths for SOC estimation were identified from PLSR output by analysing the product of absolute regression coefficient and variable importance for projection ($|\beta| \times$ VIP) (as explained in section 4.4 of Chapter 4).

An evaluation of atmospheric correction algorithms in the estimation of SOC from Hyperion image.
Ph.D. Thesis, 2018, NITK, Surathkal, India.

108

6.3 RESULTS

6.3.1 Selection of optimum number of ground targets (GTs) in EL_m and hybrid models

Number of GTs (N) were varied to calibrate EL equations (equations 6.21, 6.23 and 6.24) of EL_m, HAC_1 and HAC_2 models for calculating the gain and offset parameters. For each N number of GTs, 100 random combinations of GTs were analysed and so 100 equations (for equations 6.21, 6.23 and 6.24) were calibrated. SAM and SID indices were calculated between the field VNIR/SWIR spectra and the corresponding Hyperion reflectance spectra (except the N GTs used to calibrate the model) estimated by i) EL_m technique (red lines in Figures 6.3 and 6.4), ii) HAC_1 model (green lines in Figures 6.3 and 6.4) and iii) HAC_2 model (blue lines in Figures 6.3 and 6.4).

The variances obtained are given in Table 6.1 and 6.2. An optimum number of GTs is arrived considering the following criteria in totality:

1) Mean of SAM and SID values should be minimum,
2) Variance in SAM and SID values should be minimum, and
3) Minimum number of GTs reduce the field work and thereby make it more cost effective.

An increase of number N allows to decrease the mean SAM and SID indices and improves the quality of estimated surface reflectance spectra (Figures 6.3 and 6.4). Moreover, from N=8, the means of SAM and SID indices are stable, so the quality of estimated surface reflectance spectra is almost stable. Also, when N increases, the variance of SAM and SID indices decreases, and from N=8, the variation is negligible. (Tables 6.1 and 6.2). Same behaviour is obtained for EL_m, HAC_1 and HAC_2 models.

An evaluation of atmospheric correction algorithms in the estimation of SOC from Hyperion image.
Ph.D. Thesis, 2018, NITK, Surathkal, India.

109

Also, same behaviour is obtained whatever the tested Hyperion image (Narrabri site #1 and Narrabri site #2) (Figures 6.3, 6.4 and Tables 6.1 and 6.2). In addition considering a minimum number of GTs satisfying the purpose, the optimum number of GTs is chosen as eight in all the cases namely EL_m, HAC_1 and HAC_2 from both the images. Thus, the three atmospheric correction algorithms using modified empirical line technique (EL_m, HAC_1 and HAC_2) were run using an optimum number of eight GTs selected randomly.

An evaluation of atmospheric correction algorithms in the estimation of SOC from Hyperion image. Ph.D. Thesis, 2018, NITK, Surathkal, India.

110
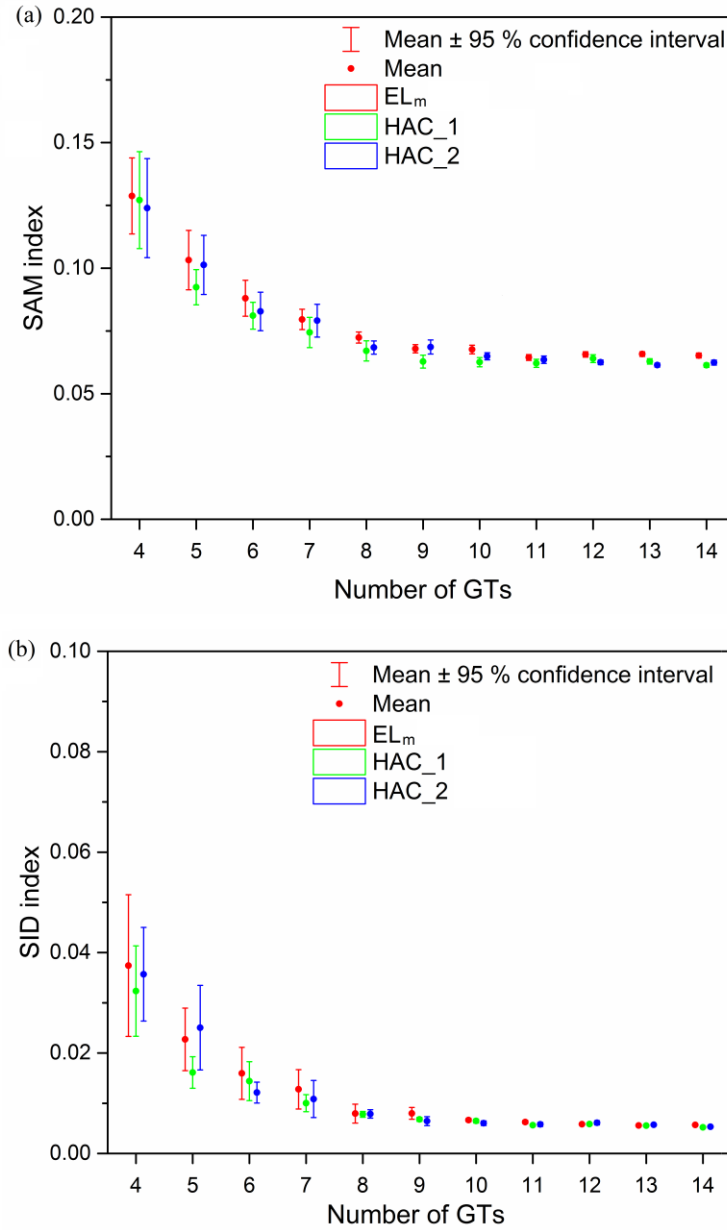
Figure 6.3 (a) SAM and (b) SID indices calculated between the field reflectance spectra and the corresponding Hyperion reflectance spectra corrected by EL_m, HAC_1 and HAC_2 models using *N* ground targets (GTs) (from 4 to 14), over Narrabri site#1 image

An evaluation of atmospheric correction algorithms in the estimation of SOC from Hyperion image.
Ph.D. Thesis, 2018, NITK, Surathkal, India.

111
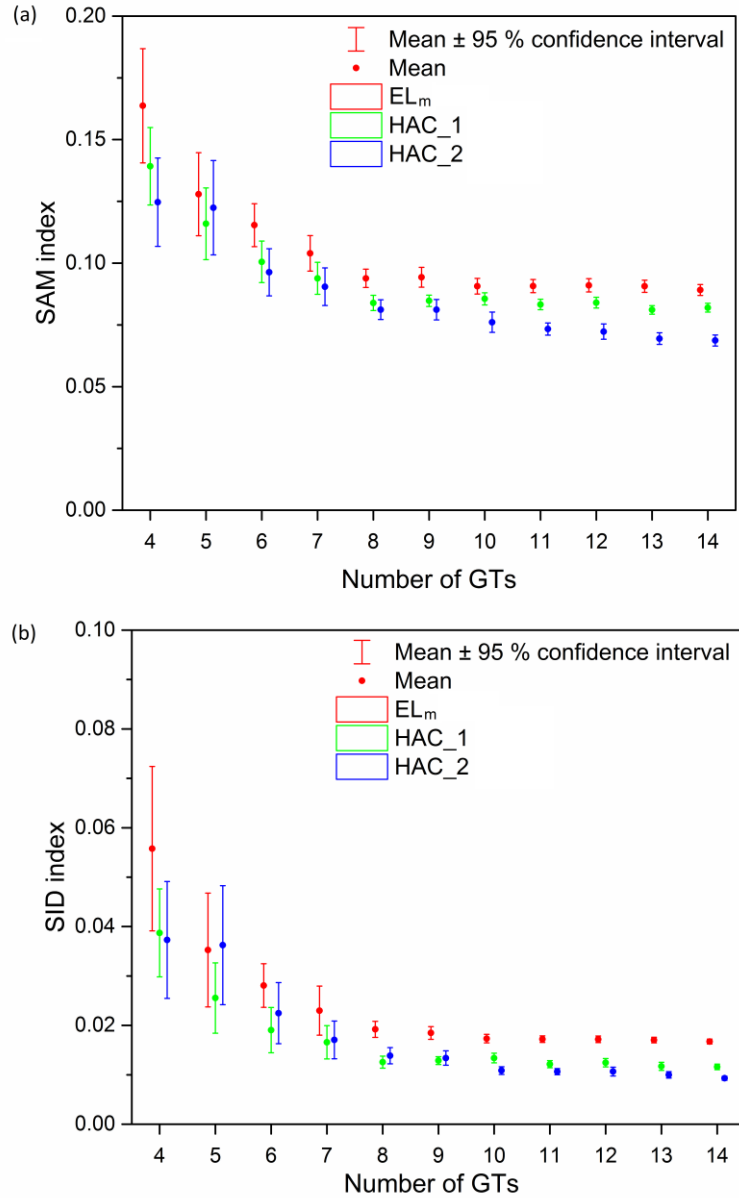
Figure 6.4 (a) SAM and (b) SID indices calculated between the field reflectance spectra and the corresponding Hyperion reflectance corrected by EL_m, HAC_1 and HAC_2 models using *N* ground targets (GTs) (from 4 to 14), over Narrabri site#2 image

An evaluation of atmospheric correction algorithms in the estimation of SOC from Hyperion image.
Ph.D. Thesis, 2018, NITK, Surathkal, India.

112

Table 6.1 Variances of SAM and SID indices of Narrabri site#1 image

No. of GTs	EL_m		HAC_1		HAC_2	
(*N*)	SAM	SID	SAM	SID	SAM	SID
4	5.87E-03	2.19E-03	9.55E-03	2.04E-03	9.99E-03	4.99E-03
5	3.59E-03	1.79E-03	1.26E-03	2.47E-04	3.56E-03	9.73E-04
6	1.32E-03	3.77E-04	7.33E-04	1.08E-04	1.51E-03	6.75E-04
7	4.20E-04	7.15E-05	9.33E-04	3.43E-04	1.10E-03	3.87E-04
8	7.00E-05	8.57E-06	1.70E-04	8.82E-05	1.78E-04	1.76E-05
9	6.81E-05	3.93E-06	1.71E-04	1.99E-05	2.03E-04	3.53E-05
10	7.81E-05	4.24E-06	8.66E-05	4.88E-06	5.11E-05	3.05E-06
11	3.59E-05	1.92E-06	6.73E-05	4.20E-06	5.43E-05	3.30E-06
12	2.93E-05	2.03E-06	6.43E-05	4.34E-06	2.28E-05	1.18E-06
13	2.34E-05	1.47E-06	2.98E-05	1.72E-06	1.62E-05	9.48E-07
14	2.50E-05	1.45E-06	1.89E-05	8.27E-07	2.44E-05	1.37E-06

An evaluation of atmospheric correction algorithms in the estimation of SOC from Hyperion image.
Ph.D. Thesis, 2018, NITK, Surathkal, India.

113

Table 6.2 Variances of SAM and SID indices of Narrabri site#2 image

No. of GTs (N)	EL$_m$		HAC_1		HAC_2	
	SAM	SID	SAM	SID	SAM	SID
4	1.37E-02	6.96E-03	6.32E-03	1.99E-03	8.21E-03	3.52E-03
5	7.26E-03	3.34E-03	5.41E-03	1.27E-03	9.35E-03	3.64E-03
6	1.94E-03	4.90E-04	1.82E-03	5.26E-04	2.33E-03	9.61E-04
7	1.33E-03	6.20E-04	1.08E-03	2.83E-04	1.49E-03	3.67E-04
8	3.54E-04	6.66E-05	2.47E-04	3.76E-05	4.10E-04	6.75E-05
9	4.09E-04	4.16E-05	1.35E-04	1.56E-05	4.37E-04	5.35E-05
10	2.59E-04	1.84E-05	1.76E-04	2.44E-05	4.09E-04	1.51E-05
11	1.83E-04	1.13E-05	1.15E-04	1.33E-05	1.55E-04	9.62E-06
12	1.86E-04	1.14E-05	1.21E-04	1.86E-05	2.46E-04	2.02E-05
13	1.56E-04	8.02E-06	7.61E-05	1.71E-05	1.42E-04	1.06E-05
14	1.26E-04	5.98E-06	7.98E-05	7.93E-06	9.83E-05	4.27E-06

An evaluation of atmospheric correction algorithms in the estimation of SOC from Hyperion image.
Ph.D. Thesis, 2018, NITK, Surathkal, India.

114

6.3.2 Spectral similarity comparison

Soil reflectance spectra over bare soil pixels were extracted from both Hyperion images (Narrabri site#1 and site#2) and were subjected after each atmospheric correction algorithms. Corresponding soil sample reflectances on the ground were considered together for further analysis.

SAM indices were used to compare soil reflectance retrieved from corrected Hyperion images with corresponding field reflectances. Summary of mean and standard deviation of SAM indices applied in three spectral domains: 400 to 1050 nm, 1500 to 1790 nm and 2000 to 2350 nm is given in Table 6.3.

Table 6.3 Mean (μ) and Standard deviation (σ) of SAM indices.

Atmospheric correction algorithm used	Domain 1 400 to 1050 nm		Domain 2 1500 to 1790 nm		Domain 3 2000 to 2350 nm	
	μ	σ	μ	σ	μ	σ
ATCOR	0.130	0.081	0.037	0.020	0.057	0.028
RT	0.113	0.031	0.032	0.011	0.090	0.013
EL$_m$	0.069	0.036	0.029	0.011	0.049	0.019
HAC_1 model	**0.067**	0.040	**0.012**	0.008	**0.022**	0.008
HAC_2 model	0.069	0.035	0.027	0.016	0.037	0.018
					In bold are represented the best values per tested domain.	

An evaluation of atmospheric correction algorithms in the estimation of SOC from Hyperion image. Ph.D. Thesis, 2018, NITK, Surathkal, India.

115

Lower SAM values (near to 0 which is considered as perfect match) indicate a better similarity with field reflectance spectrum in all domains. Among the physics-based ATCOR and RT models, RT seems to be better with lower SAM values in 400 to 1050 nm and 1500 to 1790 nm domains, while ATCOR seems to be better in 2000 to 2350 nm domain. The EL_m model provides spectra with lower SAM values than ATCOR and RT, whatever maybe the spectral domain (Table 6.3). It may be explained because of the use of field reflectance in EL_m model. The spectral similarity of Hybrid models seems to be superior to others with lower SAM values in all domains (Table 6.3). Among the hybrid models, HAC_1 model seems to be better with lower SAM values, especially in 1500 to 1790 nm and 2000 to 2350 nm domains.

Figure 6.5 shows average spectral reflectance pattern of bare soil pixels over the study sites in three spectral domains. Each corrected Hyperion average reflectance spectrum is compared with field average reflectance spectrum. It is noted that both the hybrid models produce a good spectrum, contrasting other single models (ATCOR, RT or EL_m), irrespective of the spectral domain. HAC_1 model matches with field reflectance in magnitude and shape throughout the spectral domain considered. Average magnitude seems to be underestimated by the ATCOR model having maximum variation. All reflectance spectra, except RT corrected spectra, were able to capture the dip in spectral signature of soil near 2200 nm.

An evaluation of atmospheric correction algorithms in the estimation of SOC from Hyperion image. Ph.D. Thesis, 2018, NITK, Surathkal, India.

116
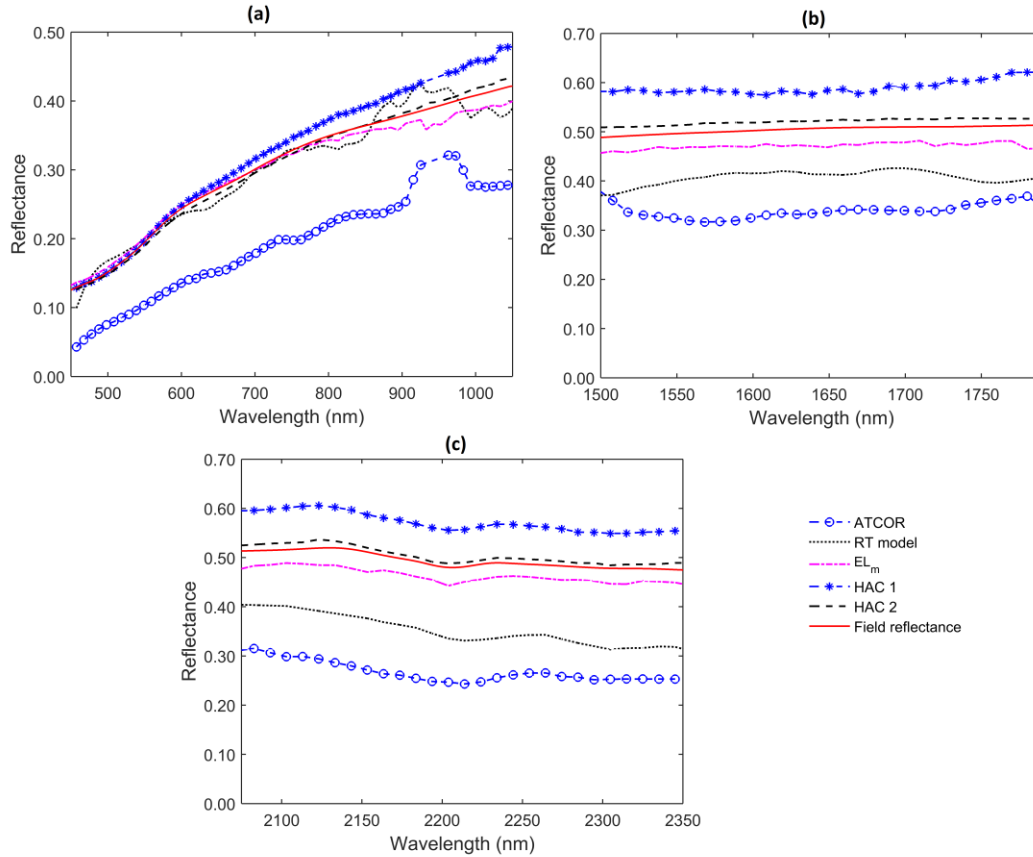
Figure 6.5 Average reflectance spectra over bare soils from corrected pixels and average field spectra, in the following spectral regions: (a) 400 to 1050 nm-Domain 1, (b) 1500 to 1790 nm-Domain 2 and (c) 2000 to2350 nm-Domain 3.

An evaluation of atmospheric correction algorithms in the estimation of SOC from Hyperion image.
Ph.D. Thesis, 2018, NITK, Surathkal, India.

117

6.3.3 PLSR analysis

PLSR models were built for SOC estimation from ATCOR, RT, EL_m, HAC_1 and HAC_2 corrected Hyperion reflectance spectra. Output of PLSR model using ATCOR corrected signal over the Narrabri sites was already presented in section 5.3.2 of Chapter 5.

As the first step, optimum number of PLS components (NF) required was identified for each model and the results are tabulated in Table 6.4. Graphs of percentage variance in the model explained by each component and estimated MSEP corresponding to ten PLS components were plotted (Table 6.4). NF was identified in each case, which minimizes MSEP in cross-validation.

Table 6.4 Results of optimum number of PLS component (NF) selection

Spectrum used	Variance in Y explained by 10 components	Estimated MSEP in Y for 10 components	NF
RT corrected			3

An evaluation of atmospheric correction algorithms in the estimation of SOC from Hyperion image. Ph.D. Thesis, 2018, NITK, Surathkal, India.

118

EL$_m$ corrected			4
HAC_1 corrected			4
HAC_2 corrected			6

Each PLSR model, run with an optimum number of PLS components, was used to estimate SOC from atmospherically corrected Hyperion spectra. Figures 6.6 to 6.9 show

An evaluation of atmospheric correction algorithms in the estimation of SOC from Hyperion image.
Ph.D. Thesis, 2018, NITK, Surathkal, India.

119

scatterplots of SOC estimation results in calibration and validation sets of RT, EL_m, HAC_1 and HAC_2. It shows qualitatively the spread of estimation with respect to 1:1 line and also the general trend of estimation. At lower SOC, the trend line shows that the estimation is overestimated whereas at higher SOC, it is underestimated. The distribution of SOC collected from Narrabri sites is skewed with more samples having SOC content from 0.5% to 1.5%, the estimation is reliable in those regions as observed from scatterplots and trend lines (Figures 6.6 to 6.9). The performance during calibration and validation are quantitatively represented using performance matrices in Table 6.5.
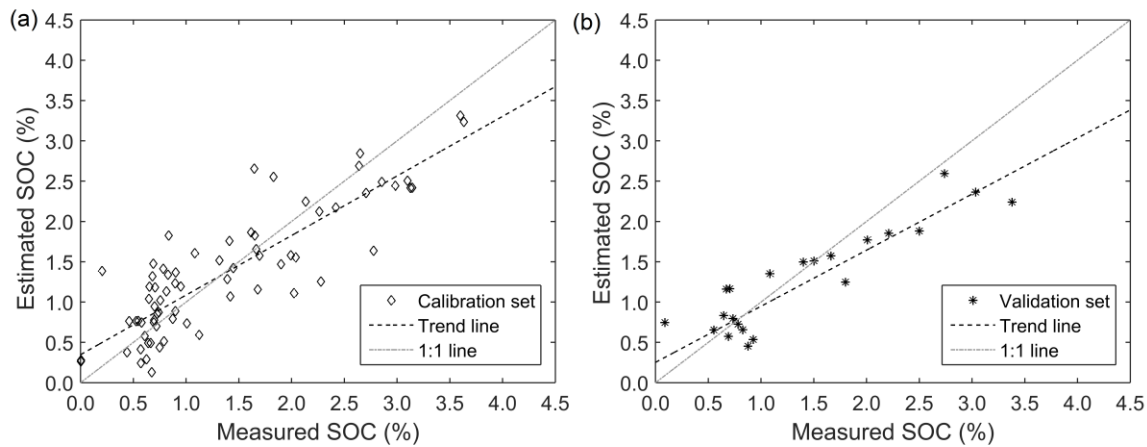
Figure 6.6 Measured vs. estimated SOC content obtained from (a) calibration set and (b) validation set of PLSR model using RT corrected signals over Narrabri sites.

An evaluation of atmospheric correction algorithms in the estimation of SOC from Hyperion image.
Ph.D. Thesis, 2018, NITK, Surathkal, India.

120
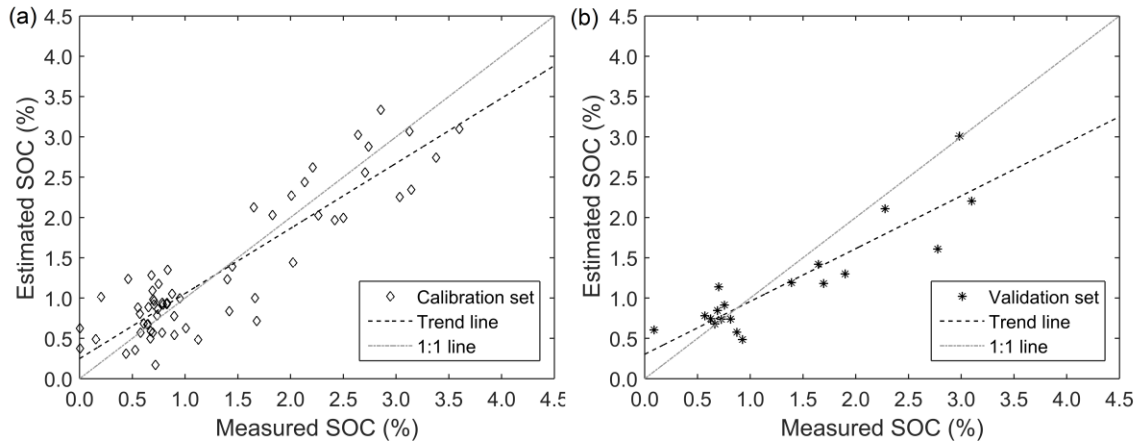
Figure 6.7 Measured vs. estimated SOC content obtained from (a) calibration set and (b) validation set of PLSR model using EL_m corrected signals over Narrabri sites.
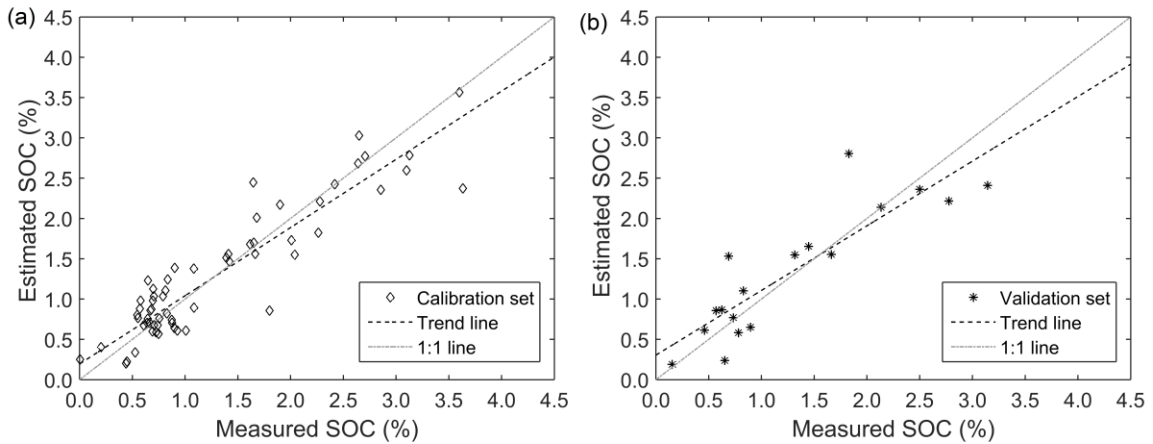
Figure 6.8 Measured vs. estimated SOC content obtained from (a) calibration set and (b) validation set of PLSR model using HAC_1 corrected signals over Narrabri sites.

An evaluation of atmospheric correction algorithms in the estimation of SOC from Hyperion image.
Ph.D. Thesis, 2018, NITK, Surathkal, India.

121
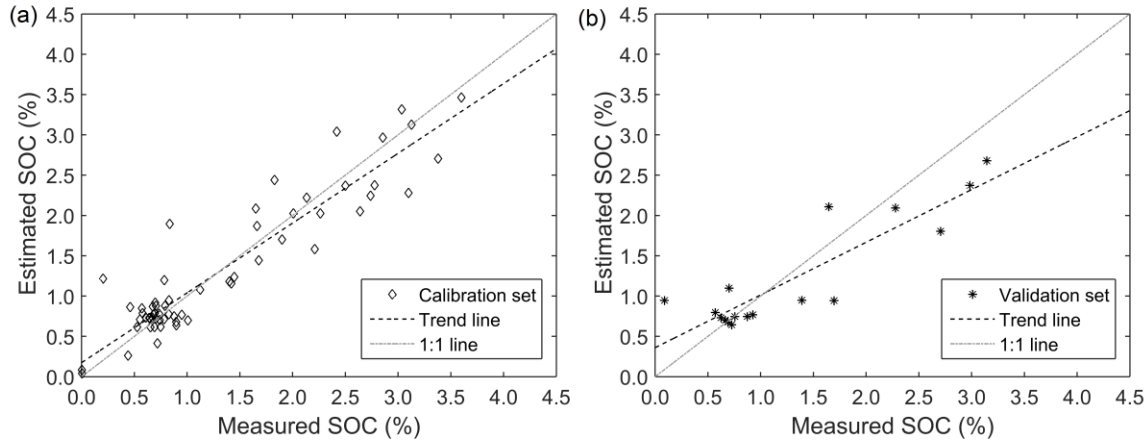
Figure 6.9 Measured vs. estimated SOC content obtained from (a) calibration set and (b) validation set of PLSR model using HAC_2 corrected signals over Narrabri sites.

Table 6.5 Performance matrices of SOC estimation using atmospherically corrected Hyperion spectra.

Atmospheric correction algorithm used	Calibration set				Validation set			
	R^2_{cal}	$RMSE_{cal}$	RPD_{cal}	$RPIQ_{cal}$	R^2_{val}	$RMSE_{val}$	RPD_{val}	$RPIQ_{val}$
ATCOR	0.76	0.44	2.07	2.83	0.71	0.47	1.90	2.60
RT	0.74	0.46	1.97	2.70	0.70	0.48	1.87	2.63
EL_m	0.81	0.40	2.30	3.29	0.74	0.45	2.02	2.60
HAC_1	0.85	0.35	2.60	3.01	**0.76**	**0.42**	**2.08**	**2.81**
HAC_2	**0.86**	**0.34**	**2.75**	**3.70**	0.75	0.44	2.08	2.58
						In bold are represented the best performances per set.		

An evaluation of atmospheric correction algorithms in the estimation of SOC from Hyperion image.
Ph.D. Thesis, 2018, NITK, Surathkal, India.

122

It is found that the choice of the atmospheric correction algorithm employed influences the results of SOC estimation from spaceborne Hyperion data. PLSR models of SOC, built using Hyperion spectra corrected by ATCOR and RT algorithms, gave similar SOC estimation performances (R^2_{val} =0.71, RPD$_{val}$=1.90, RPIQ$_{val}$=2.60 for ATCOR and R^2_{val}=0.70, RPD$_{val}$ =1.87, RPIQ$_{val}$=2.63 for RT, Table 6.5). Hyperion spectra corrected by EL$_m$ model seem to give a better SOC estimation matrices (R^2_{val}=0.74, RPD$_{val}$=2.02, RPIQ$_{val}$=2.60, Table 6.5) compared to the earlier. Based on the performance matrices SOC estimation from Hyperion spectra corrected by HAC models, which combine radiative transfer approaches and empirical approach, was better ($R^2 \geq 0.75$, RPD ≥ 2.08, and RPIQ ≥ 2.58, Table 6.5) than single models. Both HAC models perform on par with each other during both calibration and validation and it is difficult to declare one method better than another one as the differences between these indicators are too small. According to the thresholds given by Veum et al. 2015 (refer section 4.2),'Category A' models ($R^2 \geq 0.75$, RPD ≥ 2.0, and RPIQ ≥ 3.0) were achieved using EL$_m$, HAC_1 and HAC_2 corrected signals in calibration sets, whereas 'category B' models ($R^2 \geq 0.63$, RPD ≥ 1.6, and RPIQ ≥ 1.9) were achieved using others.

Significant wavelengths from PLSR estimation models, with higher value of $|\beta| \times$ VIP score, using RT, EL$_m$, HAC_1 and HAC_2 corrected Hyperion signals over the Narrabri site are presented in Table 6.6 and Figure 6.10. Results are compared with significant wavelengths identified from field reflectance estimation model (section 4.4 of Chapter 4) represented by red lines in Figure 6.10. One to one correspondence with field-PLSR model is not seen as PLSR model is an empirical model which uses statistical techniques.

An evaluation of atmospheric correction algorithms in the estimation of SOC from Hyperion image. Ph.D. Thesis, 2018, NITK, Surathkal, India.

123
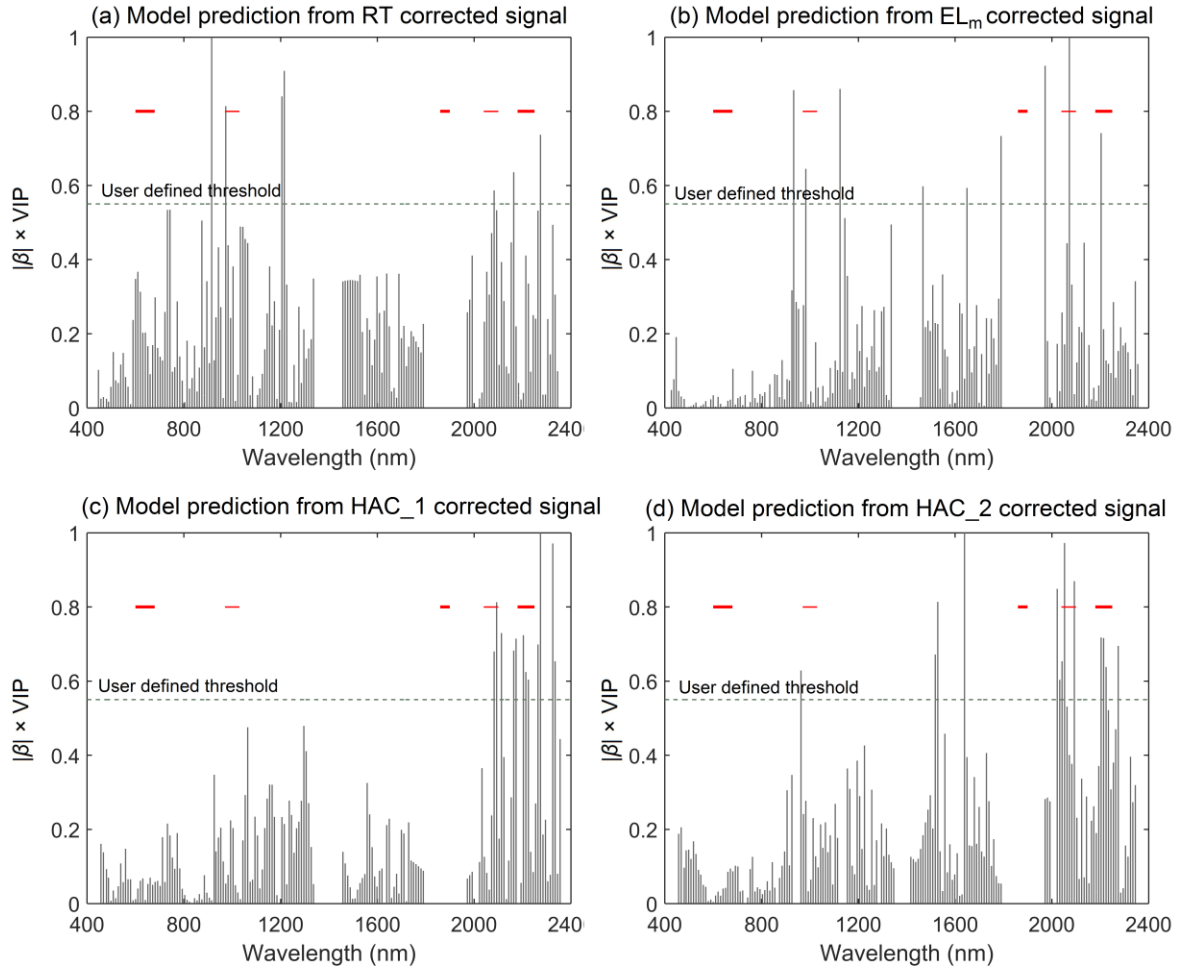
Figure 6.10 Relative scores ($|\beta| \times$ VIP) for wavelengths from PLSR estimation models using (a) RT, (b) EL_m, (c) HAC_1 and (d) HAC_2 corrected signals over Narrabri sites. Red lines in the graph represent the significant wavelength regions identified from field PLSR model.

An evaluation of atmospheric correction algorithms in the estimation of SOC from Hyperion image. Ph.D. Thesis, 2018, NITK, Surathkal, India.

124

Table 6.6 Significant wavelengths identified from Hyperion-PLSR models over Narrabri

Atmospheric correction algorithm used	Significant wavelengths identified (nm)
RT	915, 973, 1205, 1215, 2083, 2163, 2274
EL_m	932, 983, 1124, 1467, 1649, 1790, 1972, 2074, 2204
HAC_1	2083, 2093, 2113, 2163, 2173, 2204-2224, 2264, 2274, 2325, 2335
HAC_2	963, 1518, 1528, 1639, 2022- 2052, 2093, 2204- 2224, 2274

6.4 DISCUSSION

6.4.1 Atmospheric correction algorithms

Atmospheric correction algorithms were evaluated by comparing the spectral metrics of Hyperion reflectances obtained by five atmospheric correction algorithms and field spectral measurements. One of the assumptions in the article is that the surface reflectance does not change over time between field data measurements and Hyperion data acquisition. As the field spectral measurements were done using a white spectralon, the field measured reflectance may be supposed to be independent to the acquisition time. As well, as the Hyperion data were corrected for atmospheric effects, the Hyperion reflectance may be supposed to be independent to the acquisition time. Also, at the sampling sites, it is assumed that there is no alteration of soil constituents. Moisture conditions might have changed but that was difficult to separate out. The differences between field spectra and Hyperion reflectance spectra, observed in the spectral similarity analysis, may thus be due to four factors: i) difference of dates between field measurements and satellite data acquisitions, ii) quality of the white spectralon for

An evaluation of atmospheric correction algorithms in the estimation of SOC from Hyperion image. Ph.D. Thesis, 2018, NITK, Surathkal, India.

125

reflectance calibration on the field, iii) quality of the used atmospheric correction models to convert radiance into reflectance Hyperion data, and (iv) addition and consumption of soil constituents during the period between acquisition of satellite image and field measurement. So a limitation of the present study is the lack of possibility to discriminate the part of impact of each factor.

Though ATCOR and RT are physics-based algorithms tested in this study, the results indicate that both yield different results. This may be because of the difference in the equations involved or assumptions made in the radiative transfer codes. As ATCOR is a commercial software, the codes are not shared publically. While RT tried to find how the current atmospheric conditions influence the final result, ATCOR uses average atmospheric conditions. RT uses narrow SSD of 0.4 nm for wavelengths significant in SOC estimation, whereas ATCOR uses an SSD of 0.4 nm throughout the spectral domain which reduce the computational efforts. Even though RT performs well, when compared to ATCOR in 400 to 1050 nm and 1500 to 1790 nm spectral domains in terms of spectral similarity (Table 6.3), it does not do so in 2000 to 2350 nm domain. This may be because RT does not consider the influence of minor gases separately.

The better performances obtained by RT from 400 to 1790 nm may be due to the consideration of *in situ* values of surface pressure, precipitable water vapour in vertical path, aerosol optical thickness at 550 nm, and ozone concentration which influences the VNIR region of electromagnetic spectrum. The better performances obtained by ATCOR from 2000 to 2350 nm may be due to the consideration of *in situ* CO_2 which affects the SWIR region of electromagnetic spectrum. RT model may be improved by considering influence of real-time concentration of CO_2.

In EL_m and hybrid methods, an experimental approach to estimate an optimum number of GTs is performed and it was obtained as 8, and further increase in number of samples

An evaluation of atmospheric correction algorithms in the estimation of SOC from Hyperion image.
Ph.D. Thesis, 2018, NITK, Surathkal, India.

126

does not affect the accuracy greatly. It was thus achieved that the sample size chosen does not affect the end results. It brings out the robustness of the model.

Previous studies applied a different concept in selecting the number and type of GTs in EL models. Kruse et al. 1990 and Ben-Dor et al. 1994 used two targets of contrasting albedo. Hadjimitsis et al. 2009 and Hamm et al. 2012 used three contrasting targets, whereas Smith and Milton, 1999 used four diverse targets. The focus of all these studies was only on atmospheric correction algorithm, and they are considered as average techniques. Whereas in the present study the objective is not to study atmospheric components over individual targets, but it is for the retrieval of biophysical parameter (in this case the SOC) in the best possible accuracy using spaceborne data. Thus, the study used only soil targets while computing gains and offsets in EL method. Additionally, this concept can be used even if the scene under consideration does not have classical contrasting features.

In earlier studies, EL correction has mainly been applied to airborne data (Farrand et al. 1994, Clark et al. 1995, Goetz et al. 1998, Smith and Milton 1999, Ben-Dor et al. 2004, Tuominen and Lipping 2011, Hamm et al. 2012) or to multispectral spaceborne data (Karpouzli and Malthus 2003, Vaudour et al. 2008, Baugh and Groeneveld 2008, Hadjimitsis et al. 2009, Clark et al. 2011, Vaudour et al. 2014) where SNR is comparatively better. In this study, spaceborne hyperspectral data having poor SNR because of the weak signal received at the sensor are used. The modified EL method introduced in this study is rigorous and unique for low SNR data typical of spaceborne hyperspectral missions.

HAC models combined benefits of physics-based models and EL_m model. Thus these gave better results than their single model applications. The soil reflectance spectra

An evaluation of atmospheric correction algorithms in the estimation of SOC from Hyperion image. Ph.D. Thesis, 2018, NITK, Surathkal, India.

127

obtained from HAC models are comparable to lab reflectance spectra (as seen from Figure 6.5) and have best SAM values (so the minimal value, see Table 6.3).

6.4.2 Evaluation on SOC estimation

The PLSR models, built using Hyperion spectra corrected by five atmospheric correction algorithms were used for SOC estimation. The classical ways of prediction with VNIR/SWIR Hyperspectral reflectance data associated to field-measured soil properties (Gomez et al. 2008; Stevens et al. 2010; Lu et al. 2013; Gopal et al. 2015 etc.) were used to build the regression model. Building a prediction regression model from field measured SOC and field-measured surface reflectance data could be a future work, which would follow the study of Nouri et al. (2017).

All of the estimation models allowed acceptable SOC estimations (fall in categories A and B, as of Veum et al. 2015 see section 4.2, with $R^2 \geq 0.63$, RPD ≥ 1.6, and RPIQ $\geq$ 1.9, Table 6.5) on Hyperion reflectance spectra. The main purpose was to evaluate the HAC algorithms with respect to their component atmospheric algorithms. The most robust PLSR estimation models were achieved using hybrid atmospheric corrected signals ($R^2 \geq 0.75$, RPD ≥ 2.08, and RPIQ ≥ 2.58) than ATCOR or RT or EL_m corrected signals (see Table 6.5). However, the EL_m method described in this study, with an optimum number of GTs, is also a good choice as it gives better results than ATCOR or RT.

HAC_1 algorithm uses information such as real-time *in situ* climate and atmospheric data retrieved from ancillary sources and a minimum of eight field measurements over soils. Even though HAC_2 uses average atmospheric conditions and a minimum of eight field measurements over soils, they behave on par with each other. Future studies may

An evaluation of atmospheric correction algorithms in the estimation of SOC from Hyperion image.
Ph.D. Thesis, 2018, NITK, Surathkal, India.

128

concentrate on evaluating their performance under different atmospheric conditions to bring out the differences in performances if there are any.

6.5 CONCLUSIONS

In this study, HAC algorithms (HAC_1 and HAC_2) were developed for atmospheric correction of VNIR/SWIR Hyperion satellite data and were evaluated for SOC estimation in bare agricultural fields of Narrabri, Australia. HAC algorithms employ EL_m method which uses field reflectance from optimum number of GTs. HAC corrected spectra when compared with spectra corrected by their component algorithms in terms of spectral similarities and estimation accuracy, it was found that HAC performed better than component algorithms. However, the EL_m alone is also a good choice for the present study as it gives better results than ATCOR or RT. HAC_1 uses real-time *in situ* atmospheric data, a narrow SSD in significant wavelengths for SOC estimation and an optimum number of field reflectance data. However, there are still scopes for improvement of HAC_1. RT equations in the SWIR region need to be improved. The concept employed in the development of HAC_1 algorithm can be rearranged, modified and extended to extract other spectra where area of interest is in analysing different biophysical characters from spaceborne hyperspectral data. HAC_2 which combines ATCOR and EL_m methods was also found to produce similar results.

The HAC algorithms, developed using EL_m technique, may be recommended for atmospheric correction of Hyperion radiance data, when archived Hyperion reflectance data have to be used for SOC prediction mapping. To confirm our results, future works should be conducted over other study areas and for other soil property prediction. Even though, Hyperion operations ended in March 2017 after 17 years in orbit, at least five hyperspectral VNIR/SWIR satellite sensors are planned to be launched in the years to

An evaluation of atmospheric correction algorithms in the estimation of SOC from Hyperion image. Ph.D. Thesis, 2018, NITK, Surathkal, India.

129

come: PRISMA (PRecursore IperSpettrale della Missione Applicativa), EnMAP (Environmental Mapping and Analysis Program), HyspIRI (Hyperspectral Infrared Imager), SHALOM (Spaceborne Hyperspectral Applicative Land and Ocean Mission) and HYPXIM (HYPerspectral X Imagery). The launch of these forthcoming sensors will produce an increasing amount of VNIR/SWIR data over the world, so this study hopes to produce favourably new inputs in term of VNIR/SWIR spectral data treatments.

The next chapter presents summary, research conclusions, limitations and scope for future studies.

An evaluation of atmospheric correction algorithms in the estimation of SOC from Hyperion image.
Ph.D. Thesis, 2018, NITK, Surathkal, India.

130

CHAPTER 7

SUMMARY AND CONCLUSIONS

7.1 SUMMARY

In the present research work, initially a study to evaluate the accuracy of estimation of SOC from field VNIR/SWIR reflectance spectra using advanced statistical techniques viz. principal component regression, partial least square regression and artificial neural network coupled with different spectra preprocessing methods was carried out. Though the techniques used are well established in the literature,choice of a particular technique needed exploration. It was to identify the best estimation model and spectra smoothing method to be used for satellite data analysis. Also, significant wavelengths for SOC estimation were identified from supposedly error free field spectrum using PLSR model.

The primary objective of the research work was to evaluate the role of atmospheric correction algorithms in the estimation of SOC content from spaceborne hyperspectral data. Commonly used atmospheric correction algorithms ATCOR, FLAASH, 6S and QUAC algorithms were tested on EO-1 Hyperion images, and soil reflectance spectra extracted from the corrected images were used to estimate SOC content. To improve the estimation further, hybrid atmospheric correction algorithms were developed by combining physics-based methods and a modified empirical method (EL_m). These HAC algorithms were compared with their component algorithms in deriving soil spectra from Hyperion data and estimation of SOC.

An evaluation of atmospheric correction algorithms in the estimation of SOC from Hyperion image.
Ph.D. Thesis, 2018, NITK, Surathkal, India.

131

Finally, this research would open up a great scope for accurate SOC mapping when future hyperspectral missions are realised.

7.2 CONCLUSIONS

Conclusions drawn from the research with respect to the four objectives are discussed in this section.

Objective 1: To evaluate the accuracy of estimation of SOC from ground-based VNIR/SWIR reflectance spectra using advanced statistical techniques viz. principal component regression, partial least square regression and artificial neural network coupled with different spectra preprocessing methods and to identify the appropriate statistical technique for further analysis.

- The potential of field spectroscopy for soil organic carbon estimation is explored. Savitzky Golay smoothening technique is recommended as the best smoothening of reflectance spectra among moving average filter, median filter, Savitzky Golay smoothing and Gaussian smoothing. Among PCR, PLSR and ANN estimation models, PLSR model is recommended for SOC estimation in a study area when the spread and number of calibration samples are limited.

- Product of VIP scores and absolute value of PLS regression coefficients are taken for identifying significant wavelengths for SOC estimation from SG-PLSR model. Significant wavelengths identified from PLSR output of field reflectance signal are located in the 600-680 nm, 950-1050 nm, 1860-1900 nm, 2050-2090 nm and 2180-2250 nm regions.

Objective 2: To compare four popularly used atmospheric correction algorithms (QUAC, ATCOR, FLAASH, 6S) in deriving soil spectra from Hyperion data and estimation of SOC in agricultural fields of India and Australia.

An evaluation of atmospheric correction algorithms in the estimation of SOC from Hyperion image.
Ph.D. Thesis, 2018, NITK, Surathkal, India.

132

- ATCOR corrected signals estimate SOC better than FLAASH, 6S and QUAC corrected signals. The SOC spectral feature between 2050-2200 nm is retained by ATCOR corrected signal. This may be because of ATCOR's narrow spectral sampling distance in that spectral region.

- Comparing the results across study areas, Karnataka sites gives lower estimation accuracy than Narrabri sites. This is probably due to the inability to extract pure soil signals from small Karnataka fields due to mixture effects (a Hyperion pixel may straddle more than one field, and so may include several types of surface roughness and soil humidity due to the different types of ploughing between fields) than large and continuous Narrabri fields.

- Estimation of SOC from spaceborne hyperspectral imagery is influenced by:
  (i)   the type of atmospheric correction algorithm chosen, and
  (ii)   spatial arrangement of fields.

Objective 3: To explore hybrid atmospheric correction algorithm that combines the concepts of radiative transfer equations and empirical line techniques and incorporates real-time *in situ* atmospheric and climatic data.

- A hybrid atmospheric correction algorithm is developed (named as HAC_1), focusing specifically to extract soil spectra and to estimate SOC from it. It uses narrow SSD of 0.4 nm in key SOC estimating wavelength regions. It uses radiative transfer equations with real-time *in situ* atmospheric data followed by ground calibration using modified empirical line method.

- The EL_m method proposed in the study fixes an optimum number of ground targets and confirms robustness of the selected GTs on the model efficiency. In this study, the optimum number of GTs required is found as eight.

An evaluation of atmospheric correction algorithms in the estimation of SOC from Hyperion image.
Ph.D. Thesis, 2018, NITK, Surathkal, India.

133

Objective 4: To compare hybrid atmospheric correction algorithm with their component algorithms in deriving soil spectra from Hyperion data and estimation of SOC.

- Spectral similarities and thereby the SOC estimation accuracies of soil reflectance spectrum obtained from the hybrid atmospheric correction algorithms (HAC_1 and HAC_2) produced better results among its component algorithms and all tested commercial algorithms.

7.3 LIMITATIONS OF THE STUDY

In the present study, analysis was confined only to SOC contents. There was no quantitative information about other physicochemical components. It was hypothesised that there was no interaction with other soil components. However, a better knowledge of soil types and characteristics over both study areas may help to examine interaction between i) spectral features related to SOC and ii) spectral features related to others minerals (such as clay or carbonates).

7.4 SCOPE FOR FUTURE STUDIES

- The concept developed in coding the HAC_1 algorithm focuses specifically to extract soil spectra and to estimate SOC. However, it can be rearranged, modified and extended to extract other spectra where area of interest can be in analyzing different biophysical characters from spaceborne hyperspectral data.

- In this research, the performance of estimation model was evaluated in terms of R^2, RMSE, RPD and RPIQ statistics. In addition to these global indicators, an evaluation of uncertainty affecting each estimation parameter could be studied. It could guide the user for reliable estimations and calibration transferability.

An evaluation of atmospheric correction algorithms in the estimation of SOC from Hyperion image.
Ph.D. Thesis, 2018, NITK, Surathkal, India.

134

Uncertainties associated with SOC estimation obtained by Hyperion data may be due to (Gomez et al. 2015b):

1) Uncertainty in model building caused by choice made to build the calibration set.
2) Uncertainty in model building caused by choice of model dimension i.e number of varibales included in the model.
3) Uncertainty due to spatial positioning which takes into account the georeferencing errors.
4) Uncertainty of the reference lab values.

- Future research may also concentrate on testing of the atmospheric correction models over new region (different pedological context) and estimating new soil properties (e.g., textural clay).

An evaluation of atmospheric correction algorithms in the estimation of SOC from Hyperion image.
Ph.D. Thesis, 2018, NITK, Surathkal, India.

135

An evaluation of atmospheric correction algorithms in the estimation of SOC from Hyperion image.
Ph.D. Thesis, 2018, NITK, Surathkal, India.

136

APPENDIX- I

MATLAB CODES

MATLAB R2015a® version was used for the analysis. The codes used for various analysis are given below.

SIGNAL SMOOTHING METHODS

```
%------------ Savitzky Golay smoothing ---------------------------%%
sgolayfilt(X,K,F)
% smooth the signal X using a Savitzky-Golay polynomial smoothing
filter.  The polynomial order, K, must be less than the frame size, F,
and F must be odd.  The length of the input X must be >= F.  If X is a
matrix, the filtering is done on the columns of X. %%


%------------ Moving Average filter ----------------------------%%
smooth(X,F, 'moving')
% smooth the signal X using a moving average filter with span F, and F
must be odd. %%


%------------ Median filter -------------------------------------%%
medfilt1(X,N)
% smooth the signal X using a median filter of the order N. For N odd,
output is the median of X( k-(N-1)/2 : k+(N-1)/2 ). For N even, output
is the median of X( k-N/2 : k+N/2-1 ).


%------------ Gaussian filter -------------------------------------%%
g = gausswin(F); % F is the width of the smoothing window
g = g/sum(g);
Y = conv(X, g, 'same');
```

An evaluation of atmospheric correction algorithms in the estimation of SOC from Hyperion image.
Ph.D. Thesis, 2018, NITK, Surathkal, India.

137

PCR MODEL

```
% X and y are soil spectra and SOC content in calibration set; Xv and
Yv are soil spectra and SOC content in validation set %%
[n,p] = size(X);
[v,w] = size(Xv);
% Perform PCA analysis %%
[PCALoadings,PCAScores,PCAVar] = pca(X,'Economy',false);
% Perform PC regression %%
betaPCR = regress(y-mean(y), PCAScores(:,1:3));
betaPCR = PCALoadings(:,1:3)*betaPCR;
betaPCR = [mean(y) - mean(X)*betaPCR; betaPCR];
% get the beta coefficients from calibration set and predict y value%%
YPv = [ones(v,1) Xv]*betaPCR;
% Computing prediction statistics %%
TSSv= sum((Yv-mean(Yv)).^2);
RSS_PCRv= sum((Yv-YPv).^2);
rsquarev= 1- RSS_PCRv/TSSv
rmsev= sqrt(sum((Yv(:)-YPv(:)).^2)/numel(Yv))
rpd=std(Yv)/rmsev
rpiq=iqr(Yv)/rmsev
```

PLSR MODEL

```
% finding optimum no. of components to be used in the model, X = soil
reflectance; Y = SOC content %%
[Xloadings, Yloadings, Xscores, Yscores, betaPLS10, PLSPctVar]=
plsregress(X,Y,10);
figure, plot(1:10, cumsum(100*PLSPctVar(2,:)),'-bo');
xlabel('No: of PLS components');
ylabel('Percentage variance explained in Y');
% Cross validation method to find optimum no. of components to be used
in model %%
```

An evaluation of atmospheric correction algorithms in the estimation of SOC from Hyperion image.
Ph.D. Thesis, 2018, NITK, Surathkal, India.

138

```
[Xl,Yl,Xs,Ys,beta1,pctVar,PLSmsep] = plsregress(X,Y,10,'CV',10);
figure,plot(0:10,PLSmsep(2,:),'b-o');
xlabel('Number of PLS components','FontSize', 14);
ylabel('Estimated Mean Squared Prediction Error','FontSize', 14);


% getting beta coefficients from calibration set and predicting y value
[Xloadings, Yloadings, Xscores, Yscores, betaPLS]= plsregress(X,Y,5);
yfitPLS= [ones(v,1) XV]* betaPLS;
% calculating prediction statistics
TSS= sum((YV-mean(YV)).^2);
RSS_PLS= sum((YV-yfitPLS).^2);
rsquare= 1- RSS_PLS/TSS
rmse= sqrt(sum((YV(:)-yfitPLS(:)).^2)/numel(YV))
rpd=std(YV)/rmse
rpiq=iqr(YV)/rmse
```

VIP ALGORITHM

```
% X and Y are soil spectra and SOC content in calibration set, A is the
PLSR dimension %%
varX=sum(sum(X.^2));
varY=sum(sum(Y.^2));
for i=1:A
error=1;
u=Y(:,1);
niter=0;
while (error>1e-8 &&niter<1000)  % for convergence test
        w=X'*u/(u'*u);
        w=w/norm(w);
        t=X*w;
        q=Y'*t/(t'*t);  % regress Y against t;
        u1=Y*q/(q'*q);
```

An evaluation of atmospheric correction algorithms in the estimation of SOC from Hyperion image.
Ph.D. Thesis, 2018, NITK, Surathkal, India.

139

```
        error=norm(u1-u)/norm(u);
        u=u1;
        niter=niter+1;
end
p=X'*t/(t'*t);
X=X-t*p';
Y=Y-t*q';
W(:,i)=w;
T(:,i)=t;
P(:,i)=p;
Q(:,i)=q;
end

% calculation of explained variance
R2X=diag(T'*T*P'*P)/varX;
R2Y=diag(T'*T*Q'*Q)/varY;
Wstar=W*(P'*W)^(-1);
B=Wstar*Q';
Q=Q';
s=diag(T'*T*Q*Q');
%initializing
[m,p]=size(X);
[m,h]=size(T);
% calculation of VIP
VIP=[];
for i=1:p
weight=[];
      for j=1:h
        weight(j,1)= (W(i,j)/norm(W(:,j)))^2;
      end
q=s'*weight;  % explained variance by variable i
VIP(i)=sqrt(p*q/sum(s));
end
```

An evaluation of atmospheric correction algorithms in the estimation of SOC from Hyperion image.
Ph.D. Thesis, 2018, NITK, Surathkal, India.

140

RADIATIVE TRANSFER ALGORITHM

```
%------------ Estimation of TOA radiance ------------------------%%
[X, R] = geotiffread(filename)
% load Hyperion image in geotiff format %%
[rows, cols, bands] = size(X);
X=double(X);
for B = 1 : bands
     for R = 1 : rows
             for C = 1 : cols
             pixel = squeeze(X(R, C, B));
             TOA_radiance(R,C,B)=double(pixel/SF);
             % TOA_radiance is top-of-atmosphere radiance image and SF
             is scale factor matrix%%
             end
     end
end
[rows, cols, bands] = size(TOA_radiance);


%------------ Estimation of TOA reflectance ----------------------%%
%  TOA  reflectance  is  computed  by  normalizing  top-of-atmosphere
radiances to the band averaged solar irradiance %%
for B = 1 : bands
     for R = 1 : rows
             for C = 1 : cols
             pixel = squeeze(TOA_radiance(R, C, B));
             TOA_reflectance(R,C,B)=double((pi*pixel*d*d)/(E_sun*
             cosd(sza)));
             % TOA_reflectance is top-of-atmosphere reflectance image, d
             is earth-sun distance in astronomical unit, E_sun is
             Hyperion mean solar exoatmospheric irradiances, sza is Sun
             zenith angle%%
             end
```

An evaluation of atmospheric correction algorithms in the estimation of SOC from Hyperion image.
Ph.D. Thesis, 2018, NITK, Surathkal, India.

141

```
      end
end


%------------ Estimation of Optical thicknesses---------------------%%


% Rayleigh optical thickness%%
ROT= (p/p0)*(wl_micr ^(4)*(115.6406-1.335* wl_micr^(-2)))^(-1);
% ROT is Rayleigh optical thickness, wl_micr is wavelength in
micrometer, p is in situ surface pressure in mb, p0 is standard
pressure at sea level%%


% Aerosol optical thickness%%
a1=1.0274;
a2=1.2060;
if wl_micr >= 0.55
AOT= t_55*( wl_micr /.55)^(-a1);
else
AOT= t_55*( wl_micr /.55)^(-a2);
end
% t_55 is aerosol optical depth in a vertical path at 550 nm
wavelength, AOT is aerosol optical depth%%


% Water vapor optical thickness %%
WOT= (0.2385*aw*W)/(1+20.07*aw*W)^(0.45);
% WOT is water vapor optical thickness, aw is water vapour absorption
coefficients (Bird and Riordan 1986)at spectral sampling distance, W is
in situ precipitable water vapour (cm) in a vertical path%%
% Ozone optical thickness %%
OOT= ao*o3;
% OOT is Ozone vapor optical thickness, ao is ozone absorption
coefficient (Bird and Riordan 1986)at spectral sampling distance, o3 is
in situ ozone amount (atm-cm) %%
```

An evaluation of atmospheric correction algorithms in the estimation of SOC from Hyperion image.
Ph.D. Thesis, 2018, NITK, Surathkal, India.

142

```
% Uniform air optical thickness %%
UOT = (p/p0)*(1.41*au)/(1+118.93*au)^(0.45);
% UOT is uniform air optical thickness, au absorption coefficient of
uniformly mixed gaseous amount (Bird and Riordan 1986)at spectral
sampling distance%%



%-----------Estimation of sensor azimuth angle--------------------%%
% sza is sun zenith angle, vza is Sensor zenith angle, sun_az is sun
azimuth angle, sen_az is sensor azimuth angle %%
beeta= vza+sza;
% estimation of beeta which is the sum of sensor zenith angle and sun
zenith angle%%
cos_beeta=cosd(beeta);
cos_diff_sza_vza=(cos_beeta-(cosd(sza)*cosd(vza)))/(sind(sza)*
sind(vza));
%cos of (sun azimuth angle- sensor azimuth angle)%%
diff_sza_vza=acosd(cos_diff_sza_vza);
%( sun azimuth angle - sensor azimuth angle)%%
sen_az = diff_sza_vza - sun_az;
% sensor azimuth angle in degrees%%

%-----------Estimation of Rayleigh reflectance--------------------%%
cos_theeta_minus= (-1*(cosd(sza)*cosd(vza)))-(sind(sza)*sind(vza)*
(cos_diff_sza_vza));
cos_theeta_plus= ((cosd(sza)*cosd(vza)))-(sind(sza)*sind(vza)*
(cos_diff_sza_vza));
pr_theeta_minus= 0.75*(1+cos_theeta_minus*cos_theeta_minus);
pr_theeta_plus= 0.75*(1+cos_theeta_plus*cos_theeta_plus);


theeta_trans_vza=asind(1.5*sind(vza));
```

An evaluation of atmospheric correction algorithms in the estimation of SOC from Hyperion image.
Ph.D. Thesis, 2018, NITK, Surathkal, India.

143

```
term1_vza=sind(vza-theeta_trans_vza)*sind(vza-theeta_trans_vza)/
(sind(vza+theeta_trans_vza)* sind(vza+theeta_trans_vza));
term2_vza=tand(vza-theeta_trans_vza)*tand(vza-theeta_trans_vza)/
(tand(vza+theeta_trans_vza)*tand(vza+theeta_trans_vza));
r_theeta_vza=0.5*(term1_vza+term2_vza);


theeta_trans_sza=asind(1.5*sind(sza));
term1_sza=sind(sza-theeta_trans_sza)*sind(sza-
theeta_trans_sza)/(sind(sza+theeta_trans_sza)*
sind(sza+theeta_trans_sza));
term2_sza=tand(sza-theeta_trans_sza)*tand(sza-theeta_trans_sza)/
(tand(sza+theeta_trans_sza)*tand(sza+theeta_trans_sza));
r_theeta_sza=0.5*(term1_sza+term2_sza);


pr= pr_theeta_minus+((r_theeta_sza+r_theeta_vza)*pr_theeta_plus);


rayleigh_reflectance=(ROT*pr)/(4*cosd(sza)*cosd(vza));


%------------Estimation of Aerosol reflectance--------------------%%


beeta= vza+sza;
cos_beeta=cosd(beeta);
cos_diff_sza_vza=(cos_beeta-
(cosd(sza)*cosd(vza)))/(sind(sza)*sind(vza));
diff_sza_vza=acosd(cos_diff_sza_vza);
cos_scatter= (+(cosd(sza)*cosd(vza)))-(sind(sza)*sind(vza)*
(cos_diff_sza_vza));
scatter=acos(cos_scatter);
% estimation of scatter angle %%


g= 0.652;
% g= 0.652 rural aerosols %%
```

An evaluation of atmospheric correction algorithms in the estimation of SOC from Hyperion image.
Ph.D. Thesis, 2018, NITK, Surathkal, India.

144

```
pa=(1-g^2)/(1+g^2-2*g*cos(pi-scatter))^(3/2);
% aerosol scattering phase function %%


wf=0.945;
wt=0.095;
w = wf* exp(-wt*(log(wl_micr/0.4))^2);
% w is aerosol single scattering albedo %%


aerosol_reflectance=(AOT*pa*w)/(4*cosd(sza)*cosd(vza));


%------------Total transmission of the atmosphere -------------%%


T_down=exp(-(ROT+AOT+WOT+OOT+UOT)/cosd(sza));
T_up=exp(-(ROT+AOT+WOT+OOT+UOT)/cosd(vza));


% T_down is the total transmission of the atmosphere from the sun to
the surface, T_up is the total transmission of the atmosphere from the
surface to the sensor %%


%------------ Estimation of Surface reflectance -------------------%%


RT_surface_reflectance=(TOA_reflectance-rayleigh_reflectance-
aerosol_reflectance)./((T_down.*T_up) + (s_al.*( TOA_reflectance-
rayleigh_reflectance-aerosol_reflectance)));
% RT_surface_reflectance is surface reflectance obtained after solving
RT equations
```

Modified empirical line method

```
for z=1:100
no=52; % total number of ground samples
ground_index=randperm(no,N);
```

An evaluation of atmospheric correction algorithms in the estimation of SOC from Hyperion image.
Ph.D. Thesis, 2018, NITK, Surathkal, India.

145

```
pixellocation_N=pixellocation(ground_index,:);
% pixellocation is the location information of ground samples and
pixellocation_N is the location information of randomly taken N number
of samples %%

soil_row=pixellocation_N(:,1);
soil_column=pixellocation_N(:,2);
row=size(soil_row);

for i=1:row(1)
      spectrum=Hyperion_image(soil_row(i),soil_column(i),:);
      % Hyperion_image is TOA radiance image in the case of single
      modified empirical line model, or surface reflectance image
      obtained using radiative transfer equations in the case of HAC_1
      model, or surface reflectance image obtained using ATCOR in the
      case of HAC_2 model %%

      Hyperion_spectrum(i,:)=spectrum(:,1:end);
      Field_spectrum(i,:)= ground_spectrum(ground_index(i),:);
      % Field_spectrum is known field reflectance from ground targets%%
end

for i=1:bands
    x= Hyperion_spectrum(:,i);
    y= Field_spectrum (:,i);
    myfit=polyfit(x,y,1);
    gain(i)=myfit(1,1);
    offset(i)=myfit(1,2);
end
for i=1:b
    elm_refl(:,:,i)= Hyperion_image(:,:,i)*gain(i)+offset(i);
end
```

An evaluation of atmospheric correction algorithms in the estimation of SOC from Hyperion image.
Ph.D. Thesis, 2018, NITK, Surathkal, India.

146

```
ground_index2=[1:1:no];
new_index=setdiff(ground_index2,ground_index);
pixellocation_new=pixellocation(new_index,:);
soil_row_new=pixellocation_new(:,1);
soil_column_new=pixellocation_new(:,2);


for i=1:size(soil_row_new,1)
      spectrum=el_refl(soil_row_new(i),soil_column_new(i),:);
      Hyperion_spectrum_new(i,:)=spectrum(:,1:end);
      soc_new(i,:)=soc(new_index(i),:);
      Field_spectrum_new(i,:)= ground_spectrum(new_index(i),:);
      Hyperion_spectrum_new, Field_spectrum_new and soc_new are
      matrices of corrected Hyperion, field spectra and soc content
      after removing N spectra that have been used to find the gain and
      offset from the soil dataset.
end


% Calculation of SAM and SID between corrected Hyperion spectra and
field spectra %%
for S = 1 : row
a= Hyperion_spectrum_new;
c= Field_spectrum_new;
    k= sum(a.*a); sizea=size(a);sizec=size(c);
    j=sum(c.*c);
    sam = real(acos((dot(a,c))/(sqrt(k)*sqrt(j))));
    samangle(S,:)=sam;


    suma= sum(a);
    sumc =sum(c);
    proba=a/suma;
    probc=c/sumc;
```

An evaluation of atmospheric correction algorithms in the estimation of SOC from Hyperion image.
Ph.D. Thesis, 2018, NITK, Surathkal, India.

147

```
    sumx=sum(proba.*(log(proba./probc)));

    sumy=sum(probc.*(log(probc./proba)));

    SID=real(sumx+sumy);

    SIDvalue(S,:)=SID;

end

asam(z,1)=mean(samangle)

asid(z,1)=mean(SIDvalue)

end



%%********************************************************%%
```

An evaluation of atmospheric correction algorithms in the estimation of SOC from Hyperion image.
Ph.D. Thesis, 2018, NITK, Surathkal, India.

148

REFERENCES

- Abrams, M., and Hook, S. (2003). "ASTER Users Handbook. Version 2." Jet Propulsion Laboratory, Pasadena, California.

- Achard, V. and Lesage, S. (2010). "Atmospheric correction of airborne infrared hyperspectral images using neural networks." *IEEE*, 2nd Workshop on Hyperspectral Image and Signal Processing: Evolution in Remote Sensing (WHISPERS), Reykjavik, Iceland.

- ACORN 4.0. (2002). "User's Guide." Analytical Imaging and Geophysics, LLC, Boulder.

- Adler-Golden,S.M., Berk, A., Bernstein, L.S., Richtsmeier, S, Acharya, P.K, Matthew, M.W, Anderson,G.P., Allred, C.,Jeong, L. and Chetwynd, J. (1999). "FLAASH, A MODTRAN4 Atmospheric Correction Package for Hyperspectral Data Retrievals and Simulations." *Proc. 7th Ann. JPL Airborne Earth Science Workshop*, 9–14, California: JPL Publ.

- Albaladejo, J., Ortiz, R., García-Franco, N., Ruiz Navarro, A., Almagro, M., García-Pintado, J. and Martínez-Mena, M. (2013). "Land Use and Climate Change Impacts on Soil Organic Carbon Stocks in Semi-Arid Spain." *J. Soils Sediments*, 13, 265–277.

- Anne, J.P.N, Abd-Elrahman, A.H., Lewis, D.B. and Hewitt, N.A. (2014). "Modeling soil parameters using hyperspectral image reflectance in subtropical coastal wetlands." *International Journal of Applied Earth Observation and Geoinformation*, 33, 47–56.

- Bartholomeus, H.M., Schaepman, M.E., Kooistra, L., Stevens, A., Hoogmoed, W.B. and Spaargaren, O.S.P. (2008). "Spectral reflectance based indices for soil organic carbon quantification." *Geoderma*, 145 (1), 28-36.

An evaluation of atmospheric correction algorithms in the estimation of SOC from Hyperion image.
Ph.D. Thesis, 2018, NITK, Surathkal, India.

149

- Baugh, W.M. and Groeneveld, D.P. (2008). "Empirical proof of the empirical line." *International Journal of Remote Sensing* 29(3), 665–672.

- Beck, R. (2003) "EO-1 User Guide Version 2.3", *USGS Earth Resources Observation Systems Data Center (EDC)*, https://eo1.usgs.gov/documents/EO1userguidev2pt320030715UC.pdf (July 10, 2015).

- Bellon-Maurel, V. and McBratney, A. (2011). "Near-infrared (NIR) and mid-infrared (MIR) spectroscopic techniques for assessing the amount of carbon stock in soils - Critical review and research perspectives." *Soil Biology & Biochemistry*, 43, 1398-1410.

- Bellon-Maurel, V., Fernandez-Ahumada, E., Palagos, P., Roger, J.M. and McBratney, A.B. (2010). "Critical review of chemometric indicators commonly used for assessing the quality of the prediction of soil attributes by NIR spectroscopy." *Trends in Analytical Chemistry,* 29, 1073-108.

- Benassi, M., Garcia, R.D.M., Karp, A.H. and Sievert, C.E. (1984). "A high-order spherical harmonics solution to the standard problem in radiative transfer." *The Astrophysical Journal*, 280, 853-864.

- Ben-Dor, E. and Banin. A. (1995). "Near-Infrared Analysis as a Rapid Method to Simultaneously Evaluate Several Soil Properties." *Soil Science Society of America Journal*, 59, 364–372.

- Ben-Dor, E., Inbar, Y. and Chen, Y. (1997). "The Reflectance spectra of organic matter in the visible near-infrared and short wave infrared region (400-2500 nm) during a controlled decomposition process." *Remote Sens. Environ*, 61, 1-15.

- Ben-Dor, E., Kindel, B. and Goetz, A.F.H. (2004). "Quality assessment of several methods to recover surface reflectance using synthetic imaging spectroscopy data." *Remote Sensing of Environment*, 90, 389-404.

An evaluation of atmospheric correction algorithms in the estimation of SOC from Hyperion image.
Ph.D. Thesis, 2018, NITK, Surathkal, India.

150

- Ben-Dor, E., Kruse, F.A., Lefkoff, A.B. and Banin. A. (1994). "Comparison of three calibration techniques for utilization of GER 63-channel aircraft scanner data of Makhtesh Ramon, Nega, Israel." *Photogrammetric Engineering & Remote Sensing*, 60(11), 1339-1354.

- Ben-Dor, E., Levin, N., Singer, A., Karnieli, A., Braun, O. and Kidron, G.J. (2006). "Quantitative mapping of the soil rubification process on sand dunes using an airborne hyperspectral sensor." *Geoderma*, 131 (1-2), 1–21.

- Ben-Dor, E., Patkin, K., Banin, A. and Karnieli, A. (2002). "Mapping of Several Soil Properties Using DAIS-7915 Hyperspectral Scanner Data— A Case Study over Clayey Soils in Israel." *International Journal of remote sensing* 23(6), 1043-1062.

- Berk, A., Anderson, G.P., Acharya, P.K. and Shettle. E.P. (2008). "MODTRAN®5.2.0.0 User's Manual." *Spectral Sciences*, Inc. Burlington and Air Force Research Laboratory Hanscom AFB, MA.

- Berk, A., Anderson, G.P., Acharya, P.K., Bernstein, L.S., Muratov, L., Lee, J. et al. (2004). "MODTRAN5: A Reformulated Atmospheric Band Model with Auxiliary Species and Practical Multiple Scattering Options." *SPIE. International Society for Optical Engineering*, 5425, 341–347.

- Berk, A., Bernstein, L.S. and Robertson, D.C. (1989). "MODTRAN: a moderate resolution model for LOWTRAN7." Final report, GL-TR-89-0122, AFGL, Hanscom AFB, MA, 42.

- Bernstein, L. S., Adler-Golden,S. M., Sundberg, R. L., Levine,R. Y., Perkins, T. C., Berk, A., Ratkowski, A.J., Felde G. and Hoke, M. L. (2005). "A New Method for Atmospheric Correction and Aerosol Optical Property Retrieval for VIS-SWIR Multi- and Hyperspectral Imaging Sensors: QUAC (QUick Atmospheric Correction)." Geoscience and Remote Sensing Symposium, *IEEE International*, 5, 3549-3552.

An evaluation of atmospheric correction algorithms in the estimation of SOC from Hyperion image.
Ph.D. Thesis, 2018, NITK, Surathkal, India.

151

- Bernstein, L. S., Jin, X. M., Gregor, B. and Adler-Golden, S.M. (2012). "Quick Atmospheric Correction Code: Algorithm Description and Recent Upgrades." *SPIE Optical Engineering*, 51 (11), 111719.

- Bilal, M., Nichol, J. E., Bleiweiss, M. P. and Dubois, D. (2013). "A Simplified high resolution MODIS Aerosol Retrieval Algorithm (SARA) for use over mixed surfaces." *Remote Sensing of Environment*, 136, 135–145.

- Bird, R. E. and Riordan, C. (1986). "Simple solar spectral model for direct and diffuse irradiance on horizontal and tilted planes at the earth's surface for cloudless atmospheres." *J. Climate and applied Meteorology*, 25, 87-97.

- Borengasser, M., Hungate, W.S. and Watkins, R. (2008). "Hyperspectral Remote Sensing Principles and Applications." CRC Press, Taylor & Francis Group, 978‒1‒56670‒654‒4.

- Buddenbaum, H. and Steffens, M. (2012). "The Effects of Spectral Pretreatments on Chemometric Analyses of Soil Profiles Using Laboratory Imaging Spectroscopy." *Applied and Environmental Soil Science*, 274903, 12.

- Bussoletti, E. (2012). "Space Observations for Agriculture and Food Support." *Proc., 32nd session of Inter-Agency Meeting on Outer Space Activities*, Rome, March 7-9.

- Carrere, V., Briottet, X., Jacquemoud, S., Marion, R., Bourguignon, A., Chami, M, Dumont, M. et al. (2013). "HYPXIM: A Second Generation High Spatial Resolution Hyperspectral Satellite for Dual Applications." *Proc., 5thWorkshop on Hyperspectral Image and Signal Processing: Evolution in Remote Sensing*, Gainsville, FL, June 25-28.

- Casa, R., Castaldi, F., Pascucci, S.,Palombo, A. and Pignatti, S. (2013). "A comparison of sensor resolution and calibration strategies for soil texture estimation from hyperspectral remote sensing." *Geoderma*, 197–198, 17–26.

An evaluation of atmospheric correction algorithms in the estimation of SOC from Hyperion image.
Ph.D. Thesis, 2018, NITK, Surathkal, India.

152

- Chang, C. I. (1999). "Spectral information divergence for hyperspectral image analysis". In *Proceedings of the IEEE 1999 International Geoscience and Remote Sensing Symposium*, 1, 509–511.

- Chang, C.W. and Laird, D.A. (2002). "Near-infrared reflectance spectroscopic analysis of soil C and N." *Soil Science*, 167(2), 110–116.

- Chang, C.W., Laird, D.A., Mausbach, M.J. and Hurburgh, C.R. (2001). "Near-infrared reflectance spectroscopy - Principal components regression analyses of soil properties." *Soil Science Society of America Journal,* 65, 480-490.

- Chiang, Y.M., Chang, L.C. and Chang, F.J. (2004). "Comparison of Static Feedforward and Dynamic-Feedback Neural Networks for Rainfall Runoff Modeling." *Journal of Hydrology*, 290, 297-311.

- Clark R.N., G.A, Swayze, K.B. Heidebrecht, R.O. Green and A.F.H. Goetz, (1995). "Calibration to surface reflectance of terrestrial imaging spectrometry data: Comparison of methods". *Summaries of the Fifth annual JPL Airborne Earth Science Workshop,* 41-42, California: JPL Publ.

- Clark, B., Suomalainen, J. and Pellikka, P. (2011). "The selection of appropriate spectrally bright pseudo-invariant ground targets for use in empirical line calibration of SPOT satellite imagery." *ISPRS Journal of Photogrammetry And Remote Sensing*, 66(4), 429–445.

- Collins, D.G., Blattner, W.G., Wells, M.B. and Horak, H.G. (1972). "Backward MonteCarlo calculations of the polarization characteristics of the radiation emerging from spherical-shell atmospheres." *Applied Optics*, 11(11), 2684-2696.

- Conel, J. E., Green, R.O., Vane, G., Bruegge, C.J. and Alley, R.E. (1987). "AIS-2 radiometry and a comparison of methods for the recovery of ground reflectance." In G. Vane (Ed.), *Proc., 3rd Airborne Imaging Spectrometer Data Analysis Workshop* 87:30, 18-47, JPL Publ.

An evaluation of atmospheric correction algorithms in the estimation of SOC from Hyperion image. Ph.D. Thesis, 2018, NITK, Surathkal, India.

153

- Cornette, W.M. and Shanks, J.G. (1992). "Physically reasonable analytic expression for the single-scattering phase function." *Applied Optics,* 31:16, 3152–3160.

- Cozzolino, D. and Moron, A. (2006). "Potential of near-infrared reflectance spectroscopy and chemometrics to predict soil organic carbon fractions." *Soil & Tillage Research*, 85, 78–85.

- Crouvi, O., Ben-Dor, E., Beyth, M., Avigad, D. and Amit, R. (2006). "Quantitative mapping of arid alluvial fan surfaces using field spectrometer and hyperspectral remote sensing." *Remote Sensing of Environment*, 104, 103–117.

- Dalal, R. C. and Henry, R. J. (1986). "Simultaneous Determination of Moisture, Organic Carbon, and Total Nitrogen by Near Infrared Reflectance Spectrophotometry." *Soil Sci. Soc. Am. J.*, 50, 120-123.

- Das, B.S., Sarathjith, M.C., Santra, P., Sahoo, R.N., Srivastava, R., Routray, A. and Ray, S.S. (2015). "Hyperspectral Remote Sensing: Opportunities, Status and Challenges for Rapid Soil Assessment in India." *Current Science*, 108(5), 860-868.

- De Tar, W.R., Chesson, J.H., Penner, J.V. and Ojala, J.C. (2008). "Detection of soil properties with airborne hyperspectral measurements of bare fields." *American Society of Agricultural and Biological Engineers*, 51, 463-470.

- Farifteh, J., van der Meer, F.D., Atzberger, C.G. and Carranza, E.J.M. (2007). "Quantitative analysis of salt - affected soil reflectance spectra : a comparison of two adaptive methods, PLSR and ANN." *Remote sensing of environment*, 110, 59-78.

- Farrand, W.H., Singer, R.B. and Merenyi, E. (1994). "Retrieval of apparent surface reflectance from AVIRIS data: a comparison of empirical line, radiative

An evaluation of atmospheric correction algorithms in the estimation of SOC from Hyperion image.
Ph.D. Thesis, 2018, NITK, Surathkal, India.

154

transfer and spectral mixture methods." *Remote Sensing of Environment*, 47, 311–321.

- FLAASH. (2009). "FLAASH Module: User's Guide." In Version 4.3.

- Folkman, M., Pearlman, J., Liao, L. and Jarecke, P. (2001). "EO1/Hyperion hyperspectral imager design, development, characterization and prediction". In: Smith, W.L., Yasuoka, Y. (Eds.), Hyperspectral Remote Sensing of the Land and Atmosphere. *SPIE Proc*, 4151, 40–51.

- Galvao, L.S., Pizarro, M. A. and Epiphanio, J. C. N. (2001). "Variations in Reflectance of Tropical Soils: Spectral-Chemical Composition Relationships from AVIRIS data." *Remote Sens. Environ*. 75, 245–255.

- Gao, B. C., and Goetz, A. F. H. (1990). "Column Atmospheric Water Vapor and Vegetation Liquid Water Retrievals from Airborne Imaging Spectrometer Data." *Journal of Geophysical Research*, 95, 3549–3564.

- Gao, B.C. and Davis, C.O. (1997). "Development of a line-by-line-based atmosphere removal algorithm for airborne and spaceborne imaging spectrometers." *SPIE Proceedings*, 3118, 132−141.

- Gao, B.C., Heidebrecht, K.B. and Goetz, A.F.H. (1993). "Derivation of Scaled Surface Reflectances from AVIRIS Data." *Remote Sens. Environ*., 44, 165–178.

- Gao, B.C., Montes, J.M., Davis, C.O. and Goetz, A.F.H. (2009). "Atmospheric correction algorithms for hyperspectral remote sensing data of land and ocean." *Remote Sensing of Environment*, 113, S17–S24.

- Gao, Y., Cui, L., Lei, B., Zhai, Y., Shi,T., Wang, J., Chen, Y., He, H. and Wug, G. (2014). "Estimating Soil Organic Carbon Content with Visible–Near-Infrared (Vis-NIR) Spectroscopy." *Applied Spectroscopy*, 68(7), 712-722.

- Goetz A.F.H., Heidebrecht K.B., Kindel B. and Boardman J.W. (1998). "Using ground spectral irradiance for model correction of AVIRIS data." *Summaries of*

An evaluation of atmospheric correction algorithms in the estimation of SOC from Hyperion image.
Ph.D. Thesis, 2018, NITK, Surathkal, India.

155

the Seventh JPL Airborne Earth Science Workshop, 97–21, 159-168, California, JPL Publication.

- Gomez, C., Drost A.P.A., Roger J.M. (2015b). "Analysis of the uncertainties affecting predictions of clay contents from VNIR/SWIR hyperspectral data." *Remote Sensing of Environment*, 156, 58–70.

- Gomez, C., Lagacherie, P. and Coulouma, G. (2008b). "Continuum removal versus PLSR method for clay and calcium carbonate content estimation from laboratory and airborne hyperspectral measurements." *Geoderma*,148, 141–148.

- Gomez, C., Oltra-Carrió, R., Bacha, S., Lagacherie, P. and Briottet, X. (2015a). "Evaluating the Sensitivity of Clay Content Prediction to Atmospheric Effects and Degradation of Image Spatial Resolution using Hyperspectral VNIR/SWIR Imagery." *Remote Sensing of Environment*, 164, 1–15.

- Gomez, C., Viscarra-Rossel, R.A. and McBratney, A.B. (2008). "Soil Organic Carbon Prediction by Hyperspectral Remote Sensing and Field Vis-NIR Spectroscopy: An Australian Case Study." *Geoderma*, 146, 403–411.

- Gopal, B. (2014). "Measurement and Prediction of Topsoil Chemical Properties using Hyperspectral Remote Sensing Techniques." PhD diss., National Institute of Technology Karnataka, Surathkal.

- Gopal, B., Shetty, A, Ramya, B. J. (2015). "Spatial variability of topsoil chemical properties." *Indian Journal of Agricultural Research*, 49(2), 134-141. doi: 10.5958/0976-058X.2015.00019.0.

- Gopal, B., Shetty, A. and Ramya, B. J. (2014). "Prediction of topsoil nitrogen from spaceborne hyperspectral data." *Geocato International*, 30(1), 82-92.

- Gordon, H. R., Brown, J. W. and Evans, R. H. (1988). "Exact Rayleigh scattering calculations for use with the Nimbus-7 coastal zone color scanner." *Applied Optics*, 27, 862–871.

An evaluation of atmospheric correction algorithms in the estimation of SOC from Hyperion image.
Ph.D. Thesis, 2018, NITK, Surathkal, India.

156

- Gosselin, R., Rodrigue, D. and Duchesne, C. (2010). "A Bootstrap-VIP approach for selecting wavelength intervals in spectral imaging applications." *Chemometrics and Intelligent Laboratory Systems*,100, 1221.

- Green, A. A., Berman, M., Switzer, P. and Craig, M. D. (1988). "A transformation for ordering multispectral data in terms of image quality with implications for noise removal." *IEEE Transactions on Geoscience and Remote Sensing*, 26, 65–74.

- Green, R. O., Conel, J. E. and Roberts, D. A. (1993). "Estimation of aerosol optical depth and additional atmospheric parameters for the calculation of the reflectance from radiance measured by the Airborne Visible/Infrared Imaging Spectrometer", In Summaries of the *4th Annual JPL Airborne Geoscience Workshop*, JPL Publ., 93–26, 1, 73–76.

- Grey W.M.F. and North, P.R.J. (2009). "Aerosol optical depth from dual-view (A)ATSR satellite observations." In: Kokhanovsky A.A., de Leeuw G. (eds) Satellite Aerosol Remote Sensing over Land. Springer Praxis Books. Springer, Berlin, Heidelberg.

- Hadjimitsis, D. G., Clayton, C. R. I. and Retalis, A. (2009). "The use of selected pseudo-invariant targets for the application of atmospheric correction in multi-temporal studies using satellite remotely sensed imagery." *International Journal of Applied Earth Observation and Geoinformation,* 11(3), 192–200.

- Hamm, N.A.S., Atkinson, P.M. and Milton, E.J. (2012). "A per-pixel, non-stationary mixed model for empirical line atmospheric correction in remote sensing." *Remote Sensing of Environment,* 124, 666–678.

- Haubrock, S.N, Chabrillat, S., Kuhnert, M., Hostert, P. and Kaufmann, H. (2008). "Surface soil moisture quantification and validation based on hyperspectral data and field measurements." *Journal of Applied Remote Sensing.* 2, 023552, 1-26.

An evaluation of atmospheric correction algorithms in the estimation of SOC from Hyperion image.
Ph.D. Thesis, 2018, NITK, Surathkal, India.

157

- Henderson, T.L., Baumgardner, M.F., Franzmeier, D.P, Stott, D.E. and Coster, D.C. (1992). "High Dimensional Reflectance Analysis of Soil Organic Matter." *Soil Science Society America Journal*, 56, 865–872.

- Hively, W.D., McCarty, G.W., Reeves, J.B., Lang, M.W., Oesterling, R.A., and Delwiche, S.R. (2011). "Use of Airborne Hyperspectral Imagery to Map Soil Properties in Tilled Agricultural Fields." *Applied and Environmental Soil Science*, 358193, 13.

- Hodge, V. J., and Austin, J. (2004). "A Survey of Outlier Detection Methodologies." *Artificial Intelligence Review*, 22 (2), 85–126.

- Hong, S.Y., Sudduth, K.A., Kitchen, N.R., Drummond, S.T., Palm, H.L. and Wiebold, W.J. (2002). "Estimating within-field variations in soil properties from airborne hyperspectral images", *Proc., Pecora 15/Land Satellite Information IV/ISPRS Commission I/FIEOS 2002*. Denver, CO.

- IS 2720 (Part XXII). 1972. Methods of Test for Soils Part XXII Determination of Organic Matter. First Revision. New Delhi: Bureau of Indian standards.

- Jaber, S. M., Lant, C. L. and Al-Qinna, M. I. (2011). "Estimating Spatial Variations in Soil Organic Carbon Using Satellite Hyperspectral Data and Map Algebra*." International Journal of Remote Sensing*, 32 (18), 5077–5103.

- Jensen, J.R. (2006) "Remote sensing of the environment- an earth resource perspective". 2nd edition, Pearson prentice hall.

- Jiang, Q., Chen, Y., Guo, L., Fei, T. and Qi, K. (2016). "Estimating Soil Organic Carbon of Cropland Soil at Different Levels of Soil Moisture Using VIS-NIR Spectroscopy." *Remote Sensing*, 8, 755.

- Kim, M., Jeong, S., Yeom, J., Kim, H. and Ko, J. (2016). "Determination of rice canopy growth based on high resolution satellite images: a case study using RapidEye imagery in Korea." *AIMS Environmental Science*, 3(4), 631-645.

An evaluation of atmospheric correction algorithms in the estimation of SOC from Hyperion image.
Ph.D. Thesis, 2018, NITK, Surathkal, India.

158

- Kneizys, F.X., Shett1e, E.P., Gallery, W.O., Chetwynd, J.H., Abrea, L.W., Selby, J.E.A., Fenn, R.W. and McClatchey, R.W. (1980). "Atmospheric Transmittance/Radiance: Computer Code LOWTRAN5." Tech. Rep. AFGL-TR-800067, Air Force Geophysics Laboratory.

- Kneizys, F.X., Shettle, E.P., Abreau, L.W., Chetwynd, J. H., Anderson, G.P., Gallery, W.O., Selby, E.A. and Clough, S.A. (1988). "Users guide to LOWTRAN-7." In AFGL-TR-8-0177 Air Force Geophysics Laboratories, Bedford, Massachusett.

- Kruse, F. A., Raines, G. I. and Watson, K. (1985). "Analytical techniques for extracting geologic information from multichannel airborne spectroradiometer and airborne imaging spectrometer data." *Proc., 4th thematic conference on remote sensing for exploration geology*. Ann Arbor, MI.

- Kruse, F., Lefkoff, A., Boardman, J., Heidebrecht, K., Shapiro, A., Barloon, P. and Goetz, A. (1993). "The Spectral Image Processing System (SIPS)-Interactive Visualization and Analysis of Imaging Spectrometer Data." *Remote Sensing of Environment*, 44, 145–163.

- Kruse, F.A., Kierein-Young, K. S. and Boardman. J.W. (1990). "Mineral mapping at Cuprite, Nevada with a 63 channel imaging spectrometer," *Photogrammetric Engineering & Remote Sensing* 56(1), 83–92.

- Lacis, A.A., and Oinas, V. (1991). "A description of correlated k distribution method for modelling nongray gaseous absorption, thermal emission, and multiple scattering in vertically inhomogeneous atmospheres." *J. Geophys*, 96, 9027-9063.

- Lagacherie P., Gomez C., Bailly J.S., Baret F. and Coulouma, G. (2010). "The use of Hyperspectral imagery for Digital Soil Mapping in Mediterranean Areas." Digital Soil Mapping, Progress in Soil Science, 2, 93-102.

An evaluation of atmospheric correction algorithms in the estimation of SOC from Hyperion image.
Ph.D. Thesis, 2018, NITK, Surathkal, India.

159

- Lagacherie, P., Baret, F., Feret, J.B., Madeira-Netto, J. and Robbez-Masson, J. (2008). "Estimation of Soil Clay and Calcium Carbonate using Laboratory, Field and Airborne Hyperspectral Measurements." *Remote Sensing of Environment*, 112(3), 825–835.

- Lenot, X., Achard, V. and Poutier, L. (2009). "SIERRA: A new approach to atmospheric and topographic corrections for hyperspectral imagery." *Remote Sensing of Environment*, 113, 1664–1677.

- Li, L., Qiu, S.J., Liu, J.T., Liu, Q. and Lu, Z.H. (2012). "Roles of Soil Dissolved Organic Carbon in Carbon Cycling of Terrestrial Ecosystems: A Review." *J. Applied Ecology*, 23(5), 1407-14.

- Lillesand, T.M, Kiefer, R.W. and Chipman, J.W. (2009) "Remote Sensing and Image Interpretation.", 5th edition., Wiley India Pvt. Ltd., New Delhi.

- Liou, K.N. (1973). "A numerical experiment on Chandrasekhar's discrete-ordinate method for radiative transfer: application to cloud and hazy atmospheres." *Journal of Atmospheric Sciences*, 30, 1303-1326.

- López, S.M., Corral-Rivas, J.J., Díaz-Varela, R.A., Álvarez-González, J.G. and López-Sánchez, C.A. (2016). "Evaluation of Radiometric and Atmospheric Correction Algorithms for Aboveground Forest Biomass Estimation Using Landsat 5 TM Data." *Remote Sensing,* 8, 369.

- Lopinto, E., and Ananasso, C. (2013). "The Prisma Hyperspectral Mission." Proceedings of EARSeL Symposium, Matera, Italy, June 3-6.

- Lu, P., Wang ,L., Niu, Z., Li, L. and Zhang, W. (2013). "Prediction of soil properties using laboratory VIS–NIR spectroscopy and Hyperion imagery." *J Geochem Explor*. 132, 26–33.

- Maesschalck, R.D., Estinne, F. and Candolfi, A. (1999). "The development of calibration models for spectroscopic data using principal component regression." *International journal of chemistry*, 2, 19.

An evaluation of atmospheric correction algorithms in the estimation of SOC from Hyperion image.
Ph.D. Thesis, 2018, NITK, Surathkal, India.

160

- Malkmus, W. (1967). "Random Lorentz band model with exponential-tailed S line intensity distribution function." *Journal of the Optical Society America*, 57, 323−329.

- Mandanici, E. (2010). "Implementation of Hyperion Sensor Routine in 6SV Radiative Transfer Code." *Proc. Hyperspectral Workshop*, Frascati, Italy, March 17–19. The Netherlands: ESA Communications

- Marcello. J., Eugenio, F., Perdomo, U. and Medina, A. (2016). "Assessment of Atmospheric Algorithms to Retrieve Vegetation in Natural Protected Areas Using Multispectral High Resolution Imagery." *Sensors,* 16, 1624.

- Mark, H. and Workman, J.Jr. (2003). "Statistics in Spectroscopy." Second Edition, Elsevier Academic Press, USA.

- Martin, P.D., Malley, D.F., Manning, G. and Fuller, L. (2002). "Determination of Soil Organic Carbon and Nitrogen at the Field Level using Near-Infrared Spectroscopy." *Canadian J. soil science*, 82(4), 413–422.

- Matarrese, R., Ancona, V., Salvatori, R., Muolo, M.R., Uricchio, V.F. and Vurro, M. (2014). "Detecting soil organic carbon by CASI hyperspectral images." *Geoscience and Remote Sensing Symposium*, IEEE International, IGARSS 2014, 3284- 3287.

- McBratney, A.B., Stockmann, U., Angers, D.A, Minasny, B. and Field, D.J. (2014). "Challenges for soil organic carbon research." In: Hartemink, A.E., McSweeney, K. (Eds.), *Soil Carbon*. Springer International Publishing Switzerland 2014, 3–16.

- McCarty, G. W., Reeves, J. B., Reeves, V. B., Follett, R. F. and Kimble, J. M. (2002). "Mid-Infrared and Near-Infrared Diffuse Reflectance Spectroscopy for Soil Carbon Measurements." *Soil Science Society of America Journal*, 66, 640–646.

An evaluation of atmospheric correction algorithms in the estimation of SOC from Hyperion image.
Ph.D. Thesis, 2018, NITK, Surathkal, India.

161

- Mehmood T., Liland K.H., Snipen L. and Sb S. (2012). "A Review of Variable Selection Methods in Partial Least Squares Regression." *Chemometrics and Intelligent Laboratory Systems*, 118, 62-69.

- Miglani, A., Ray, S.S., Vashishta, D.P. and Parihar, J.S. (2011). "Comparison of Two Data Smoothing Techniques for Vegetation Spectra Derived From EO-1 Hyperion." *Journal of the Indian Society of Remote Sensing*, 39(4), 443-453.

- Minasny, B., McBratney, A.B., Tranter, G. and Murphy, B.W. (2008). Using soil knowledge for the evaluation of mid-infrared diffuse reflectance spectroscopy for predicting soil physical and mechanical properties. *European Journal of Soil Science*, 59(5), 960-971.

- Minu, S. and Shetty, A. (2015). Atmospheric correction algorithms for hyperspectral imageries: A review." *International Research Journal of Earth Sciences, 3*, 14–18.

- Minu, S. and Shetty, A. (2018). "Prediction accuracy of soil organic carbon from ground based visible near-infrared reflectance spectroscopy" *Journal of the Indian Society of Remote Sensing*. pp. 1-7.

- Minu, S., Shetty, A. and Gopal, B. (2016). "Review of Preprocessing Techniques used in Soil Property Prediction from Hyperspectral Data." *Cogent Geoscience*, 2(1), 1145878.

- Minu, S., Shetty, A., Minasny, B. and Gomez, C. (2017). "The role of atmospheric correction algorithms in the prediction of soil organic carbon from Hyperion data." *International journal of remote sensing*. 38(23), 6435-6456.

- Morgan, C.L.S., Waiser, T.H., Brown, D.J. and Hallmark, T. (2009). "Simulated in situ characterization of soil organic and inorganic carbon with visible near-infrared diffuse reflectance spectroscopy." *Geoderma*, 151, 249–256.

An evaluation of atmospheric correction algorithms in the estimation of SOC from Hyperion image.
Ph.D. Thesis, 2018, NITK, Surathkal, India.

162

- Moses, W.J., Bowles, J.H., Lucke, R.L. and Corson, M.R. (2012). "Impact of signal-to-noise ratio in a hyperspectral sensor on the accuracy of biophysical parameter estimation in case II waters." *Optics Express*, 20(4), 4309- 4330.

- Nouri, M., Gomez, C., Gorretta, N. and Roger, J.M. (2017). "Clay content mapping from airborne hyperspectral Vis-NIR data by transferring a laboratory regression model." *Geoderma,* 298, 54–66.

- O'Neill, N.T., Zagolski, F., Bergeron, M., Royer, A., Miller, J. and Freemantle, J. (1997). "Atmospheric correction validation of CASI images acquired over the BOREAS Southern study area." *Canadian Journal of Remote Sensing*, 23 (2), 143-162.

- Peng, X., Shi, T., Song, A., Chen, Y. and Gao, W. (2014). "Estimating Soil Organic Carbon Using VIS/NIR Spectroscopy with SVMR and SPA Methods." *Remote Sensing*, 6, 2699-2717.

- Peon, J., Fernandez, S., Recondo, C. and Calleja, J.F. (2017). "Evaluation of the spectral characteristics of five hyperspectral and multispectral sensors for soil organic carbon estimation in burned areas." *International Journal of Wildland Fire*, 26(3), 230-239.

- Qu, Z., Goetz, A.F.H. and Heidbrecht, K.B. (2001). "High accuracy atmosphere correction for hyperspectral data (HATCH)." *Proc., Ninth JPL Airborne Earth Science Workshop,* JPL Publ. 00-18, 373-381.

- Qu, Z., Kindel, B.C. and Goetz, A.F.H. (2003). "The High Accuracy Atmospheric Correction for Hyperspectral Data (HATCH) Model." *IEEE Transactions on Geoscience and Remote Sensing*, 41, 1223-1231.

- Richter, R. (1996). "A spatially adaptive fast atmosphere correction algorithm." *International Journal of Remote Sensing*, 11, 159– 166.

- Richter, R. (1998). "Correction of satellite imagery over mountainous terrain." *Applied Optics*, 37, 4004−4015.

An evaluation of atmospheric correction algorithms in the estimation of SOC from Hyperion image.
Ph.D. Thesis, 2018, NITK, Surathkal, India.

163

- Richter, R. and Schlaepfer, D. (2012). "Atmospheric/Topographic Correction for Satellite Imagery." In ATCOR-2/3 User Guide. Version-8.2. Switzerland: ReSe Applications Schläpfer.

- Richter, R., and Schlaepfer, D. (2002). "Geo-atmospheric processing of airborne imaging spectrometry data, Part 2: atmospheric/topographic correction." *International Journal of Remote Sensing,* 23(13), 2631−2649.

- Richter, R., Schlapfer, D. and Muller, A. (2006). "An automatic atmospheric correction algorithm for visible/NIR imagery", *International Journal of Remote Sensing*, 27, 2077–2085.

- Rinnan, A., Berg, F.V.D. and Engelsen, S.B. (2009). "Review of the most common pre-processing techniques for near-infrared spectra." *Trends in Analytical Chemistry*, 28(10), 1201-1222.

- Roberts, D. A., Yamaguchi, Y. and Lyon, R. (1986). "Comparison of various techniques for calibration of AIS data," *Proc., 2nd Airborne Imaging Spectrometer Data Analysis Workshop*, JPL Publication Laboratory, Pasadena, CA. 86-35, 21–30.

- Rodger, A. and Lynch, M.J. (2001). "Determining atmospheric column water vapour in the 0.4–2.5 μm spectral region". *Proc., AVIRIS Workshop 2001*. Pasadena, California.

- Rojas-Lertxundi, S., Lopez, J.R., Huerta, S. and Bringas, P.G. (2015). "Motion Capture Systems for Jump Analysis." HAIS, LNAI 9121, 111–124.

- Rothman, L. S., Gamache, R. R., Tipping, R.H., Rinsland, C.P. et al. (1992). "The HITRAN molecular database: editions of 1991 and 1992." *Journal of Quantitative Spectroscopy & Radiative Transfer*, 48, 469-507.

- Rothman, L. S., Jacquemart, D., Barbe, A., Benner, D. C., Birk, M., Brown, L. R. et al. (2005). "The HITRAN 2004 molecular spectroscopic database." *Journal of Quantitative Spectroscopy and Radiative Transfer*, 96, 139−204.

An evaluation of atmospheric correction algorithms in the estimation of SOC from Hyperion image.
Ph.D. Thesis, 2018, NITK, Surathkal, India.

164

- Rothman, L.S., Barbe, A., Benner, D.C., Brown, L.R., Camy-Peyret, C., Carleer, M.R. et al. (2003). "The HITRAN molecular spectroscopic database: edition of 2000 including updates through 2001." *Journal of Quantitative Spectroscopy and Radiative Transfer*, 82, 5−44.

- Roy, D.P., Wulder, M.A., Loveland, T.R., et al. (2014). "Landsat-8: science and product vision for terrestrial global change research." *Remote Sensing of Environment,* 145, 154–172.

- San, B.T., and Suzen, M.L. (2010). "Evaluation of different atmospheric correction algorithms for EO-1 Hyperion imagery." *International archives of the Photogrammetry, Remote Sensing and Spatial Information Science*, 38 (8), 392–397.

- Sarkhot, D.V., Grunwald, S., Ge, Y. and Morgan, C.L.S. (2011). "Comparison and Detection of Total and Available Soil Carbon Fractions using Visible/Near-Infrared Diffuse Reflectance Spectroscopy." *Geoderma*, 164, 22–32.

- Savitzky, A. and Golay, M.J.E. (1964). "Smoothing and Differentiation of Data by Simplified Least Squares Procedures." *Analytical Chemistry*, 36, 1627.

- Selige, T., Böhner J., and Schmidhalter. U. (2006). "High Resolution Topsoil Mapping using Hyperspectral Image and Field Data in Multivariate Regression Modeling Procedures." *Geoderma*, 136, 235–244.

- Shaw, G.A. and Burke, H.K. (2003). "Spectral Imaging for Remote Sensing." *Lincoln Laboratory Journal*, 14(1), 3-28.

- Shettle, E. P. and Fenn, R. W. (1975) "Models of the Atmospheric Aerosol and Their Optical Properties." *Proc. Advisory Group for Aerospace Research and Development*, 183.

An evaluation of atmospheric correction algorithms in the estimation of SOC from Hyperion image.
Ph.D. Thesis, 2018, NITK, Surathkal, India.

165

- Shettle, E.P. and Weinman, J.A. (1970). "The transfer of solar irradiance through in homogeneous turbid atmospheres evaluated by Eddington's approximation." *Journal of atmospheric sciences*, 27, 1048-1055.

- Smith, G. M. and Milton, E. J. (1999). "The use of the empirical line method to calibrate remotely sensed data to reflectance." *International Journal of Remote Sensing*, 20(13), 2653–2662.

- Staenz, K., Szeredi, T., and Schwarz, J. (1998). "ISDAS - a system for processing/ analysing hyperspectral data." Technical note. *Canadian Journal of Remote Sensing*, 24, 99−113.

- Steinberg, A., Chabrillat, S., Stevens, A., Segl, K. and Foerster, S. (2016). "Prediction of Common Surface Soil Properties Based on Vis-NIR Airborne and Simulated EnMAP Imaging Spectroscopy Data: Prediction Accuracy and Influence of Spatial Resolution." *Remote Sens.*, 8, 613.

- Stevens, A., Miralles, I. and van-Wesemael, B. (2012). Soil Organic Carbon Predictions by Airborne Imaging Spectroscopy: Comparing Cross-Validation and Validation. *Soil Science Society of America Journal,* 76, 2174-2183.

- Stevens, A., Udelhoven, T., Denis, A., Tychon, B., Lioy, R., Hoffmann, L. and Wesemael, B.V. (2010). "Measuring soil organic carbon in croplands at regional scale using airborne imaging spectroscopy". *Geoderma*.158:32–45.

- Stevens, A., van Wesemael, B., Bartholomeus, H., Rosillon, D., Tychon, B. and Ben-Dor, E. (2008). "Laboratory, field and airborne spectroscopy for monitoring organic carbon content in agricultural soils." *Geoderma* 144, 395–404.

- Stevens, A., Van-Wesemael, B., Vandenschrick, G., Touré, S. and Tychon, B. (2006). "Detection of Carbon Stock Change in Agricultural Soils using Spectroscopic Techniques." *Soil Science Society of America Journal*, 70, 844–850.

An evaluation of atmospheric correction algorithms in the estimation of SOC from Hyperion image.
Ph.D. Thesis, 2018, NITK, Surathkal, India.

166

- Stuffler, T., Kaufmann, H., Hofer, S., Förster, K. P., Schreier, G., Müller, A, Eckardt, A. et al. (2007). "The EnMAP Hyperspectral Imager-An Advanced Optical Payload for Future Applications in Earth Observation Programmes." *Acta Astronautica*, 61, 115–120.

- Tanre, D., Deroo, C., Duhaut, P., Herman, M. and Morcrette, J. J. (1990). "Description of a computer code to simulate the satellite signal in the solar spectrum - The 5S code." *International Journal of Remote Sensing*, 11, 659-668.

- Tanré, D., Deschamps, P. Y., Devaux, C. and Herman, M. (1988). "Estimation of Saharan aerosol optical thickness from blurring effects in thematic mapper data." *Journal of Geophysical Research*, 93(12), 15955–15964.

- Tuominen, J. and Lipping, T. (2011). "Atmospheric correction of hyperspectral data using combined empirical and model based method." *Proc., 7th EARSeL SIG Imaging Spectroscopy workshop*, 11–13 April 2011, Scotland.

- Uno, Y., Prasher, S.O., Patel, R.M., Strachan, I.B., Pattey, E. and Karimi, Y. (2005). "Development of field-scale soil organic matter content estimation models in Eastern Canada using airborne hyperspectral imagery." *Canadian Biosystems Engineering*, 47, 1.9-1.14.

- USDA (2009). "Soil Quality Indicators: Total Organic Carbon." *Natural Resources Conservation Service* https://www.nrcs.usda.gov/Internet/FSE_DOCUMENTS/nrcs143_019177.pdf (May 2, 2015).

- Van der Meer, F. (2001). "Basic Physics of spectrometry", In: Van der Meer, F. and de Jong, S. (2001). *Imaging Spectroscopy: Basic Principles and Prospective Applications*, Kluwer Academic Publishers, the Netherlands.

- Vaudour, E., Gilliot, J.M., Bel, L., Bréchet, L., Hadjar, D., Hamiache, J. and Lemonnier, Y. (2014). "Uncertainty of soil reflectance retrieval from SPOT and Rapid Eye multispectral satellite images using a per-pixel bootstrapped empirical

An evaluation of atmospheric correction algorithms in the estimation of SOC from Hyperion image.
Ph.D. Thesis, 2018, NITK, Surathkal, India.

167

line atmospheric correction over an agricultural region." *International Journal of Applied Earth Observation and Geoinformation,* 26, 217–234.

- Vaudour, E., Moeys, J., Gilliot, J.M. and Coquet, Y. (2008). "Spatial retrieval of soil reflectance from SPOT multispectral data using the empirical line method." *International Journal of Remote Sensing,* 29(19), 5571–5584.

- Vermote, E. F., Saleous, N.E., Justice, C.O, Kaufman, Y.J., Privette, J.L., Remer, L., Roger, J.C. and Tanre, D. (1997b). "Atmospheric correction of visible to middle-infrared EOS-MODIS data over land surfaces: Background, operational algorithm and validation." *NASA Publications,* 31.

- Vermote, E.F., Tanre, D., Deuze, J.L., Herman, M. and Morcrett, J.J. (1997a). "Second simulation of the satellite signal in the solar spectrum, 6S: an overview." *IEEE Transactions on Geoscience and Remote Sensing*, 35, 675-686.

- Veum, K.S., Sudduth, K.A., Kremer, R.J. and Kitchem, N.R. (2015). "Estimating a soil quality index with VNIR reflectance spectroscopy." *Soil Science Society of America Journal,* 79, 637–649.

- Viscarra-Rossel, R. A., Walvoort, D. J. J., McBratney, A. B., Janik, L. J. and Skjemstad, J.O. (2006). "Visible, Near-Infrared, Mid-Infrared or Combined Diffuse Reflectance Spectroscopy for Simultaneous Assessment of Various Soil Properties." *Geoderma*, 131, 59–75.

- Viscarra-Rossel, R.A. and Behrens, T. (2010). "Using Data Mining to Model and Interpret Soil Diffuse Reflectance Spectra." *Geoderma*, 158, 46–54.

- Vohland, M. and Emmerling, C. (2011). "Determination of Total Soil Organic C and Hot Water Extractable C from VIS-NIR Soil Reflectance with Partial Least Squares Regression and Spectral Feature Selection Techniques." *European Journal of Soil Science*, 62, 598–606.

- Wang, J., He, T., Lv, C., Chen, Y. and Jian, W. (2010). "Mapping soil organic matter based on land degradation spectral response units using Hyperion images."

An evaluation of atmospheric correction algorithms in the estimation of SOC from Hyperion image.
Ph.D. Thesis, 2018, NITK, Surathkal, India.

168

International Journal of Applied Earth Observation and Geoinformation. 12S, S171-S180.

▪ Wijewardane, N.K., Ge, Y., Wills, S. and Loecke, T. (2016). "Prediction of Soil Carbon in the Conterminous United States: Visible and Near Infrared Reflectance Spectroscopy Analysis of the Rapid Carbon Assessment Project." *Soil Science Society of America Journal*, 80, 973–982.

▪ Wold S., Sjostrom M. and Eriksson L. (2001). "PLS-regression: A basic Tool of Chemometrics." *Chemometrics and Intelligent Laboratory Systems*, 58, 109-130.

▪ Wold, S., Martens, H. and Wold, H. (1983). "The multivariate calibration problem in chemistry solved by the PLS method." *Lecture Notes in Mathematics*, Springer Verlag, Heidelberg, 286-293.

▪ Zhang, T., Li, L. and Zheng, B. (2009). "Partial least squares modeling of Hyperion image spectra for mapping agricultural soil properties." Proceedings of SPIE, *The International Society for Optical Engineering*, 7454, 74540P-1 - 74540P-12.

▪ Zheng, B. (2008). "Using satellite hyperspectral imagery to map soil organic matter, total nitrogen and total phosphorus." MSc thesis, Department of earth science, Indiana University.

An evaluation of atmospheric correction algorithms in the estimation of SOC from Hyperion image.
Ph.D. Thesis, 2018, NITK, Surathkal, India.

169

PUBLICATIONS

International journals

1. **Minu, S**., Shetty, A. and Gomez, C. (2018) "Hybrid Atmospheric Correction Algorithms and evaluation on VNIR/SWIR Hyperion satellite data for Soil Organic Carbon prediction." ***Accepted for publication*** in *International Journal of Remote Sensing*.
doi: 10.1080/01431161.2018.1483087. (Taylor & Francis publication)

2. **Minu, S**. and Shetty, A. (2018) "Prediction accuracy of soil organic carbon from ground based visible near-infrared reflectance spectroscopy" *Journal of the Indian Society of Remote Sensing*. pp. 1-7.
doi: 10.1007/s12524-017-0744-0 (Springer publication)

3. **Minu, S**., Shetty, A., Minasny, B. and Gomez, C. (2017). "The role of atmospheric correction algorithms in the prediction of soil organic carbon from Hyperion data." *International journal of remote sensing*, 38(23), 6435-6456.
doi: 10.1080/01431161.2017.1354265. (Taylor & Francis publication)

4. **Minu, S**., Shetty, A. and Gopal, B. (2016). "Review of preprocessing techniques used in soil property prediction from hyperspectral data." *Cogent Geoscience*, 2, 1145878. doi:10.1080/23312041.2016.1145878 (Taylor & Francis publication)

5. **Minu, S.** and Shetty, A. (2015). "Atmospheric Correction Algorithms for Hyperspectral Imageries: A Review." *International Research Journal of Earth Sciences*, 3(5), 14-18.
http://www.isca.in/EARTH_SCI/Archive/v3/i5/3.ISCA-IRJES-2015-020.pdf

Conference Proceedings

1. **Minu, S.,** Mundol, A.A. and Shetty, A. (2016). "Comparison of Prediction Accuracy of Soil Organic Carbon from Reflectance Spectroscopy", In Proceedings of National Symposium on "Recent Advances in Remote Sensing and GIS with Special Emphasis on Mountain Ecosystems" December 7-9, 2016, ISRS Dehradun, 432.

BIODATA

Name	: Ms. Minu S
Date of Birth	: 14/05/1988
Address	: Parappurathu (H)
	Puliyannoor P.O.
	Pala, Kerala
Telephone	: +91-9962211701
Email:	minu.s88@gmail.com
Qualification	: B.Tech (Civil Engineering)
	Govt. Rajiv Gandhi Institute of technology,
	Kottayam (2006-2010).
	M.Tech (Remote Sensing and GIS)
	National Institute of Technology Karnataka
	Surathkal (2010-2012)
Publications	: International Journal: 05
	International Conference: 03
	National Conference: 01